A quantum chemical study of CH and CC bond activation on transition metals

Please check the document version of this publication:

• A submitted manuscript is the version of the article upon submission and before peer-review. There can be important differences between the submitted version and the official published version of record. People interested in the research are advised to contact the author for the final version of the publication, or visit the DOI to the publisher's website.
• The final author version and the galley proof are versions of the publication after peer review.
• The final published version features the final layout of the paper including the volume, issue and page numbers.

[Link to publication](#)

A Quantum Chemical Study of CH and CC Bond Activation on Transition Metals

H. Burghgraef

A QUANTUM CHEMICAL STUDY OF CH AND CC BOND ACTIVATION ON TRANSITION METALS

A QUANTUM CHEMICAL STUDY OF CH AND CC BOND ACTIVATION ON TRANSITION METALS

PROEFSCHRIFT

ter verkrijging van de graad van doctor aan de
Technische Universiteit Eindhoven, op gezag van
de Rector Magnificus, prof.dr. J.H. van Lint,
voor een commisie aangewezen door het College
van Dekanen in het openbaar te verdedigen op
dinsdag 6 juni 1995 om 14.00 uur

door

Hielke Burghgraef

geboren te Stedum

Dit proefschrift is goedgekeurd door de promotoren:

prof.dr. R.A. van Santen
en
prof.dr. E.J. Baerends

copromotor: dr. A.P.J. Jansen

Voor mijn ouders

Chapter 1

Introduction

1.1   General introduction

Together with oil and coal, natural gas (methane) forms one of the basic sources of fossil energy we nowadays need. These sources can be used for traffic purposes, the generation of electricity in power plants, and as a basic material in the production of a large number of chemicals. Since our energy demand is still increasing and the amount of oil is limited, coal and natural gas become more and more important, together with other sources of energy like wind-, solar-, and nuclear energy. The application of wind and solar energy is increasing, but still limited. The application of nuclear energy results in a long-term waste problem (fission) or the need of extremely high temperatures (fusion). The application of the fossil energy sources results in waste products contributing to the greenhouse effect. Nevertheless, this last form of energy is nowadays mostly needed to cover the energy demands. To produce other chemicals, coal and methane must first be converted to a so-called synthesis gas, which is a mixture of hydrogen and carbon monoxide. In practice this is achieved by gasification (coal) and steam reforming or oxidation (methane). As its name is suggesting, the synthesis gas can be converted to a variety of products depending on reaction conditions and the catalyst used[1]. The conversion of methane is thus an important issue in chemistry. However, methane is a very stable species with strong tetrahedral CH bonds, which are difficult to activate. Therefore, the conversion problem is also a very interesting one.

One way methane activation can be achieved is adsorbing it on transition metal surfaces. The fact that surfaces can induce reaction of such a stable species can be understood by realising that neighbouring metal atoms in the bulk metal are no longer present at a surface. The consequence is that not enough metal metal bonds can be formed, and the

surface metal atoms will become reactive and/or the surface will reconstruct. In principle, the reactiveness and the ability to reconstruct can be studied in detail by computing the electronic structure, which governs these processes. However, we have not studied or allowed for surface reconstruction processes, although we recognise that it can be a very important process. Instead, we have assumed a cluster model for the surface with metal-metal bond distances as in the bulk. The cluster can be viewed as a large molecule and its electronic structure can in principle be computed with standard methods. The effect of the surrounding metal not included in the cluster can be treated by embedding techniques, or by extending the cluster thereby diminishing the effect of the metal surroundings. In this thesis we have chosen for this last option.

How do we compute the electronic structure? In principle, one can use standard Hartree-Fock (HF) theory, which must be followed by Configuration Interaction (CI) to include the very important correlation contribution to the energy in transition metals. However, the larger the cluster the better it is expected to model a surface, which makes application of HF-CI virtually impossible, as will be explained later. A promising alternative is possible by applying density functional theory, which includes correlation and is well suited for fairly large systems. One implementation of density functional theory is the local density approximation (LDA). In this thesis, we have used LDA in combination with gradient corrected terms to allow for the non-uniform electron density in molecules. A next step is computation of kinetical properties like rate constants and sticking coefficients. We have done this by applying transition state theory. This implies an equilibrium situation between reactants and transition state, the description of the internal state distributions by Boltzmann distributions, and the separability of one degree of freedom (the reaction coordinate) from all others. Furthermore, rotational and vibrational frequencies at various parts of the potential energy surface, the actual barrier height (with inclusion of zero-point energies), and the rate of barrier passage need to be known. However, all these data is accessible.

Density functional theory, in particular the LDA-method is more thoroughly discussed in section 1.2. We will see that the main advantages over conventional HF theory are the local exchange potential, the inclusion of correlation and the applicability to large systems. The concept of partition function is discussed in section 1.3. We will derive partition function formulae for translational, rotational, and vibrational degrees of freedom, and we will see how they enter in the transition state theory formula for the rate constant. In chapter 2 we will discuss a first model for the activation of methane by starting from the simplest possible cluster case: the single metal atom. Of course, it is clear that there are many differences between such a simple model and a real surface, but it offers

a starting point, which we can use when going to larger, more realistic cluster models. Chapter 3 deals with these larger clusters. We have judged the various cluster models by comparing the adsorption behaviour of the expected and experimentally detected products of methane dissociation: adsorbed methyl and hydrogen. A one layer 7-atom cluster and a 13-atom spherical cluster turned out to be the best cluster models. In addition to adsorbed methyl and hydrogen, we have also studied subsequent dehydrogenation steps on both clusters leading eventually to adsorbed carbon and hydrogen. To investigate the role of the transition metal, we have studied both nickel and cobalt systems. It turned out that on average adsorption energies on cobalt are larger than those on nickel. Reaction energies are strongly moderated on 13-atom clusters compared to 7-atom clusters. In chapter 4 we have studied in detail methane dissociation producing adsorbed methyl and hydrogen. We determined barrier heights on both clusters and both metals and made a kinetic analysis by computing rate constants and sticking coefficients. On both 7-atom clusters the reaction is strongly endothermic. This endothermicity is strongly reduced on the 13-atom clusters. Reactions on nickel and cobalt are comparable. Chapter 5 deals with the alternative class of reactions which can occur, once adsorbed methyl and hydrogen are formed: CC bond formation reactions. We studied the formation of adsorbed ethynyl (CCH) from adsorbed carbon and methylidyne (CH), adsorbed vinylidene (CCH_2) from adsorbed carbon and methylene (CH_2), and adsorbed ethylidyne (CCH_3) from adsorbed carbon and methyl. This last reaction was studied in more detail by determining the transition state, because ethylidyne is unambiguously detected experimentally. The CC bond formation of C/CH_3 is comparable on the 7-atom clusters. On the 13-atom clusters cobalt is significantly more active. However, finite cluster effects were observed for all studied CC bond formation reactions.

1.2   Electronic structure calculations

In quantum mechanics the state of a system consisting of N particles is fully described by the wave function $\Psi(\vec{r}_1, \vec{r}_2, \ldots, \vec{r}_N, t)$, where $\vec{r}_i$ denotes the position (and spin) of particle i, and t denotes time. When the potential energy is not an explicit function of time, the space- and time variables can be separated and the wave function can be written as a product of a space dependent part and a time dependent part:

$$\Psi(\vec{r}_1, \vec{r}_2, \ldots, \vec{r}_N, t) = \psi(\vec{r}_1, \vec{r}_2, \ldots, \vec{r}_N)\Theta(t). \tag{1.1}$$

If we are dealing with a molecule, our system consists generally of N electrons and M nuclei. It is common practice to separate the motion of the electrons and the nuclei (Born Oppenheimer approximation), because the wave function can then be factorised in a part describing the N electrons and a part describing the M nuclei. This is physically justified by the very large difference between the masses of electrons and those of the nuclei. The equation of motion describing such a system of N electrons, where we have implicitly separated of the part describing the M nuclei, becomes

$$H\psi(\vec{r}_1, \vec{r}_2, \ldots, \vec{r}_N) = E\psi(\vec{r}_1, \vec{r}_2, \ldots, \vec{r}_N), \tag{1.2}$$

where H is the Hamilton operator (Hamiltonian), and E its eigenvalue the energy. Solutions of eq. (1.2) depend parametrically on the nuclear geometry. The Hamilton operator has the form

$$-\sum_{i=1}^{N} \frac{h^2}{8\pi^2 m_i} \left(\frac{\partial^2}{\partial x_i^2} + \frac{\partial^2}{\partial y_i^2} + \frac{\partial^2}{\partial z_i^2} \right) - \sum_{i=1}^{N}\sum_{n=1}^{M} \frac{e^2 Z_n}{|\vec{r}_i - \vec{R}_n|} + \sum_{i=1}^{N}\sum_{j>i}^{N} \frac{e^2}{|\vec{r}_i - \vec{r}_j|}, \tag{1.3}$$

or, in atomic units,

$$-\frac{1}{2}\sum_{i=1}^{N} \nabla_i^2 - \sum_{i=1}^{N}\sum_{n=1}^{M} \frac{Z_n}{|\vec{r}_i - \vec{R}_n|} + \sum_{i=1}^{N}\sum_{j>i}^{N} \frac{1}{|\vec{r}_i - \vec{r}_j|}, \tag{1.4}$$

where i, j sum over the N electrons and n over the M nuclei. The first term denotes the kinetic energy of the electrons, the second term the potential energy of the electrons in the field of the nuclei, and the last term the averaged electrostatic (Coulomb) energy between the electrons. Inspection of eq. (1.4) shows that the first two terms are one-electron operators, and the third term a two-electron operator.

Thus the hamilton operator can also be written:

$$H = \sum_{i=1}^{N} h(i) + \sum_{i=1}^{N} \sum_{j>i}^{N} g(i,j). \tag{1.5}$$

The exact N-electron wave function can be expanded in antisymmetric products:

$$\psi(\vec{r}_1, \vec{r}_2, \ldots, \vec{r}_N) = \sum_i \psi_i^{antisymm.}(\vec{r}_1, \vec{r}_2, \ldots, \vec{r}_N). \tag{1.6}$$

These products must be antisymmetric, because electrons are fermions, implying that under the interchange of any two electrons the wave function must change sign. Products meeting the antisymmetry requirement are the so-called Slater determinants:

$$\psi_S(\vec{r}_1, \vec{r}_2, \ldots, \vec{r}_N) = \sqrt{\frac{1}{N!}} \begin{vmatrix} \psi_1(\vec{r}_1) & \psi_2(\vec{r}_1) & \cdots & \psi_N(\vec{r}_1) \\ \psi_1(\vec{r}_2) & \psi_2(\vec{r}_2) & \cdots & \psi_N(\vec{r}_2) \\ \vdots & \vdots & \ddots & \vdots \\ \psi_1(\vec{r}_N) & \psi_2(\vec{r}_N) & \cdots & \psi_N(\vec{r}_N) \end{vmatrix}, \tag{1.7}$$

where the $\psi_i(\vec{r}_j)$ are any set of orthonormal one-electron functions (orbitals, each a product of a spatial orbital ($\phi_i(\vec{r}_j)$) and a spin function (α or β)). If we retain only one term in expansion (1.6) and minimize the total energy of the system, being the expectation value of the hamiltonian, we get effectively a one-electron eigenvalue problem[2]:

$$f(1)\psi_i(\vec{r}_1) = \epsilon_i\psi_i(\vec{r}_1). \tag{1.8}$$

Here, the single electron has been chosen to be electron 1. The orbital energy (eigenvalue) of $\psi_i(\vec{r}_1)$ is given by ϵ_i. Eqns. (1.8) denote the Hartree-Fock equations; its solutions $\psi_i(\vec{r}_1)$ are known as the Hartree-Fock orbitals. The Fock operator, $f(1)$, is given by:

$$f(1) = h(1) + \sum_j^N \mathcal{J}_j(1) - \sum_j^N \mathcal{K}_j(1), \tag{1.9}$$

where $\mathcal{J}_j(1)$ is called the coulomb operator and is defined as

$$\mathcal{J}_j(1)\psi_i(\vec{r}_1) \equiv \left[\int d\vec{r}_2 \frac{|\psi_j(\vec{r}_2)|^2}{|\vec{r}_1 - \vec{r}_2|} \right] \psi_i(\vec{r}_1), \tag{1.10}$$

and $\mathcal{K}_j(1)$ is called the exchange operator and is defined as

$$\mathcal{K}_j(1)\psi_i(\vec{r}_1) \equiv \left[\int d\vec{r}_2 \frac{\psi_j^*(\vec{r}_2)\psi_i(\vec{r}_2)}{|\vec{r}_1 - \vec{r}_2|}\right]\psi_j(\vec{r}_1). \tag{1.11}$$

The first term of the Fock operator contains again the kinetic energy and the potential energy of the electrons in the field of the nuclei. The second term contains the Coulomb electrostatic interaction. It gives the interaction of electron 1 with the average potential field due to all other electrons j. The last term is due to the antisymmetry of the wave function and is called the exchange term. It has no classical analogue and it is non-local. In practice, the Hartree-Fock orbitals are expanded in some finite basis (with m basis functions) and solved by iteration. This means that for calculating the Coulomb and exchange term of eqns. (1.10)–(1.11), we have to compute m^4 integrals, which is extremely time consuming for even moderate m and N.

An alternative for Hartree-Fock theory and the non-local exchange part was proposed by Slater[3] in 1951. He invoked the uniform electron gas model to produce a local exchange part, resulting in the $X\alpha$ or Hartree-Fock-Slater equation. The local potential in this scheme is given by:

$$v_x(\vec{r}) = -\frac{3}{2}\alpha\left(\frac{3}{\pi}\rho(\vec{r})\right)^{1/3}, \tag{1.12}$$

where the parameter α was set equal to unity in the original description.

A new development was presented by Hohenberg, Kohn and Sham[4]. They showed that the ground state energy of an electronic system can be written as a functional of the density. This led to the development of the Kohn-Sham orbital equations, which can be written as:

$$[-\frac{1}{2}\nabla^2 + v_{eff}(\vec{r})]\psi_i(\vec{r}) = \epsilon_i\psi_i(\vec{r}), \tag{1.13}$$

$$v_{eff}(\vec{r}) = v(\vec{r}) + \int \frac{\rho(\vec{r}\,')}{\vec{r} - \vec{r}\,'}d\vec{r}\,' + v_{xc}(\vec{r}), \tag{1.14}$$

$$\rho(\vec{r}) = \sum_i^N |\psi_i(\vec{r})|^2. \tag{1.15}$$

However, an explicit form for $v_{xc}(\vec{r})$ is needed. This can be obtained by adopting the so-called local density approximation (LDA) for exchange and correlation energy. This method, which is used throughout this thesis, approximates the exchange and correlation energy by:

$$E_{xc}(\rho(\vec{r})) = E_{xc}[\rho] = \int \rho(\vec{r})\epsilon_{xc}(\rho(\vec{r}))d\vec{r}, \tag{1.16}$$

where $\epsilon_{xc}(\rho(\vec{r}))$ indicates the exchange and correlation energy per particle of a uniform electron gas of density $\rho(\vec{r})$. It can be divided into exchange and correlation contributions:

$$\epsilon_{xc}(\rho(\vec{r})) = \epsilon_{xc}[\rho] = \epsilon_x[\rho] + \epsilon_c[\rho]. \tag{1.17}$$

The exchange part was already derived by Dirac[5] in 1930 for a uniform electron gas and is given by:

$$\epsilon_x[\rho] = -\frac{3}{4}\left(\frac{3}{\pi}\rho(\vec{r})\right)^{(1/3)} \tag{1.18}$$

The corresponding exchange-correlation potential now becomes (using eq. (1.16)):

$$v_{xc}(\vec{r}) = \frac{\delta E_{xc}[\rho]}{\delta\rho(\vec{r})} = \epsilon_{xc}[\rho] + \rho(\vec{r})\frac{\delta\epsilon_{xc}[\rho]}{\delta\rho(\vec{r})}. \tag{1.19}$$

Substituting eq.(1.18) into eq. (1.19) and neglecting the correlation part results in:

$$v_x(\vec{r}) = -\left(\frac{3}{\pi}\rho(\vec{r})\right)^{(1/3)}. \tag{1.20}$$

The correlation part for a uniform electron gas is accounted for by interpolation of quantum Monte Carlo simulations of Ceperley and Alder[6] by Vosko, Wilk and Nusair[7], providing an analytical form. Application to a molecule amounts to assuming that the exchange correlation energy for a non-uniform system can be obtained by applying the uniform electron gas results to infinitesimal portions of the non-uniform electron distribution and then summing over all space the individual contributions.

It can be seen by comparing the Hartree-Fock-Slater formula for the local potential (eq. 1.12) and the Kohn-Sham result (eq. 1.20) that the two are equivalent, if correlation is ignored and α is set to 2/3. As a result the value of α was treated as a variable in many Hartree-Fock-Slater calculations. As stated, LDA has been widely applied to problems in molecular and solid state physics with remarkably good results. Bond lengths and -angles are reproduced with an accuracy of 0.02 Å and 1°, respectively. However, binding energies are in some cases overestimated by several eV's. The accuracy for vibrational frequencies is about 70 cm^{-1}. The discrepancies in binding energy have led to the development of methods taking into account small changes in the density instead of assuming a locally constant density. Becke proposed a non-local correction term to LDA giving rise to a gradient corrected exchange functional[8]. Stoll *et al.*[9] accounted for correlation beyond the uniform electron gas model between electrons of different spin, which has been shown[10] to be the major part of the correlation energy. Both the Becke correction for exchange and the Stoll correction for correlation have been used throughout this thesis.

1.3   Kinetic calculations

In this section the concept of partition function is discussed and how it can be used for computing the rate constant according to transition state theory[11]. The theory has been originally developed by Eyring[12], and Evans and Polanyi[13]. We start with the general definition of a partition function (Q):

$$Q \equiv \sum_i e^{\frac{-\epsilon_i}{kT}}. \tag{1.21}$$

Here, i sums over all quantum states, ϵ_i is the energy of state i, k Boltzmann's constant, and T temperature. The value of Q can loosely be interpreted as the number of states that are accessible to the system at the temperature of interest. We will now give explicit forms of the partition functions for translations, rotations, and vibrations. We start with the formula for the translational energy (E_t).

$$E_t = (p_x^2 + p_y^2 + p_z^2)/2m = p^2/2m, \tag{1.22}$$

where p_x, p_y, and p_z are the momenta in the $x-$, $y-$, and $z-$direction; m denotes the mass.

The translational partition function (Q_t) therefore becomes

$$Q_t = \sum_i e^{\frac{-\epsilon_i^t}{kT}}, \tag{1.23}$$

or

$$Q_t = \frac{1}{h^3} \int \int \int \int \int \int dp_x dp_y dp_z dx dy dz \; e^{\frac{-p^2}{2mkT}}, \tag{1.24}$$

where we have substituted the translational energy expression, and replaced the sum over the very narrow spaced states by a six-dimensional integral over phase-space coordinates. The minimum volume per representative point is h^3, and therefore the minimum normalised phase space element becomes $(1/h^3)dp_x dp_y dp_z dx dy dz$, where h is Planck's constant. Eq. (1.24) can be rearranged to

$$Q_t = V \left(\frac{1}{h} \int_{-\infty}^{\infty} dp_x \; e^{\frac{-p_x^2}{2mkT}} \right)^3, \tag{1.25}$$

where V is the volume, obtained by integrating over space coordinates.

This is a standard integration[14] resulting in

$$Q_t = V \left(\frac{2\pi mkT}{h^2} \right)^{3/2} . \tag{1.26}$$

Its equivalent in two dimensions is given by

$$Q_t = S \left(\frac{2\pi mkT}{h^2} \right) , \tag{1.27}$$

where S is the surface area.

The rotational partition function (Q_r) is somewhat more complicated. In fact, for molecules with three different moments of inertia, Q_r can not be derived in closed form. However, we will start with a relatively simple case, where the three moments of inertia are the same $(I_a = I_b = I_c)$. Such a molecule is called a spherical top, and CH_4 belongs to this category. We start with the rotational energy expression (E_r) for a spherical top.

$$E_r = \frac{J(J+1)h^2}{8\pi^2 I_a} , \tag{1.28}$$

where J is a rotational quantum number and can take the values 0, 1, 2, ..., ∞. Therefore, our expression for the rotational partition function is given by:

$$Q_r = \sum_{J=0}^{\infty} e^{\frac{-\epsilon_r}{kT}} = \frac{1}{\sigma} \sum_{J=0}^{\infty} (2J+1)^2 e^{-\frac{J(J+1)h^2}{8\pi^2 I_a kT}} . \tag{1.29}$$

The factor $(2J+1)^2$ accounts for degenerate J-levels. The factor $1/\sigma$ occurs, because we have to count only distinguishable positions into which the molecule can be turned by a simple rigid rotation. σ is called the symmetry factor and equals the number of indistinguishable rotations.

The rotational energy levels of the molecules studied in this thesis lie close enough together for a large number to be populated (at normal temperatures). Thus a good approximation will be replacement of the sum in eq. (1.29) by an integral. Also, in the temperature range studied, high values of J are important, and we may thus approximate $(2J+1)^2$ by $4J^2$. This gives

$$Q_r = \frac{1}{\sigma} \int_0^{\infty} 4J^2 e^{\frac{J(J+1)h^2}{8\pi^2 I_a kT}} . \tag{1.30}$$

This is a again a standard integration[14] and the result is

$$Q_r = \frac{\pi^{1/2}}{\sigma} \left(\frac{8\pi^2 I_a kT}{h^2}\right)^{3/2}.$$ (1.31)

The other case we will encounter in this thesis are molecules with three different moments of inertia ($I_a \neq I_b \neq I_c$). Such molecules are called asymmetric tops. The result for the rotational partition function is a generalisation of eq (1.31):

$$Q_r = \frac{\pi^{1/2}}{\sigma} \left(\frac{8\pi^2 I_a kT}{h^2}\right)^{1/2} \left(\frac{8\pi^2 I_b kT}{h^2}\right)^{1/2} \left(\frac{8\pi^2 I_c kT}{h^2}\right)^{1/2}.$$ (1.32)

The moments of inertia I_a, I_b, and I_c need to be known to compute the rotational partition functions. They are the eigenvalues of the moment of inertia tensor **I**, whose diagonal elements are given by

$$I_{xx} = \sum_{j=1}^{n} m_j[(y_j - y_{CM})^2 + (z_j - z_{CM})^2],$$ (1.33)

$$I_{yy} = \sum_{j=1}^{n} m_j[(x_j - x_{CM})^2 + (z_j - z_{CM})^2],$$ (1.34)

$$I_{zz} = \sum_{j=1}^{n} m_j[(x_j - x_{CM})^2 + (y_j - y_{CM})^2],$$ (1.35)

and whose off-diagonal elements are given by

$$I_{xy} = \sum_{j=1}^{n} m_j[(x_j - x_{CM})(y_j - y_{CM})],$$ (1.36)

where m_j is the mass of the jth nucleus, and x_j its cartesian x-coordinate, etc. j counts the number of nuclei n. x_{CM}, y_{CM}, and z_{CM}, are the centre of mass coordinates; they are given by

$$x_{CM} = \frac{1}{M} \sum_{j=1}^{n} m_j x_j,$$ (1.37)

$$y_{CM} = \frac{1}{M} \sum_{j=1}^{n} m_j y_j,$$ (1.38)

$$z_{CM} = \frac{1}{M} \sum_{j=1}^{n} m_j z_j, \qquad (1.39)$$

where M is the sum of the n masses.

Finally, we will discuss the vibrational partition function. We start with the energy expression for a harmonic oscillator given by

$$E_v = (v + \frac{1}{2})h\nu, \qquad (1.40)$$

where v is the vibrational quantum number and takes the values 0, 1, 2, ..., ∞. ν is the vibrational frequency of the harmonic oscillator.

It follows straightforward from the definition of the partition function that

$$Q_v = \sum_i e^{\frac{-\epsilon_v}{kT}} = \sum_{v=0}^{\infty} e^{-(v + \frac{1}{2})\frac{h\nu}{kT}} = e^{-\frac{1}{2}\frac{h\nu}{kT}} \left(\frac{1}{1 - e^{-\frac{h\nu}{kT}}} \right). \qquad (1.41)$$

The vibrational frequency ν needs to be known to compute the vibrational partition function. It is obtained as follows. Consider a molecule consisting of N atoms. We express the potential energy function V, which is obtained by solving eq. (1.2) for the nuclear positions of interest, in terms of internal coordinates (s_i):

$$2V = V_0 + 2\sum_i^{3N} \left(\frac{\partial V}{\partial s_i} \right)_0 s_i + \sum_{i,j}^{3N} \left(\frac{\partial^2 V}{\partial s_i \partial s_j} \right)_0 s_i s_j + \cdots \qquad (1.42)$$

By choosing the zero-point of energy properly, V_0 can be eliminated. Furthermore, at the potential energy minimum all first derivatives are equal to zero. Finally, cubic, quartic and higher order terms are zero in the harmonic approximation. This leaves us with

$$2V = \sum_{i,j}^{3N} \left(\frac{\partial^2 V}{\partial s_i \partial s_j} \right)_0 s_i s_j = \sum_{i,j}^{3N} F_{ij} s_i s_j. \qquad (1.43)$$

We express the kinetic energy (T) as:

$$2T = \sum_i^{3N} m_i \left(\frac{d\xi_i}{dt} \right)^2 = \sum_i^{3N} m_i \dot{\xi}_i^2, \qquad (1.44)$$

where ξ_i are the cartesian displacement coordinates. To compute the vibrational frequencies, the internal coordinates s_i and the cartesian displacement coordinates must be related.

This relation is

$$s_i = \sum_{j}^{3N} B_{ji}\xi_i, \tag{1.45}$$

where the coefficients B_{ji} depend on the geometry of the system studied. When the coefficients B_{ji} are determined, the kinetic energy can be written in terms of internal coordinates:

$$2T = \sum_{i,j}^{3N} G_{ij}^{-1} \dot{s}_i \dot{s}_j. \tag{1.46}$$

The problem of finding the frequencies is now equivalent with solving the eigenvalue problem[15]

$$\mathbf{GFs} = \lambda\mathbf{s}. \tag{1.47}$$

Diagonalisation of the **GF** matrix thus gives the eigenvalues λ which are related to the frequencies ν according to

$$\lambda = 4\pi\nu^2. \tag{1.48}$$

We will now derive an expression for the rate constant in terms of the partition functions. Consider the following (isomerisation) reaction in the gas phase

$$A \rightleftharpoons A^\dagger \xrightarrow{k_f} P, \tag{1.49}$$

where A denotes the reactant molecule, $A^\dagger$ the transition state, P the product, and k_f the (forward) reaction rate constant. If the reactant and the transition state can be considered to be in equilibrium with their surroundings, their internal state distributions can be taken as Boltzmann distributions, and the partition function concept is applicable. When equilibrium is established between the reactant A and the transition state $A^\dagger$, we can then write down for the equilibrium constant K:

$$K = \frac{[A^\dagger]}{[A]} = \frac{N_A^\dagger}{N_A} = \frac{Q_A^\dagger}{Q_A} e^{\frac{-E}{kT}}. \tag{1.50}$$

Here, $[A]$ denotes the concentration of molecule A, N_A the number of molecules A, and Q_A the (overall) partition function of molecule A, which is a product of the translational, vibrational and rotational partition function. The same holds for $A^\dagger$. The exponential term accounts for the energy difference between the reactant and the transition state at the electronic potential energy surface, because zero-point vibrational energies are thus far included in the vibrational partition function (see eq. (1.41)). At this stage, the transition state partition function still includes all 3N modes. However, we now assume that one vibration has a distinct character and is separable from all other modes. It corresponds to such a loose vibration that there is no restoring force: the transition state complex forms the product P. For this one degree of freedom (the reaction coordinate), we have to evaluate eq. (1.41) in the limit of zero vibrational frequency:

$$\lim_{\nu \to 0} \left(\frac{1}{1 - e^{-\frac{h\nu}{kT}}} \right) = \frac{1}{1 - (1 - (h\nu/kT))} = \frac{kT}{h\nu}, \tag{1.51}$$

where the zero-point vibrational energies are now included in the energy barrier.
Eq.(1.50) now rearranges in

$$\frac{[A^\dagger]}{[A]} = \frac{kT}{h\nu} \frac{Q_A^\dagger}{Q_A} e^{\frac{-E'}{kT}}, \tag{1.52}$$

or

$$\nu[A^\dagger] = [A] \frac{kT}{h} \frac{Q_A^\dagger}{Q_A} e^{\frac{-E'}{kT}}. \tag{1.53}$$

Here, $Q_A^\dagger$ denotes the overall transition state partition function of molecule A excluding the reaction coordinate. The left-hand sight of eq.(1.53) is the product of the concentration of the transition state and the frequency of its conversion to product, and is therefore the rate of reaction v. We thus get:

$$v = [A] \frac{kT}{h} \frac{Q_A^\dagger}{Q_A} e^{\frac{-E'}{kT}}. \tag{1.54}$$

Using the definition of the rate constant, which is

$$v = k_f[A], \tag{1.55}$$

we arrive at the transition state expression for the rate constant

$$k_f = \frac{kT}{h} \frac{Q_A^\dagger}{Q_A} e^{\frac{-E'}{kT}}, \tag{1.56}$$

which we will write as

$$k^{TST} = \frac{kT}{h} \frac{Q_A^\dagger}{Q_A} e^{\frac{-E}{kT}}. \tag{1.57}$$

1.4   References

1. J.R. Rostrup-Nielsen, *Catalysis- science and technology, Vol. 5*,
   edited by J.R. Anderson and M. Boudart (Springer-Verlag, Berlin, 1984).
2. A. Szabo, N.S. Ostlund, *Modern quantum chemistry*,
   (McGraw-Hill, New York, 1982).
3. J.C. Slater, Phys. Rev. **81** (1951) 385.
4. P. Hohenberg, W. Kohn, Phys. Rev. B **136** (1964) 864.
   W. Kohn, L.J. Sham, Phys. Rev. A **140** (1965) 1133.
5. P.A.M. Dirac, Proc. Cambridge Phil. Soc. **26** (1930) 376.
6. D.M. Ceperley, B.J. Alder, Phys. Rev. Lett. **45** (1980) 566.
7. S.H. Vosko, L. Wilk, M. Nusair, Can. J. Phys. **58** (1980) 1200.
8. A.D. Becke, Phys. Rev. A **38** (1988) 3098.
9. H. Stoll, C.M.E. Pavlidou, H. Preuss, Theor. Chim. Acta **49** (1978) 143.
   H. Stoll, E. Golka, H. Preuss, Theor. Chim. Acta **55** (1980) 29.
10. B.O. Roos, P.E.M. Siegbahn, *Modern theoretical chemistry*,
    edited by H.F. Schaefer III, (Plenum Press, New York, 1977).
11. D.A. McQuarrie, *Statistical mechanics*, (Harper and Row, New York, 1976).
    K.J. Laidler, *Chemical kinetics*, (Harper and Row, New York, 1987).
    R.D. Levine, R.B. Bernstein, *Molecular reaction dynamics and chemical reactivity*,
    (Oxford University Press, Oxford, 1987).
    R.A. van Santen, J.W. Niemantsverdriet, *Chemical Kinetics and Catalysis*,
    (Lecture notes, Eindhoven, 1992).
12. H. Eyring, J. Chem. Phys. **3** (1935) 107.
13. M.G. Evans, M. Polanyi, Trans. Faraday Soc. **31** (1935) 875.
14. M. Abramowitz, I.A. Stegun, *Handbook of mathematical functions*,
    (Dover Inc, New York, 1965).
15. E.B. Wilson, J.C. Decius, P.C. Cross, *Molecular vibrations. Theory of infrared and raman vibrational spectra*, (McGraw-Hill, New York, 1955).

Chapter 2

Insertion of nickel and cobalt in the CH bond of methane. Electronic structure calculations and kinetics

abstract

The insertion of a transition metal atom in the CH bond of CH_4 is calculated using density functional theory by determining the transition state and the dissociated state of $HMCH_3$, where M is nickel or cobalt. A barrier for nickel insertion of 41 kJ/mol is found and its origin is discussed. The insertion is exothermic by 34 kJ/mol. The barrier height for cobalt insertion is 79 kJ/mol, and the overall reaction is endothermic by 6 kJ/mol. From the potential energy surface at the transition state and the dissociated state vibrational and rotational frequencies are obtained. Unimolecular and bimolecular transition state theory is used for the calculation of rate constants, sticking coefficients and activation energies for the insertion reactions as well as the elimination reactions. Activation energies for nickel or cobalt insertion in both CH_4 and CD_4 are small compared with other theoretical work. A moderate kinetic isotope effect for the insertion reactions is found, whereas no significant kinetic isotope effect is found for the elimination reactions. Hydrogen tunneling corrections on rate coefficients are also evaluated, but their effect is negligible.

2.1   Introduction

The conversion of hydrocarbons on transition metal surfaces is industrially and theoretically of great interest. For example, the steam reforming of natural gas, of which CH$_4$ is the major constituent, over a nickel catalyst is a commercial process to produce hydrogen, but occurs only at elevated temperatures[1]. Some of the first mechanistic studies of CH$_4$ dissociative chemisorption on transition metals were those of Winters[2]. The apparent activation energies of CH$_4$ on a tungsten surface were discussed in terms of tunneling of hydrogen through a potential barrier, vibrational excitation of CH$_4$ and the lifetime of undissociated CH$_4$ on the surface (precursor model). At the same time, Stewart and Ehrlich[3] found that dissociative adsorption of CH$_4$ on rhodium surfaces could be enhanced by increasing only the CH$_4$ gas temperature (T_g). Also, a large kinetic isotope effect (KIE) was found and Stewart *et al.* attributed this to a dominant role of vibrational activation in the CH$_4$ activation process. Since both experiments suggested the importance of vibrational excitation, laser vibrational excitation experiments on rhodium surfaces were carried out[4], but were unsuccessful. Rettner *et al.*[5] showed in a subsequent study on W(110) that vibrational excitation enhances the CH$_4$ chemisorption, but that this enhancement is not significantly larger than for an equal amount of energy in translation modes. They could not rule out the possibility that individual vibrational modes contribute disproportionally to the observed sticking probability, but in that case other vibrational modes would be less effective, thus explaining the unsuccessful laser experiments. In later work on CH$_4$ on rhodium[6], Brass and Ehrlich studied thermal activation by raising the gas temperature or the metal surface temperature (T_s). They found that initial sticking coefficients increased in all cases with temperature. Therefore, they suggested[7] that dissociation occurs both through activated direct chemisorption (dependent on T_g) and through molecular precursors (dependent on T_s) and they explained the observation of different activation energies for CH$_4$ and CD$_4$ again in terms of internal vibrational excitation of CD$_4$ and CH$_4$. Beebe *et al.*[8] also performed thermal activation experiments under isothermal conditions for several low indices nickel single crystal surfaces. Again, a large KIE of a factor 20 was found on Ni(100), whereas none was seen on the Ni(110) surface; no CD$_4$ experiments on Ni(111) were carried out. Chorkendorff *et al.*[9] however, performing the same isothermal experiments for CH$_4$ on Ni(100), found an activation energy of twice that of Beebe. Beebe also compared his measured sticking coefficients with those calculated from molecular beam experiments on Ni(111)[10] and Ni(100)[11]. The agreement with Ni(111) was good, with Ni(100) poor. In another dispute Lo and Ehrlich[12] claimed that the experimental KIE of CH$_4$/CD$_4$ chemisorption on W(211), whether translationally

or vibrationally activated, could not be described by a tunneling model in which barrier parameters were chosen to match the experimental activation energy. Their results were reanalyzed by Kay and Coltrin[13] who showed that the experimental results were entirely consistent with a tunneling mechanism provided a more intricate model for the tunneling transmission coefficient was used. In return, Lo *et al.* derived a more generally applicable relation for tunneling and again denounced the tunneling model after comparison with their experimental findings. After additional exchange of comments between both sides, we conclude that a tunneling mechanism could not be totally eliminated, as demonstrated by Kay *et al.*, but also couldn't account totally for the small experimental KIE as was pointed out by Lo *et al.*.

By making use of molecular beam techniques in combination with ultrahigh vacuum surface electron spectroscopy, it is nowadays possible to study experimentally the dynamics of the CH_4/CD_4 decomposition under low pressure conditions, giving far more detailed experimental information. The first CH_4 dissociation molecular beam experiment (on W(110)) was performed by Rettner *et al.*[14], which showed a roughly exponential increase of the sticking coefficient (S) with the normal component of the incident energy, E_n. The experiments also showed a large KIE and an increase in S with nozzle temperature, which was explained by enhanced vibrational excitation. The authors pointed out that the dependence of S on E_n suggested a concerted tunneling mechanism instead of a molecular precursor model followed by tunneling. In another experiment Lee *el al.*[10] used a single Ni(111) crystal and obtained similar results, but by making use of EELS vibrational spectroscopy they demonstrated also that the initial step in dissociative chemisorption is the breaking of a single CH bond and the formation of adsorbed CH_3 and H. They also argued that the critical requirement for CH_4 dissociation is angular deformation of CH_4 to allow a NiC bond to form. In this model S is sensitive for excitation of CH_4 bending modes, explaining the dependence of S with nozzle temperature and partly the KIE. The strong dependence of S on E_n was to increase transfer of translational energy to bending vibration energy on impact of CH_4 with the surface (called splats and eventually giving rise to new experimental methods like inert gas atoms induced chemisorption [15]). Tunneling can contribute to this model but is not essential; also molecular precursors play no role in this model. Similar studies have been performed by Luntz and Bethune [16] and Schoofs *et al.*[17] on Pt(111). The only new feature emerging was a complex dependence of S on E_n, T_g and T_s, noted by Luntz and Bethune, but unnoticed by Schoofs *et al.*. Also, Luntz and Bethune did not present a model to explain the observed complex dependence, but remarked that this could not be explained by any known single model. In another series of papers however, Luntz and Harris [18] presented a model in which quantum chemical tun-

neling is dominant; the tunneling process is interpreted as a quantum dynamics problem
involving a three dimensional potential energy surface. They gave however only qualitative
results.

In conclusion, many kinetic and molecular beam studies have been performed resulting
in different activation energies, sticking coefficients and KIE's for each kind of experiment
and condition. Precursor models, accounting for a strong dependence of S on T_s, direct dis-
sociative chemisorption models, accounting for a strong dependence of S on T_g and mixed
models, relating S, E_n, T_g and T_s, have been invoked. Nevertheless, this wealth in models
has not resolved the relationship between the factors controlling the reaction mechanism
of the chemisorptive dissociation of CH$_4$ on transition metal surfaces completely.

As a first model in the investigation of the electronic factors determining the CH$_4$
dissociation on transition metals, we have investigated the elimination of a nickel or cobalt
atom (M) from the dissociated state:

$$\text{HMCH}_3 \xrightarrow{k_{uni,eli.}} \text{CH}_4 + \text{M} \tag{2.1}$$

as well as the reverse reaction, insertion of a nickel or cobalt atom in a CH bond of CH$_4$:

$$\text{CH}_4 + \text{M} \xrightarrow{k_{bi,ins.}} \text{HMCH}_3 \tag{2.2}$$

by means of an *ab initio* approach. Using the potential energy surfaces at the transi-
tion state (TS) and at the dissociated state (DS), we have calculated vibrational frequen-
cies. The TS and DS geometries allow the calculation of rotational constants. According
to transition state theory, the rate coefficients for nickel/cobalt (oxidative) addition and
nickel/cobalt (reductive) elimination have been calculated in terms of translational, vibra-
tional, and rotational partition functions. Activation energies and pre-exponential factors
have been calculated from Arrhenius plots. Technical details of the calculations are dis-
cussed in section 2.2. In section 2.3 the electronic structure calculations are presented and
discussed. In section 2.4 kinetic calculations and the application of transition state theory
is discussed. In section 2.5 we summerise results and draw conclusions.

2.2   Methods

We have performed quasi-relativistic calculations based on density functional theory (DFT) using the implementation of Baerends' group[19]. The exchange-correlation potential used is based on Quantum Monte Carlo simulations of Ceperley and Alder[20] of a homogeneous electron gas which are parametrised by Vosko, Wilk and Nusair[21]. To correct for the overbinding inherent to the local density approximation (LDA)[22], we haved used a gradient corrected exchange energy functional[23] in combination with the Stoll correction[24] for correlation. Molecular orbitals are expressed by the LCAO method using Slater orbitals, integrals are evaluated numerically[25] and adsorption energies are calculated by Ziegler's transition state method[26]. For carbon the 1s electrons are frozen; for nickel and cobalt the electrons up to 3p are frozen. Relativistic effects were taken into account by first order perturbation theory[27]. The basis sets are of double ζ quality with the exception of the nickel and cobalt d-orbitals, which are triple ζ 's. On all atoms polarisation functions are included. The geometric parameters which were optimised are shown
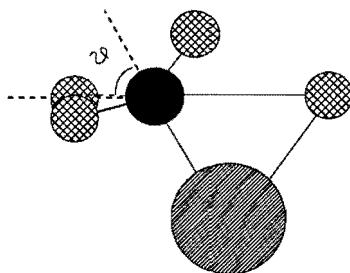
Fig. 2.1.
Definition of optimised parameters. Hydrogen atoms are denoted by diagonally cross-hatched circles, carbon by a filled black circle, and the transition metal atom by a diagonally hatched circle. The dotted lines denote the C_{3v}-axes of the CH_3-group in the reactant- and the TS. The MC bond, the MH bond, the CH bond, together with the CH_3 tilt angle with respect to the activated bond (θ) were optimised.

in fig 2.1. The CH_3 fragment was fixed with CH distances of 1.09 Å and HCH angles of 109.48° as in CH_4, because it was shown experimentally to be very similar[10] in the TS and the DS. The TS and the DS were explicitly calculated by a four dimensional grid in the MC, MH and CH distances and the CH_3 tilt angle with respect to the activated CH bond (θ). Vibrational calculations were performed by the conventional GF method[28]. Kinetical properties were calculated using transition state theory[29], including quantum tunneling corrections based on an unsymmetrical Eckart potential[30].

2.3   Electronic structure calculations

Results of calculations on the atomic states of nickel and cobalt are shown in table 2.1. The implementation of the programme allows only the calculation of low and high spin states. Therefore, it is not possible to calculate the separate *J*-states. Also the calculation of the separate Ni d^{8}s^2 (^{3}F) and Ni d^{8}s^2 (^{3}P) state is not possible, because the d^{8}s^2 high spin state corresponds with a linear combination of both. This is also the case for several atomic states of cobalt.   However, we can calculate *J*-averaged low and high

Table 2.1. Energies (kJ/mol) of *J*-averaged atomic states relative to the Ni d^{9}s^1(^{3}D) state and the Co d^{7}s^2(^{4}F + ^{4}P) state.

System	*J*-averaged state	Experiment^a	DFT	MRCI + Q^b	ACPF^c	CASPT2^d
Ni	d^{9}s^1(^{3}D)	0	0	0	0	0
Ni	d^{8}s^2(^{3}F)	3		-18		-8
Ni	d^{9}s^1(^{1}D)	32	17	44	29	31
Ni	d^{8}s^2(^{3}F + ^{3}P)	65	67			
Ni	d^{8}s^2(^{1}D)	153	157			
Ni	d^{10}(^{1}S)	167	234	181		168
Co	d^{7}s^2(^{4}F)	-47		0		
Co	d^{8}s^1(^{4}F)	-7		77		
Co	d^{7}s^2(^{4}F + ^{4}P)	0	0			
Co	d^{8}s^1(^{4}F + ^{4}P)	34	0			
Co	d^{8}s^1(^{2}F)	37		108		
Co	d^{8}s^1(^{2}F + ^{2}P)	76	31			
Co	d^{8}s^1(a^{2}D + b^{2}D)	177	93			
Co	d^{7}s^2(^{2}G + ^{2}P + ^{2}H + ^{2}G)	192	173			
Co	d^9(^{2}D)	277	259			

^{a} see ref.[33]

^{b} see ref.[31]

^{c} see ref.[34]

^{d} see ref.[32]

spin states and in the case of certain orbital occupations linear combinations of the various terms. Table 2.1 shows that a correct ordering of atomic states is obtained for both nickel and cobalt. Extensive MRCI calculations[31] including f- and g-functions in the basis set, and CASSCF plus second order perturbation theory (CASPT2) calculations[32] give the Ni d^{8}s^2 (^{3}F) state as the ground state contrary to experiment[33]. However, the other states are calculated in agreement with experiment, especially with the CASPT2 method. For the Average Coupled Pair Functional (ACPF)-method[34], only the difference between

the Ni d^9s^1 (^3D) and Ni d^9s^1 (^1D) state could be found in the literature, but this is very accurate. Optimal parameters and binding energies of the reactant, the transition state (TS) and the dissociated state (DS) of Ni/CH$_4$ and Co/CH$_4$ are shown in table 2.2. They

Table 2.2. Geometries (Å) and energies (kJ/mol) for the Ni/CH$_4$ reactant, HNiCH$_3$ (^1A') TS, HNiCH$_3$ (^1A') DS, Co/CH$_4$ reactant, HCoCH$_3$(^2A') TS, and HCoCH$_3$ (^2A') DS.

System	Method	R_{MC}	R_{MH}	R_{CH}	θ	E
HNiCH$_3$ (^1A') DS	DFT	1.92	1.46	2.55	29.9°	-34
HNiCH$_3$ (^1A') TS	DFT	2.02	1.49	1.37	21.3°	41
Ni/CH$_4^a$	DFT	∞	∞	1.08	0.0°	0
HNiCH$_3$ (^1A') DS	MRCI + Q^b	1.98	1.47	2.55	27.0°	18
HNiCH$_3$ (^1A') TS	MRCI + Q	2.12	1.49	1.62	19.5°	83
Ni/CH$_4^c$	MRCI + Q	∞	∞	1.09	0.0°	0
HNiCH$_3$ (^1A') DS	ACPF^b	1.98	1.47	2.55	27.0°	-14
HNiCH$_3$ (^1A') TS	ACPF	2.12	1.49	1.62	19.5°	75
Ni/CH$_4^c$	ACPF	∞	∞	1.09	0.0°	0
HCoCH$_3$ (^2A') DS	DFT	1.97	1.49	2.69	31.4°	6
HCoCH$_3$ (^2A') TS	DFT	2.02	1.48	1.53	26.8°	79
Co/CH$_4^a$	DFT	∞	∞	1.08	0.0°	0
HCoCH$_3$ (^2A') DS	MRCI + Q^b	1.98	1.47	2.55	27.0°	42
HCoCH$_3$ (^2A') TS	MRCI + Q	2.12	1.49	1.62	19.5°	101
Co/CH$_4^c$	MRCI + Q	∞	∞	1.09	0.0°	0

^{a} Ni d^9s^1 (^3D) + CH$_4$ or Co d^7s^2 (^4F) + CH$_4$

^{b} see ref.[36]. MRCI optimised geometries. For cobalt the nickel optimised geometries were used

^{c} Ni d^9s^1 (^1D) + CH$_4$ or Co d^8s^1 (^2F) + CH$_4$

were obtained by fitting the energy calculated on grid points in the reactant, the TS and the DS region to a second order polynomial in the MC, MH and CH distances and the CH$_3$ tilt angle θ. The obtained (fitted) energy was tested by making another set of calculations with the optimal geometrical parameters. The deviation between fitted and calculated energies was negligible. We have shifted our TS and DS of cobalt with 57 kJ/mol, which is the experimental difference between the Co d^7s^2 (^4F)-state and the Co d^7s^2 (^4P)-state to eliminate the contribution of the excited Co d^7s^2 (^4P)-state in our *J*-averaged ground state and obtain a more realistic reactant energy. We compute a barrier for cobalt insertion of 79 kJ/mol, and an overall reaction energy of 6 kJ/mol endothermic. For nickel, we compute a barrier for insertion of 41 kJ/mol, and an overall reaction energy of 34 kJ/mol. For both transition metal atoms, the DS is a bent state, as in the case of NiH$_2$ [35].

Electron distributions based on a Mulliken population analysis show that during the insertion process both the nickel and the cobalt atom maintain an open shell configuration, i.e. a d^9s^1-like state for nickel and a d^8s^1-like state for cobalt. The reason for this is that a single electron in both s- and d-shell can efficiently hybridise when low spin coupled, thereby avoiding strong steric repulsion between closed shell CH₄ and a closed s- or d-shell of the transition metal atom. Also, the open d-orbital and s-orbital can more easily form the two bonds to CH₃ and hydrogen. Blomberg *et al.* have shown[35] that this efficient s-d hybridisation has its consequence in a low barrier and a bent minimum as compared to the less efficient s-p hybridisation resulting in a high barrier and a linear minimum. Electron density difference maps of the TS with respect to the transition metal atom and CH₄ in the TS geometry in the mirror plane are shown in fig. 2.2 for both nickel and cobalt.
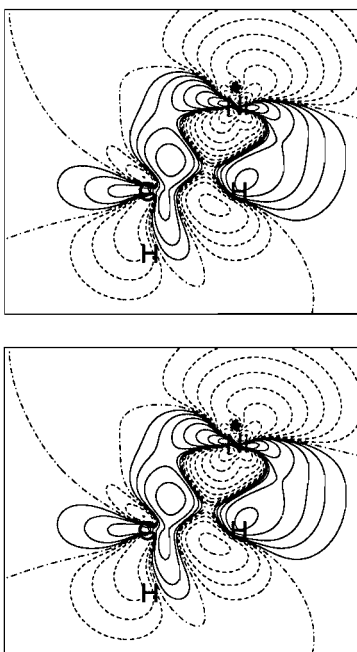
Fig. 2.2.
Contour plots of the electron density differences.
ρ (HNiCH₃^{TS}) - ρ (Ni) - ρ (CH₄^{TS}) (top), and ρ (HCoCH₃^{TS}) - ρ (Co) - ρ (CH₄^{TS}) (bottom).
Solid contours denote increase, dashed lines denote decrease in electron density (in electrons Å^{-3}).
Contour values: $0.00, \pm 0.006, \pm 0.016, \pm 0.035, \pm 0.075, \pm 0.159, \pm 0.336, \pm 0.709, \pm 1.505,$ and ± 3.185.

They show the metal d-orbital involvement at the TS. Also the activation of the CH bond, and the formation of MC and MH bonds is clearly visible. The overlap populations at the TS of 0.19 for NiH, 0.14 for NiC, 0.11 for CoH, and 0.14 for CoC confirm this. At the DS the overlap populations for CH_3 and H with nickel are 0.32 and 0.27, those with cobalt 0.29 and 0.21 respectively, suggesting a stronger bond for CH_3. Fig. 2.3 shows the local density of states (LDOS) of the antibonding σ orbital located between CH_3 and the activated H at the $HNiCH_3$ (TS) and at large distance. At the TS this antibonding orbital is dispersed significantly in four MO's of which three are above the Fermi level (denoted by the zero of energy) and one is beneath it. This one is the highest occupied molecular orbital (HOMO), which is the dissociating CH bond. Therefore, the character of the HOMO is clearly partially antibonding. At a larger distance (4.36 Å), the same antibonding σ is almost a pure MO, far above the Fermi level and therefore not occupied. To determine the origin of the barrier for nickel insertion, we performed two series of calculations. In one series, we investigated the effect of stretching a CH bond by stretching this bond in CH_4 from 1.08 Å to 1.37 Å (the TS-value). We found a destabilisation of 85 kJ/mol.
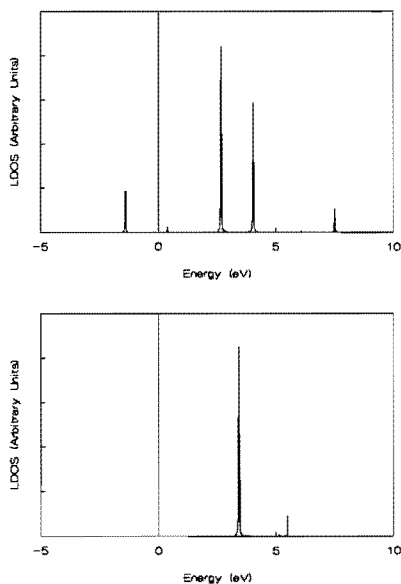
Fig. 2.3.
Local density of states (LDOS) of the antibonding σ orbital (σ^*) located between C and activated H at the $HNiCH_3$ (TS) geometry (top) and at 4.36 Å (bottom).

In another series, we investigated the effect of the Pauli repulsion, associated by the approach of a nickel atom, by enlarging the NiC distance, starting at its TS value, and keeping the CH distance at its TS value. We found a small destabilisation of the complex. The much larger destabilisation of CH$_4$ by stretching one bond in the absence of nickel (85 kJ/mol) vs. the same stretch in the presence of nickel (41 kJ/mol), in combination with the smooth destabilisation of the TS-complex when the NiC distance is enlarged, shows that the Pauli repulsion associated with the second trajectory, does not control the barrier height for dissociation. In other words the TS barrier is mainly determined by the need to minimise the energy cost to stretch the CH bond.

We can compare our data with those of Blomberg *et al.*[36], For nickel, the geometrical parameters are practically the same, except for the CH stretch at the TS. We find a TS in which the CH bond is significantly less stretched. We therefore compute a significantly lower barrier. If we had assumed the nickel atom to be in its lowest singlet state (d^{9}s^1 (^{1}D)) as Siegbahn *et al.* did, instead of its lowest state (d^{9}s^1 (^{3}D)), the barrier would lower another 17 kJ/mol. The calculated energy difference between the TS and the DS is 65 kJ/mol (MRCI) and 75 kJ/mol (DFT), but our low TS barrier results in a strong exothermic state. Blomberg *et al.*[36] also calculated the energetics of the nickel insertion reaction using the optimal geometrical parameters determined with the MRCI-method, but using a larger basis set and a different method, the internally contracted average coupled pair functional (IC-ACPF)-method. Although the IC-ACPF method results in a lower Ni d^{9}s^1 (^{1}D) state, which is used by the authors as the Ni/CH$_4$ reactant, and which is in better agreement with experiment than the MRCI -value, they nevertheless find a lowering of the nickel insertion barrier of 8 kJ/mol. Also, they computed a larger energy difference between the TS and the DS of 24 kJ/mol and the nickel insertion becomes now exothermic by 14 kJ/mol, which is both more in agreement with our results. A separate IC-ACPF geometry optimalisation would further lower their barrier and make the insertion reaction even more exothermic. For cobalt, Blomberg *et al.*[36] computed a barrier of 101 kJ/mol using their nickel optimised geometry and the Co d^{8}s^1 (^{2}F) state as an asymptote. Their overall reaction energy was 42 kJ/mol endothermic. It is difficult to compare the energy barriers of cobalt, because they are given with respect to different atomic states, which can not be connected, and because Blomberg *et al.* did not optimise the TS and the DS for cobalt insertion separately. They calculated an elimination barrier of 59 kJ/mol, where we found a value of 73 kJ/mol. If we compare our separately optimised nickel- and cobalt geometries, we see that the main difference is the CH distance in both the TS and the DS, which is 0.14–0.16 Å larger in the case of cobalt. This suggests a higher barrier for cobalt insertion and a more or less the same barrier for cobalt elimination, as indeed we find.

2.4 Kinetic calculations

Transition state theory allows the calculation of rate coefficients in terms of local properties of the potential energy surface (PES) and therefore in principle requires no calculations on the dynamics of the reacting system; we only need vibrational and rotational frequencies. The transition state theory formulae for the unimolecular and bimolecular rate coefficients of eqns. (2.1)–(2.2) at the high pressure limit are given by[29]:

$$k_{uni.\ eli.} = k_{uni.\ eli.}^{TST} = \frac{k_B T}{h} \frac{(Q_v Q_r)^\dagger}{Q_v Q_r} e^{\frac{-E_{crit}}{k_B T}} \tag{2.3}$$

$$k_{bi.\ ins.} = k_{bi.\ ins.}^{TST} V = \frac{k_B T V}{h} \frac{(Q_v Q_r)^\dagger}{Q_t Q_v Q_r} e^{\frac{-E'_{crit}}{k_B T}} \tag{2.4}$$

In eqns. (2.3)–(2.4) k_B denotes Boltzmann's constant, T temperature, V volume, and h Planck's constant. Q_t, Q_v and Q_r are the translational, vibrational and rotational partition functions of the M/CH_4 reactant, the TS, or the DS. The translational partition function describes the relative translation of the transition metal atom and CH_4. A dagger ($\dagger$) denotes transition state partition functions. E_{crit} is the minimum energy at which reaction can occur (critical energy), and includes the zero point vibrational energy differences. Therefore, to evaluate $k_{uni.\ eli.}^{TST}$ and $k_{bi.\ ins.}^{TST}$, we need to calculate the translational, vibrational and rotational partition functions of the M/CH_4 reactant, the TS and the DS. However, if partition functions are the same in the DS and the TS, or in the M/CH_4 reactant and the TS, they cancel and we need only to evaluate partition functions which differ. Also, if a vibrational frequency is high ($h\nu \gg k_B T$), the partition function gives a factor of 1.0 and therefore has effectively no contribution to the rate constant.

To find out which degrees of freedom cancel, we characterised them at the different geometries. At the TS and the DS we have the following degrees of freedom: three translations of the centre of mass, three overall rotations, three CH stretches in CH_3, one CH_3 tilt in the mirror plane (θ), one CH_3 tilt perpendicular to the mirror plane, three internal bending modes in CH_3, one internal CH_3 rotation around the C_{3v}-axis, one CH stretch, one MC stretch and one MH stretch. At the reactant we have the following degrees of freedom: three translations of the centre of mass, three relative translations, three overall rotations of CH_4, three CH stretches in CH_3, three internal bending modes in CH_3, one CH_3 tilt in the mirror plane (θ), one CH_3 tilt perpendicular to the mirror plane and one CH stretch. This choice of modes results in the cancellation of partition functions of the

following modes: three translations of the centre of mass, three CH stretches of CH_3, three internal bending modes in CH_3, and one CH_3 tilt perpendicular to the mirror plane. One internal CH_3 rotation at the TS and the DS against one overall CH_4 rotation. Therefore, we have to compute at the TS and the DS the partition functions for the CH stretch, the MC stretch, the MH stretch, θ, and three overall rotations, and at the reactant three relative translations, a CH stretch, θ, and two overall rotations of CH_4. The masses of the atoms allow the calculation of the partition functions of the relative translations. Together with the masses, the geometries allow the calculation of the moments of inertia and subsequently the rotational constants and the rotational partition functions. To calculate vibrational partition functions, a harmonic vibrational analysis at the TS and the DS in the MH, MC and CH distances, and θ, and at the reactant in the CH distance and θ was carried out. The vibrational frequencies for the reactant, the TS and the DS of Ni/CH_4, Ni/CD_4, Co/CH_4, and Co/CD_4 are displayed in table 2.3.

Table 2.3. Vibrational frequencies, ν_i (cm^{-1}), for the Ni/CH_4 reactant, HNiCH$_3$(^{1}A') TS, HNiCH$_3$(^{1}A') DS, the Co/CH_4 reactant, HCoCH$_3$(^{2}A') TS, HCoCH$_3$(^{2}A') DS, and their isotopic substitutes.

System	ν_1	ν_2	ν_3	ν_4
M/CH_4	2951	2438		
M/CD_4	2131	1929		
HNiCH$_3$(^{1}A') TS	1988	1743	682i	607
DNiCD$_3$(^{1}A') TS	1540	1258	511i	586
HNiCH$_3$(^{1}A') DS	2238	1583	672	505
DNiCD$_3$(^{1}A') DS	1605	1250	529	469
HCoCH$_3$(^{2}A') TS	2290	549i	427	136
DCoCD$_3$(^{2}A') TS	1620	428i	388	136
HCoCH$_3$(^{2}A') DS	1544	1448	252	140
DCoCD$_3$(^{2}A') DS	1104	1026	252	138

For the reactant the frequencies can be best compared with the normal frequencies of CH_4 and CD_4. We find for the CH stretch a frequency of 2951 cm^{-1} and for θ a frequency of 2438 cm^{-1}. For CD_4 these values are respectively 2131 cm^{-1} and 1929 cm^{-1}. The experimental values are 2917/3020 cm^{-1} for the symmetrical/asymmetrical stretch modes and 1534 cm^{-1} for the twofold degenerate bending modes of CH_4. For CD_4, these values are 2109/2259 cm^{-1} and 1092 cm^{-1} respectively[37]. For the CH stretch our values are reasonably well, for θ our values are 800–900 cm^{-1} too high. This is due to the fact that we calculated the pure stretch and CH_3 tilt and not the normal coordinates, which should lower the frequencies. Our choice of modes, however, results in the partition function

cancellation as discussed above. The occurrence of one imaginary frequency in the TS region shows that we have indeed found the transition state. The imaginary frequency is strongly dominated by the CH stretch. the frequencies of the TS and the DS for cobalt are somewhat lower than those of nickel, probably due to the somewhat larger MC distance, MH distance, CH distance, and θ at these geometries. Now, according to eqns. (2.3)-(2.4) rate constants can be evaluated. The results are shown in table 2.4 for CH_4 and CD_4 at different temperatures.

Table 2.4 Unimolecular ($k_{uni.\ eli.}$) (s^{-1}) and bimolecular ($k_{bi.\ ins.}$) (m^3 mol^{-1} s^{-1}) rate constants and their isotopic substitution ratios, classical sticking coefficients (S^{TST}), quantum sticking coefficients (S^{QM}) and ratio of quantum chemical rate to classical chemical rate (Γ^*) for different temperatures (T) (K) for Ni/CH_4, Ni/CD_4, Co/CH_4, and Co/CH_4.

System	T	$k_{bi.\ ins.}$	k^{CH_4}/k^{CD_4}	$k_{uni.\ eli.}$	k^{CH_4}/k^{CD_4}	S^{TST}	S^{QM}	Γ^*
Ni/CH_4	250	$2.14 \cdot 10^{+0}$		$6.55 \cdot 10^{-3}$		$1.40 \cdot 10^{-08}$	$2.89 \cdot 10^{-08}$	2.064
Ni/CD_4	250	$3.38 \cdot 10^{-1}$	6.33	$3.62 \cdot 10^{-3}$	1.81	$2.41 \cdot 10^{-09}$	$3.56 \cdot 10^{-09}$	1.478
Ni/CH_4	500	$1.09 \cdot 10^{+4}$		$2.67 \cdot 10^{+5}$		$5.04 \cdot 10^{-05}$	$6.00 \cdot 10^{-05}$	1.190
Ni/CD_4	500	$3.63 \cdot 10^{+3}$	3.00	$1.81 \cdot 10^{+5}$	1.48	$1.83 \cdot 10^{-05}$	$2.02 \cdot 10^{-05}$	1.102
Ni/CH_4	750	$2.20 \cdot 10^{+5}$		$9.55 \cdot 10^{+7}$		$8.29 \cdot 10^{-04}$	$8.97 \cdot 10^{-04}$	1.082
Ni/CD_4	750	$9.62 \cdot 10^{+4}$	2.29	$6.83 \cdot 10^{+7}$	1.40	$3.96 \cdot 10^{-04}$	$4.14 \cdot 10^{-04}$	1.045
Ni/CH_4	1000	$1.10 \cdot 10^{+6}$		$1.82 \cdot 10^{+9}$		$3.59 \cdot 10^{-03}$	$3.76 \cdot 10^{-03}$	1.047
Ni/CD_4	1000	$5.53 \cdot 10^{+5}$	1.99	$1.34 \cdot 10^{+9}$	1.36	$1.97 \cdot 10^{-03}$	$2.02 \cdot 10^{-03}$	1.026
Co/CH_4	250	$1.54 \cdot 10^{-6}$		$9.54 \cdot 10^{-3}$		$9.81 \cdot 10^{-15}$	$1.73 \cdot 10^{-14}$	1.761
Co/CD_4	250	$1.25 \cdot 10^{-7}$	12.32	$6.02 \cdot 10^{-3}$	1.58	$8.66 \cdot 10^{-16}$	$1.14 \cdot 10^{-15}$	1.311
Co/CH_4	500	$1.02 \cdot 10^{+1}$		$3.06 \cdot 10^{+5}$		$4.61 \cdot 10^{-08}$	$5.15 \cdot 10^{-08}$	1.117
Co/CD_4	500	$2.08 \cdot 10^{+0}$	4.90	$2.33 \cdot 10^{+5}$	1.31	$1.02 \cdot 10^{-08}$	$1.09 \cdot 10^{-08}$	1.070
Co/CH_4	750	$2.43 \cdot 10^{+3}$		$1.06 \cdot 10^{+8}$		$8.94 \cdot 10^{-06}$	$9.40 \cdot 10^{-06}$	1.051
Co/CD_4	750	$6.74 \cdot 10^{+2}$	3.61	$8.23 \cdot 10^{+7}$	1.30	$2.70 \cdot 10^{-06}$	$2.78 \cdot 10^{-06}$	1.031
Co/CH_4	1000	$4.21 \cdot 10^{+4}$		$2.01 \cdot 10^{+9}$		$1.34 \cdot 10^{-04}$	$1.38 \cdot 10^{-04}$	1.029
Co/CD_4	1000	$1.36 \cdot 10^{+4}$	3.09	$1.55 \cdot 10^{+9}$	1.30	$4.70 \cdot 10^{-05}$	$4.78 \cdot 10^{-05}$	1.018

Γ^* denotes the ratio of quantum chemical rate to classical chemical rate as calculated by transition state theory. In the quantum chemical rate we corrected for tunneling effects by assuming that our reaction coordinate can be described by a one dimensional unsymmetrical Eckart potential energy function[30]. For the boundaries of the Eckart function, we have taken the potential energy difference between the TS and the reactant and the TS and the DS, respectively, resulting in an upper bound for the tunneling correction. The justification for this one dimensional model is that analysis of our vibrational data shows that at the saddlepoint the reaction coordinate consists almost purely of the CH stretch.

We can see that at low temperatures ($T = 250$ K) tunneling has a pronounced effect on the reaction rate (a factor of 2.064 for Ni/CH₄ and a factor of 1.761 for Co/CH₄), and that tunneling is quite different for hydrogen and deuterium (a factor of 2.064 for Ni/CH₄ and a factor of 1.478 for Ni/CD₄). At high temperatures ($T = 1000$ K) classical rates and quantum chemical rates, which are simply obtained from table 2.4 by multiplication of $k_{uni.\ eli.}$ or $k_{bi.\ ins.}$ with Γ^*, are almost the same, as it should be.

Classical sticking coefficients (S^{TST}) are calculated in the following manner. First, we calculated the hard sphere pre-exponential (A^{HS}) by treating CH₄ and M as hard spheres[38].

$$A^{HS} = \pi\, d^2 \sqrt{\frac{8\, k_B\, T}{\pi\, \mu_{MCH_4}}} \tag{2.5}$$

In eq. (2.5) $\pi\, d^2$ represents the hard sphere collision cross section and $\sqrt{(8\, k_B\, T)/(\pi\, \mu_{MCH_4})}$ the mean speed according to the Maxwell distribution. d is given by the sum of the hard sphere radii of CH₄ and M, which are $1.91 \cdot 10^{-10}$ m for CH₄[39], $1.62 \cdot 10^{-10}$ m for Ni[40], and $1.67 \cdot 10^{-10}$ m for Co[40]. The sticking coefficient is now simply the ratio of $k_{bi.\ ins.}$ and A^{HS} and is therefore effectively the reaction probability per hard sphere collision. Analogous, the quantum chemical sticking coefficient (S^{QM}) can be calculated as the ratio of $k^{QM}_{bi.\ ins.}$ and A^{HS}. The KIE is almost negligible for the elimination reactions but pronounced for the insertion reactions. This is more clearly seen from fig. 2.4, which shows Arrhenius plots for Ni/CH₄/CD₄-, Co/CH₄/CD₄-, and Ni/Co/CH₄ insertion/elimination.

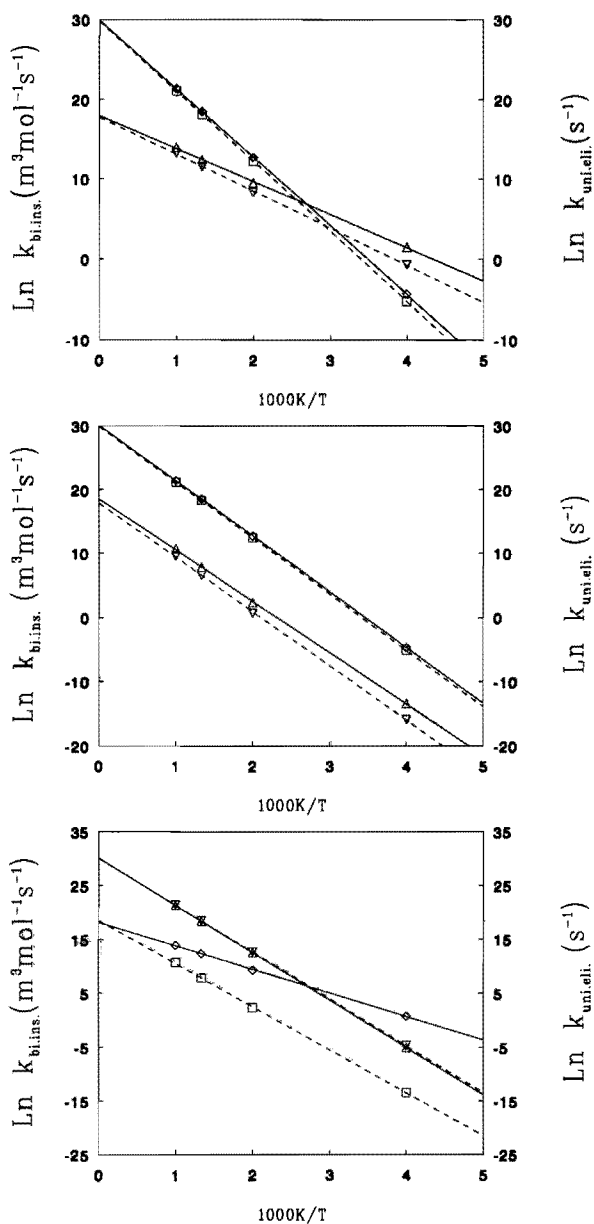**Fig. 2.4.**
Arrhenius plots for bimolecular insertion ($k_{bi.ins.}$) and unimolecular elimination ($k_{uni.eli.}$) of Ni/CH_4/CD_4 (top), Co/CH_4/CD_4 (middle), and Ni/Co/CH_4 (bottom). The following markers are used. $\triangle$: $k_{bi.ins.}$ Ni/Co/CH_4, $\triangledown$: $k_{bi.ins}$ Ni/Co/CD_4, $\diamond$: $k_{uni.eli.}$ Ni/Co/CH_4, $\square$: $k_{uni.eli.}$ Ni/Co/CD_4.

The plot data is summerised in table 2.5. The electronic energy, E, denotes the energy difference between the TS, the DS, and the reactant at the electronic potential energy surface (not including zero point energies). In the critical energy, E_{crit}, the differences in zero point energy for the TS, the DS and the reactant have been taken into account. The slope of the Arrhenius plots is reflected in the activation energy, E_{act}, and the intercept in the pre-exponential, A.

Table 2.5. Electronic energy (E) (kJ/mol), critical energy (E_{crit}) (kJ/mol), activation energy (E_{act}) (kJ/mol), and Arrhenius pre-exponential (A) for addition (m^3 mol^{-1} s^{-1}) and elimination (s^{-1}) for Ni/CH$_4$, Ni/CD$_4$, CoCH$_4$, and Co/CD$_4$.

System	Reaction	E	E_{crit}	E_{act}	A
Ni/CH$_4$	insertion	41	35	36	$7.62 \cdot 10^{+07}$
Ni/CD$_4$	insertion	41	38	39	$5.56 \cdot 10^{+07}$
Ni/CH$_4$	elimination	75	71	73	$1.16 \cdot 10^{+13}$
Ni/CD$_4$	elimination	75	72	74	$9.43 \cdot 10^{+12}$
Co/CH$_4$	insertion	79	64	66	$1.05 \cdot 10^{+08}$
Co/CD$_4$	insertion	79	67	70	$5.39 \cdot 10^{+07}$
Co/CH$_4$	elimination	73	70	72	$1.13 \cdot 10^{+13}$
Co/CD$_4$	elimination	73	71	73	$9.68 \cdot 10^{+12}$

We see that inclusion of zero point energies lowers the insertion barrier of Ni/CH$_4$ by 6 kJ/mol and of Co/CH$_4$ by 15 kJ/mol reflecting the relatively low frequencies at the TS and the high stretching mode frequency for CH$_4$. The effect of isotopic substitution is to lower vibrational frequencies for both the TS and the reactant. Therefore, the lowering effect on the insertion barrier is smaller (3 kJ/mol for Ni/CD$_4$, 12 kJ/mol for Co/CD$_4$). For the elimination barrier, we see the same trends but less pronounced, i.e. 4 kJ/mol for Ni/CH$_4$, 3 kJ/mol for Ni/CD$_4$, 3 kJ/mol for Co/CD$_4$, and 2 kJ/mol for Co/CD$_4$. The activation energy displays the effect on the barrier, when excited rotational and vibrational levels are populated: a temperature averaged barrier. The population of high vibrational frequency excited levels, e.g. CH stretch mode in the reactant or the MH stretch in the DS, will remain small at elevated temperatures, because of its high frequency and thereby associated high energy. On the contrary, the population of relatively low vibrational frequency excited levels, as those in the TS, will strongly increase, as is reflected in the vibrational partition functions and the barrier for insertion will thus increase (1–2 kJ/mol for Ni, 2–3 kJ/mol for Co). The absolute value of the temperature averaged barrier will depend on the values of the translational, vibrational and rotational partition functions at the TS, the DS and the reactant.

The pre-exponential factor on going from the DS to the TS is connected with the entropy of activation ($\Delta S^{\ddagger}$) according to:

$$A^{TST} = \frac{e\, k_B\, T}{h}\; e^{\frac{\Delta S^{\ddagger}}{k_B}} \tag{2.6}$$

and is therefore a measure for the gain or loss in entropy. At ordinary temperatures the pre-exponential in eq. (2.6) is approximately 10^{13}. The pre-exponentials for nickel and cobalt elimination are approximately 10^{13}, which indicates that $\Delta S^{\ddagger}$ is approximately zero. The entropy in the DS and the TS is therefore the same. In combination with the relatively low frequencies for both the TS and the DS (see table 2.3.), we conclude that both states are loosely bound. This can also be concluded by investigating the pre-exponential for the bimolecular insertion reaction. The pre-exponential factor on going from the reactant to the TS at ordinary temperatures for a volume of 1 m^3 is approximately 10^5 m^3 mol^{-1} s^{-1}, where we have accounted for the loss of the translational degrees of freedom by substituting for the translational partition function. Therefore, our values of 10^7–10^8 denote also a loose transition state.

Only experimental data on the bimolecular rate constant for the nickel cation insertion in CH$_4$ was found in the literature. Tonkyn *et al.*[41] found a rate constant of $7.0 \cdot 10^{-18}$ m^3 s^{-1} at $T = 300$ K. We find at $T = 300$ K a rate constant of approximately $3.47 \cdot 10^{-22}$ m^3 s^{-1}. Although this is much lower, a cation can be expected to be much more reactive. Beebe *et al.*[8] find activation energies of 53, 27 and 56 kJ/mol for the decomposition of CH$_4$ on Ni(111), Ni(100), and Ni(110) surfaces, respectively. For CD$_4$ these values are 53 kJ/mol for Ni(110) and 62 kJ/mol for Ni(100). Initial CH$_4$ sticking coefficients at $T = 500$ K are of the order 10^{-8} to 10^{-7}. Chorkendorff *et al.*[9], however, measured an activation energy of 52 kJ/mol on Ni(100). Our activation energies are much lower, probably because we have no steric repulsion between surface atoms and CH$_4$. Our single atom sticking coefficients at $T = 500$ K are higher (10^{-5}) than those found for a surface, but we see the same temperature behaviour; larger sticking coefficients for higher temperatures. We find at $T = 250$ K a ratio of the sticking coefficients of hydrogen to deuterium of 8.29, at $T = 500$ K a ratio of 3.04 and at $T = 750$ K a ratio of 2.22. This is not too far away from a Ni(111) surface sticking coefficient ratio of 8.0 in the temperature region between 640 K and 830 K as found by the molecular beam experiments of Lee *et al.*[10]. In general, the occurrence and absolute value of isotopic substitution, is very different for different surfaces. Therefore, the conclusion of Steward *et al.*[3] that transition state theory cannot account for the experimentally observed isotope effects seems premature.

2.5   Conclusions

We have carried out DFT calculations to determine the TS, the DS, height and origin of the barrier of reactions (2.1)–(2.2). In addition, we calculated rotational and vibrational frequencies and used transition state theory to calculate rate constants and sticking coefficients. We also made an estimate of hydrogen and deuterium tunneling effects, which turned out to be small. The barrier for insertion of a nickel atom turns out to be 41 kJ/mol, the barrier for cobalt insertion 79 kJ/mol. For nickel elimination we find a barrier of 75 kJ/mol and for cobalt elimination of 73 kJ/mol. The higher insertion barrier of cobalt and the almost equal barrier for elimination is due to the looser structure of the TS and the DS of cobalt. We have shown that the origin of the barrier is due to stretching of the CH bond.

The obtained barrier height of 41 kJ/mol for the insertion is low compared with experimental results for Ni(100), Ni(110) and Ni(111) surfaces, but we expect better agreement with experiment when clusters are used to model the surface. Steric repulsion due to the neighbouring surface atoms can then be taken into account. Also, a higher coordination number of the central nickel atom will tend to decrease its reactivity. Preliminary results on a one layer 7 atom cluster also showed up a more extended CH bond of 1.63 Å in the transition state, which also will result in a higher barrier.

This would be in contrast with Swang *et al.*[42] who computed a barrier for CH₄ dissociation on a Ni(100) surface, modelled by a two layer 13 atom cluster, of 37 kJ/mol and estimated the barrier to be 62-71 kJ/mol. Their calculated CH bond length was 1.51 Å. They calculated a barrier for CH₄ dissociation of 75 kJ/mol for a single nickel atom[36], corresponding with a CH bond length of 1.62 Å. Therefore, they found a lowering of their calculated barrier of 38 kJ/mol with respect to one nickel atom, which can thus partly be understood in terms of a less extension of the activated CH bond.

Calculated frequencies and rate coefficients could only partially be compared with experimental data. Frequencies for CH₄ are too high, because normal modes were not calculated; the frequency shift for CD₄ seems correct. No experimental rate constant for the insertion of a nickel atom was available, but the rate constant for insertion of the cation can be treated as un upper limit. Our one atom sticking coefficients are low as are experimental ones. Calculated pre-exponentials were connected with change in entropy for insertion and dissociation. They indicate a loose transition state.

2.6 References

1. J.R. Rostrup-Nielsen, *Catalysis- science and technology, Vol. 5*,
   edited by J.R. Anderson and M. Boudart (Springer-Verlag, Berlin, 1984).
2. H.F. Winters, J. Chem. Phys. **62** (1975) 2454.
   H.F. Winters, J. Chem. Phys. **64** (1976) 3495.
3. C.N. Stewart, G. Ehrlich, J. Chem. Phys. **62** (1975) 4672.
4. S.G. Brass, D.A. Reed, G. Ehrlich, J. Chem. Phys. **70** (1979) 5244.
   J.T. Yates, J.J. Zinck, S. Sheard, W.H. Weinberg, J. Chem. Phys. **70** (1979) 2266.
5. C.T. Rettner, H.E. Pfnür, D.J. Auerbach, J. Chem. Phys. **84** (1986) 4163.
6. S.G. Brass, G. Ehrlich, Surf. Sci. **187** (1987) 21.
   S.G. Brass, G. Ehrlich, J. Chem. Phys. **87** (1987) 4285.
7. S.G. Brass, G. Ehrlich, Phys. Rev. Lett. **57** (1986) 2532.
8. T.P. Beebe, D.W. Goodman, B.D. Kay, J.T. Yates,
   J. Chem. Phys. **87** (1987) 2305.
9. I. Chorkendorff, I. Alstrup, S. Ulmann, Surf. Sci. **227** (1990) 291.
10. M.B. Lee, Q.Y. Yang, S.L. Tang, S.T. Ceyer, J. Chem. Phys. **85** (1986) 1693.
    M.B. Lee, Q.Y. Yang, S.T. Ceyer, J. Chem. Phys. **87** (1987) 2724.
    S.T. Ceyer, J.D. Beckerle, M.B. Lee, S.L. Tang, Q.Y. Yang, M.A. Hines,
    J. Vac. Sci. Tech. A **5** (1987) 501.
11. A.V. Hamza, R.J. Madix, Surf. Sci. **179** (1987) 25.
12. T.C. Lo, G. Ehrlich, Surf. Sci. **179** (1987) L19.
    T.C. Lo, G. Ehrlich, Surf. Sci. **198** (1988) L380.
    T.C. Lo, G. Ehrlich, Surf. Sci. **205** (1988) L813.
13. B.D. Kay, M.E. Coltrin, Surf. Sci. **198** (1988) L375.
    B.D. Kay, M.E. Coltrin, Surf. Sci. **205** (1988) L805.
14. C.T. Rettner, H.E. Pfnür, D.J. Auerbach, Phys. Rev. Lett. **54** (1985) 2716.
15. S.T. Ceyer, Science **249** (1990) 133.
    J.D. Beckerle, A.D. Johnson, Q.Y. Yang, S.T. Ceyer,
    J. Chem. Phys. **91** (1989) 5756.
    J.D. Beckerle, Q.Y. Yang, A.D. Johnson, S.T. Ceyer,
    J. Chem. Phys. **86** (1987) 7236.
16. A.C. Luntz, D.S. Bethune, J. Chem. Phys. **90** (1989) 1274.
17. G.R. Schoofs, C.R. Arumainayagam, M.C. McMaster, R.J. Madix,
    Surf. Sci. **215** (1989) 1.

18. A.C. Luntz, J. Harris, Surf. Sci. **258** (1991) 397.
    A.C. Luntz, J. Harris, J. Vac. Sci. Tech. A **10** (1992) 2292.
    A.C. Luntz, J. Harris, J. Chem. Phys. **96** (1992) 7054.

19. Amsterdam density functional (ADF) programme developed by Baerends *et al.*.
    E.J. Baerends, D.E. Ellis, P. Ros, Chem. Phys. **2** (1973) 41.
    P.M. Boerrigter, G. te Velde, E.J. Baerends, Int. J. Quantum Chem. **33** (1988) 87.
    G. te Velde, E.J. Baerends, J. Comput. Phys. **99** (1992) 84.
    D. Post, E.J. Baerends, J. Chem. Phys. **78** (1983) 5663.
    E.J. Baerends, A. Rozendaal, *Quantum chemistry: the challenge of transition metals and coordination chemistry*, edited by A. Veillard (Reidel, Dordrecht, 1986), p. 159.
    P.J. van den Hoek, A.W. Kleyn, E.J. Baerends,
    Comm. Atom. Molec. Phys. **23** (1989) 93.

20. D.M. Ceperley, B.J. Alder, Phys. Rev. Lett. **45** (1980) 566.

21. S.H. Vosko, L. Wilk, M. Nusair, Can. J. Phys. **58** (1980) 1200.
    J.P. Perdew, A. Zunger, Phys. Rev. B **23** (1981) 5048.

22. A.D. Becke, Int. J. Quantum Chem. **27** (1985) 585.

23. A.D. Becke, Phys. Rev. A **38** (1988) 3098.

24. H. Stoll, C.M.E. Pavlidou, H. Preuss, Theor. Chim. Acta **49** (1978) 143.
    H. Stoll, E. Golka, H. Preuss, Theor. Chim. Acta **55** (1980) 29.

25. G. te Velde, E.J. Baerends, J. Comput. Phys. **99** (1992) 84.

26. T. Ziegler, A. Rauk, Theor. Chim. Acta **46** (1977) 1.

27. J.G. Snijders, E.J. Baerends, Mol. Phys. **36** (1978) 1789.
    J.G. Snijders, E.J. Baerends, P. Ros, Mol. Phys. **38** (1979) 1909.

28. E.B. Wilson, J.C. Decius, P.C. Cross, *Molecular vibrations. Theory of infrared and raman vibrational spectra* (McGraw-Hill, New York, 1955).

29. R.G. Gilbert, S.C. Smith, *Theory of unimolecular and recombination reactions* (Blackwell, Oxford, 1990).

30. H.S. Johnston, J.Heicklen, J. Phys. Chem. **66** (1962) 532.
    H.S. Johnston, D. Rapp, J. Am. Chem. Soc. **83** (1961) 1.

31. C.W. Bauschlicher, P.E.M. Siegbahn, L.G.M. Petterson,
    Theor. Chim. Acta **74** (1988) 479.
    P.E.M. Siegbahn, M.R.A. Blomberg, C.W. Bauschlicher,
    J.Chem. Phys. **81** (1984) 1373.

32. K. Andersson, B.O. Roos, Chem. Phys. Lett. **191** (1992) 507.

33. C.E. Moore, *Atomic energy levels*
    (National Bureau of Standards, Washington D.C., 1952).

34. M.R. Blomberg, P.E.M. Siegbahn, M. Svensson, J. Phys. Chem. **95** (1991) 4313.

35. M.R. Blomberg, P.E.M. Siegbahn, J. Chem. Phys. **78** (1983) 5682.
    M.R. Blomberg, P.E.M. Siegbahn, J. Chem. Phys. **78** (1983) 986.
    M.R. Blomberg, U. Brandemark, L. Petterson, P.E.M. Siegbahn,
    Int. J. Quantum Chem. **23** (1983) 855.

36. M.R. Blomberg, U. Brandemark, P.E.M. Siegbahn,
    J. Am. Chem. Soc. **105** (1983) 5557.
    M.R. Blomberg, P.E.M. Siegbahn, U. Nagashima, J. Wennerberg,
    J. Am. Chem. Soc. **113** (1991) 424.

37. G. Herzberg, *Electronic spectra of polyatomic molecules*
    (Van Nostrand, New York, 1966).

38. P.W. Atkins, *Physical Chemistry* (Oxford University Press, Oxford, 1978).

39. G.W.C. Kaye, T.H. Laby, *Tables of physical and chemical constants*
    (Longmans, London, 1957).

40. C.F. Fischer, *The Hartree Fock method for atoms* (Wiley, New York, 1954).

41. R. Tonkyn, M. Ronan, J.C. Weisshaar, J. Phys. Chem. **92** (1988) 92.

42. O. Swang, K. Faegri Jr, O. Gropen, U. Wahlgren, P.E.M. Siegbahn,
    Chem. Phys. **156** (1991) 379.

Chapter 3

Methane activation and dehydrogenation on nickel and cobalt. A computational study

abstract

We have studied the adsorption of CH_3 and H on nickel clusters of various size and -shape. As a next step we have chosen a one layer 7-atom cluster and a spherical 13-atom cluster to model the nickel- and cobalt surface and we have studied the adsorption of CH_3, CH_2, CH, C, and H on these clusters. Starting from gas phase CH_4, the formation of adsorbed CH_3 (CH_{3a}) and adsorbed H (H_a) is endothermic on all clusters, but the endothermicity is strongly reduced on the 13-atom clusters (142 kJ/mol on Ni_7, 135 kJ/mol on Co_7, 30 kJ/mol on Ni_{13}, and 8 kJ/mol on Co_{13}). The formation of adsorbed CH_2 (CH_{2a}) and H_a from CH_{3a} is endothermic by 25–40 kJ/mol on all clusters, except on Co_7 (3 kJ/mol exothermic), mainly because of the much stronger adsorption of CH_2 on this cluster. The formation of adsorbed CH (CH_a) and H_a from CH_{2a} is exothermic on all clusters, but the exothermicity differs a factor two between the 7- and 13-atom clusters (61 kJ/mol on Ni_7, 60 kJ/mol on Co_7, 27 kJ/mol on Ni_{13}, and 32 kJ/mol on Co_{13}). Finally, the formation of adsorbed C (C_a) and H_a from CH_a is strongly endothermic on the 7-atom clusters, but the endothermicity is again strongly reduced on the 13-atom clusters (92 kJ/mol on Ni_7, 77 kJ/mol on Co_7, 27 kJ/mol on Ni_{13}, and 14 kJ/mol on Co_{13}).

3.1 Introduction

One of the most important catalytic reactions on surfaces is the reforming of CH_4 producing higher hydrocarbons. Various carbonacious species have been proposed to be intermediates during this reaction, but the exact nature of these intermediates is still under discussion. The group of Ceyer[1] reported the existence of CH_3 and CH on a Ni(111) surface using HREELS. Kaminsky *et al.*[2] observed all CH_x fragments on Ni(111) using SIMS, and according to them the stability of carbon, methylidyne, methylene, and methyl is similar. In this study we will discuss the energetics, adsorbate-substrate distance, and -frequency of all possible single carbon CH_x-species and H on cobalt and nickel, which have been modelled by various cluster models. First, we will investigate the advantages and disadvantages of the different cluster models by means of the chemisorption behaviour of CH_3 and H, followed by the study of methane dissociation and subsequent dehydrogenation of the CH_x-species on our best cluster models, which are a one layer 7-atom cluster and a spherical 13-atom cluster. Thus, we have studied the following reactions on nickel and cobalt clusters.

$$CH_4 + M_x \rightleftharpoons CH_{3a} + H_a \tag{3.1}$$

$$CH_{3a} \rightleftharpoons CH_{2a} + H_a \tag{3.2}$$

$$CH_{2a} \rightleftharpoons CH_a + H_a \tag{3.3}$$

$$CH_a \rightleftharpoons C_a + H_a \tag{3.4}$$

For reaction (3.1) M = Ni or Co, and x = 7 or 13.

Details of the calculations are discussed in section 3.2. In section 3.3.1 we present and discuss CH_3- and H adsorption on various nickel clusters. In section 3.3.2 we discuss the chemisorption of the other CH_x-species on Ni_7 and Ni_{13}. In section 3.3.3 the chemisorption of H and all CH_x-species on Co_7 and Co_{13} is discussed. In section 3.4 we summerise results and draw some conclusions.

3.2 Methods

We have carried out quasi-relativistic calculations based on density functional theory (DFT) using the Amsterdam Density Functional programme package (ADF) developed by Baerends *et al.*[3]. The exchange-correlation potential used is based on quantum Monte Carlo simulations of Ceperley and Alder[4] of a homogeneous electron gas which are parametrised by Vosko, Wilk and Nusair[5]. To correct for the overbinding inherent to the local density approximation (LDA)[6], we haved used a gradient corrected exchange energy functional[7] in combination with the Stoll correction[8] for correlation. For carbon a frozen core potential is used for the 1s electrons; for nickel and cobalt the electrons up to 3p are frozen. Relativistic effects were taken into account by first order perturbation theory[9]. S- and p-orbitals are of double ζ quality, d orbitals of triple ζ quality. On all atoms polarisation functions are included. Rösch *et al.*[10] and Kühnholz *et al.*[11] have shown that clusters can model substrate surfaces and the bulk metal within DFT. Therefore, we have used Ni, Ni_7-, $Ni_{7,3}$-, $Ni_{7,3,3}$-, and Ni_{13}-clusters as substrate models for nickel. This last cluster does not model a specific crystal plane, but consists of a central nickel atom surrounded by 12 atoms in a hexagonal-closed-packed fashion for reasons of symmetry. In this cluster, all surface nickel atoms form bonds with five other nickel atoms and there are no low coordinated boundary atoms, eliminating possible boundary effects. For all nickel clusters the bond distance was fixed at the bulk value of 2.49 Å. The various substrate models are shown in fig. 3.1. For cobalt we modelled the substrate using the one layer 7-atom cluster and the 13-atom cluster described above. The cobalt bond distance was fixed at 2.50 Å, which is the bulk value.

Adsorption energies are calculated using Ziegler's transition state method[12] and are given relative to the gas phase fragments with the same geometry. These are the following. For all CH_x-species we kept the CH distances at 1.08 Å. For CH_3 the HCH angles are 109.48° as are the substrate-CH angles. For CH_2 the HCH angle is 109.48° and the substrate-CH angles are 125.26°. For CH the substrate-CH angles are 180°. The electronic states with respect to which the adsorption energies of the species are given are for C the ^3P -state, for CH the $^2\Pi$ state, for CH_2 the $^1A_1$ -state and for CH_3 the $^2A_1$ -state. We have also evaluated the energy difference between CH_2 ($^1A_1$) and CH_2 ($^3\Sigma_g$), and between CH_3 ($^2A_1$) and CH_3 ($^2A_2''$), which are the experimental ground states.
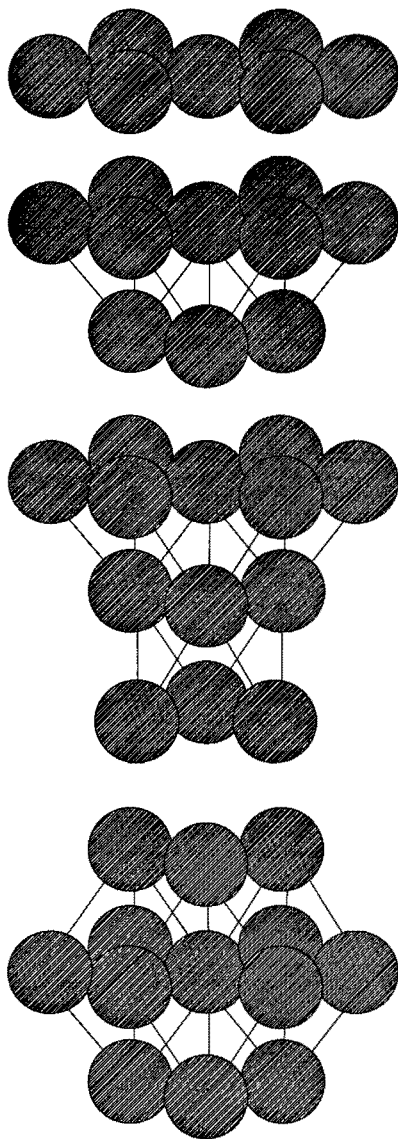
Fig. 3.1.
Different clusters modelling the substrate: M_7-cluster, $M_{7,3}$-cluster, $M_{7,3,3}$-cluster, M_{13}-cluster.
For all clusters the bond distance of the bulk was used, i.e. 2.49 Å for Ni, 2.50 Å for Co.

3.3 Results and Discussion

3.3.1 CH$_3$ and H adsorption on nickel clusters

To find a suitable model for the substrate, we have studied the chemisorption of CH$_3$ and H on various nickel clusters. The results are shown in table 3.1. CH$_3$ clearly prefers

Table 3.1. CH$_3$- and H chemisorption data on various nickel clusters. z denotes the adsorbate-substrate distance, E_{ads} the adsorption energy, and ν the adsorbate-substrate stretch frequency.

adsorbate	substrate	site	$z(\text{Å})$	E_{ads} (kJ/mol)	ν (cm^{-1})
CH$_3$[a]	Ni	1-fold	1.97	296	447
CH$_3$	Ni$_7$	1-fold	2.06	97	387
CH$_3$	Ni$_7$	2-fold	1.92	61	245
CH$_3$	Ni$_7$	3-fold	1.96	64	307
CH$_3$	Ni$_{7,3}$	1-fold	2.02	113	231
CH$_3$	Ni$_{7,3}$	2-fold	2.03	86	308
CH$_3$	Ni$_{7,3}$	3-fold	2.06	76	310
CH$_3$	Ni$_{7,3,3}$	1-fold	2.09	109	324
CH$_3$	Ni$_{7,3,3}$	2-fold	1.98	94	491
CH$_3$	Ni$_{7,3,3}$	3-fold	1.88	83	550
CH$_3$	Ni$_{13}$	1-fold	1.99	179	465
CH$_3$	Ni$_{13}$	2-fold	1.87	152	292
CH$_3$	Ni$_{13}$	3-fold	1.90	143	271
H	Ni	1-fold	1.50	304	1976
H	Ni$_7$	1-fold	1.48	203	1913
H	Ni$_7$	2-fold	1.04	229	1472
H	Ni$_7$	3-fold	0.90	241	1014
H	Ni$_{7,3}$	1-fold	1.53	224	1951
H	Ni$_{7,3}$	2-fold	1.10	218	1670
H	Ni$_{7,3}$	3-fold	0.95	253	1724
H	Ni$_{7,3,3}$	1-fold	1.48	212	1703
H	Ni$_{7,3,3}$	2-fold	1.12	231	1774
H	Ni$_{7,3,3}$	3-fold	0.87	242	2118
H	Ni$_{13}$	1-fold	1.51	235	1764
H	Ni$_{13}$	2-fold	1.13	253	1119
H	Ni$_{13}$	3-fold	1.14	272	1284

[a] All CH$_3$ adsorption energies drop 34 kJ/mol if we allow for relaxation to adopt the preferred planar (^{2}A$_2''$) configuration.

the 1-fold site on Ni$_7$, followed by the 3-fold site and the 2-fold site. The adsorption energies

of respectively 97 kJ/mol, 64 kJ/mol and 61 kJ/mol are far lower than values calculated by others. If we allow for relaxation of CH_3 in the gas phase to adopt the preferred planar geometry, all adsorption energies decrease by 34 kJ/mol. Extending our cluster model by adding a second layer of 3 atoms enlarges the adsorption energy with 12–25 kJ/mol. Adding another third layer of 3 atoms enlarges the energy with 12–33 kJ/mol w.r.t. to Ni_7-cluster. Comparing the $Ni_{7,3}$- and $Ni_{7,3,3}$-clusters, the 2-fold and 3-fold positions are favoured another 8 kJ/mol, but the 1-fold site shifts 4 kJ/mol downwards. This is an example of the oscillation of adsorption energy with cluster size and/or -shape, although the effect is relatively small. Using the Ni_{13}-cluster, the adsorption energy increases significantly for all sites with an approximately equal amount (79–91 kJ/mol) w.r.t. the Ni_7-cluster, resulting in energies of 179 kJ/mol for the 1-fold site, 152 kJ/mol for the 2-fold site, and 143 kJ/mol for the 3-fold site. Resuming the site preference, on all clusters the 1-fold position is clearly preferred, followed by the 2-fold and 3-fold position, whose adsorption energy is closer to each other than to the 1-fold chemisorption energy. The only exception is the Ni_7-cluster where the 2- and 3-fold site have almost the same energy with a slight preference for the 3-fold site. For the most preferred site on Ni_7, the 1-fold site, we have also optimised the adsorption energy as a function of CH bond distance, adsorbate-substrate distance and HCH-angle simultaneously. It turned out that in the optimal geometry the CH bonds had increased (from 1.08 Å to 1.11 Å), the adsorbate-substrate distance shortened (from 2.06 Å to 1.95 Å), and the substrate-CH angles increased (from 109.48° to 112.15°). However, the adsorption energy w.r.t. to CH_3 fragment in the same geometry in the gas phase increases only marginal with 3 kJ/mol. We therefore conclude that relaxation of the adsorbate affects the adsorption energy very little.

The ability to move along the surface (mobility) is in our model inversely proportional to the difference in adsorption energy between the most preferred site and the next-most preferred site. The energy difference between the sites can be interpreted as the barrier which has to be overcome to move along the surface, where we have implicitly assumed that there is no intermediate geometry with a worse adsorption energy than the next-most preferred site. Therefore, the higher this barrier the lower the mobility. This mobility barrier is 33 kJ/mol for the Ni_7-cluster, 27 kJ/mol for the $Ni_{7,3}$-cluster, 15 kJ/mol for the $Ni_{7,3,3}$-cluster, and 27 kJ/mol for the Ni_{13}-cluster, indicating that CH_3 is quite mobile on all these clusters. Adsorbate-substrate distances range between 1.99–2.10 Å for the 1-fold sites, 1.87–2.03 Å for the 2-fold sites, and 1.87–2.06 Å for the 3-fold sites. The adsorbate-substrate stretch frequency varies strongly among the sites and among the clusters on first sight, but on closer inspection the 1-fold site frequency has a much lower value than the 2-fold site- and 3-fold site frequency on the $Ni_{7,3}$- and $Ni_{7,3,3}$-clusters. We attribute this

effect to the oscillation of frequencies on cluster size and/or shape equivalently to the well known oscillation of adsorption energy on cluster size and/or shape. On the Ni_7- and Ni_{13}-clusters, this trend is just the opposite and more in line with our expectation.

Siegbahn *et al.*[13] performed MRCCI calculations and used so-called bond prepared clusters. For CH_3 adsorption on $Ni(111)$ modelled by a Ni_3-cluster, a value of 174 kJ/mol was calculated. Using the same cluster with the more extended basis and more reference states, they found a value of 205 kJ/mol for the high coordinated positions. In a previous study[14] on $Ni(111)$ now modelled by a $Ni_{3,1}$-, $Ni_{3,7,7,3}$-, and a $Ni_{12,7,3}$-cluster, they concluded on the basis of energies and frequencies that CH_3 adsorbs at a 3-fold site. They calculated the adsorption energy for this site in the range 188–209 kJ/mol and estimated it to be in the range 209–230 kJ/mol. For the 1-fold site modelled by a single atom and a $Ni_{7,3}$-cluster, their estimate was 180–201 kJ/mol.

Yang and Whitten[15] performed *ab initio* valence orbital CI calculations and used an embedded cluster modelling a $Ni(111)$ surface. They calculated for the 1-fold position of CH_3 an adsorption energy of 142 kJ/mol, a surface-CH_3 distance of 2.03 Å, and a surface-CH_3 stretch frequency of 416 cm^{-1}. For the 2-fold position, they found an energy of 149 kJ/mol, a surface-CH_3 distance of 1.98 Å, and a surface-CH_3 frequency of 296 cm^{-1}. Finally, for the 3-fold position an adsorption energy of 162 kJ/mol, a surface-CH_3 distance of 1.83 Å, and a surface-CH_3 frequency of 369 cm^{-1} was calculated.

The only experimental data on CH_3 adsorption on $Ni(111)$ is the surface-CH_3 stretch frequency, which is 370 cm^{-1}[1]. On the basis of this frequency our best model for a $Ni(111)$ surface, which is the $Ni_{7,3,3}$-cluster, suggests adsorption at the 1-fold site, as does the Ni_7-cluster. Therefore, both frequency and adsorption energy point to adsorption at the 1-fold site. Also on the Ni_{13}-cluster the 1-fold position is clearly preferred. It is clear that our results differ significantly from those of Siegbahn and Yang and Whitten. They agree on the preferred adsorption site, which is according to them 3-fold, but their computation of the adsorption energy differs 47-68 kJ/mol, if we use Siegbahn's best estimate. Although Siegbahn used bond prepared clusters the adsorption energy still varies significantly between the different clusters. Furthermore, Schüle *et al.*[14] expect the 1-fold vibrational frequency to be around 600 cm^{-1} based on their single atom model, whereas Yang and Whitten give for this frequency a value of 416 cm^{-1}. If we compare our single atom data with our 1-fold Ni_7-cluster (table 3.1.), it shows that in the single atom case the adsorption energy and vibrational frequency are much higher, suggesting that it is not straightforward to compare a single nickel atom with a $Ni(111)$ surface. On our Ni_7 cluster we calculate the highest stretch frequency for the 1-fold position, followed by the 3-fold and 2-fold site. Yang and Whitten find the same order, but all their frequencies are 30–60 cm^{-1} higher.

If we compare the experimental surface-CH_3 stretch frequency with our computed results, the 1-fold site on the Ni_7-cluster seems the best model for CH_3 adsorption. Adsorption at the various sites on $Ni_{7,3}$- and $Ni_{7,3,3}$-clusters results in more or less the same adsorption energy, but the adsorbate-substrate stretch frequencies at the 1-fold site are significantly below those on the 2-fold and 3-fold sites, which runs contrary to chemical intuition and is also in disagreement with the computed frequencies of Yang and Whitten. Their adsorbate-substrate stretch frequencies are always highest on 1-fold sites. The Ni_7-, $Ni_{7,3}$-, and $Ni_{7,3,3}$-cluster models have all as their main disadvantage a strongly endothermic dissociation of CH_4 (reaction 3.1), whereas it should be more or less thermoneutral. This is remedied by choosing the Ni_{13}-cluster as our substrate model. In this model, all twelve surface atoms are equally unsaturated with bonds, i.e. five bonds instead of the bulk value of twelve, and therefore it forms a relatively strong bond with any adsorbate. In this cluster boundary effects can not occur, contrary to all other substrate models.

For H adsorption on Ni_7-cluster, we calculated a preference for the 3-fold site, with a surface-H distance of 0.90 Å, an adsorption energy of 241 kJ/mol and a surface-H frequency of 1014 cm^{-1}. Adding a second layer affects the adsorption sites very differently, destabilising the 2-fold site by 10 kJ/mol and stabilising the 1-fold site by 22 kJ/mol. For the $Ni_{7,3,3}$-cluster the adsorption energies resemble strongly those on the Ni_7 cluster. The largest difference is for the 1-fold site which is stabilised now by 10 kJ/mol. For the Ni_{13}-cluster the adsorption energies are shifted more or less the same by 24–32 kJ/mol, resulting in a favoured 3-fold site with adsorption energy of 272 kJ/mol. The barrier to move along the surface is 13 kJ/mol on the Ni_7 cluster, 29 kJ/mol on the $Ni_{7,3}$-cluster, 11 kJ/mol on the $Ni_{7,3,3}$-cluster, and 19 kJ/mol on the Ni_{13}-cluster. Again the stretch frequencies vary strongly between the different cluster models, but the value for the 3-fold site on the Ni_7-cluster is quite close to the experimental value. The 3-fold site frequencies on the $Ni_{7,3}$- and $Ni_{7,3,3}$-clusters seem too high, and in the case of the $Ni_{7,3,3}$-cluster it is again higher than the 1-fold site frequency. Panas *et al.*[16] studied high coordinated adsorption of hydrogen using many clusters modelling Ni(111) surfaces. Averaging over the different cluster models, they found a value of 258 kJ/mol for clusters modelling the Ni(111) surface. No data on frequencies or adsorbate-substrate distances was given. Yang and Whitten[13] found for hydrogen a preference for the 3-fold site, with an adsorption energy of 259 kJ/mol, a surface-H distance of 1.16 Å, and a surface-H frequency of 1043 cm^{-1}, which is in good agreement with our results on Ni_7. For the 2-fold site they found an adsorption energy of 248 kJ/mol, a surface-H distance of 1.31 Å and a surface-H frequency of 1183 cm^{-1}. For the 1-fold site they computed an adsorption energy of 187 kJ/mol, a surface-H distance of 1.61 Å and a surface-H frequency of 2332 cm^{-1}. Except for the

1-fold adsorption energy, this is also in good agreement with our results quantitatively. For hydrogen adsorption on Ni(111) more experimental data is available. The experimental site preference for H is 3-fold with a surface-H distance of 1.15 Å[17], an adsorption energy of 261 kJ/mol[18], and a surface-H frequency of 1120 cm^{-1}[19].

We conclude that there is good agreement between our results and those of Siegbahn *et al.* and Yang and Whitten with respect to hydrogen adsorption. All groups produce adsorption energies, surface-H distances and surface-H frequencies, which compare well with the available experimental data. On the other hand, the computed CH$_3$ chemisorption data differ significantly between the groups, while experimental data is scarce. A possible origin of these differences is the treatment of the nickel d-orbitals. Yang and Whitten include for their local surface region of four nickel atoms the valence d-orbitals. All other nickel atoms are described by an effective core potential (ECP). Also, the inclusion of two more nickel atoms in the second layer of their cluster favours now hydrogen adsorption at the hollow (fcc) site by 2 kJ/mol, whereas without these two nickel atoms the filled (hcp) site is favoured by 15 kJ/mol[20], indicating the susceptibility of their cluster choice. Siegbahn *et al.* described all nickel atoms modelling hollow (3-fold) sites by ECP's. For on top bonding, the directly bonding metal atom was described at the all electron level. In all cases effects of 3d-correlation have not been included. In the case of oxygen adsorbed in the fourfold hollow site of Cu(100), this correlation effect turned out to be 55 kJ/mol[21]. Rösch *et al.*[10] have shown in a DFT study on small to medium sized clusters that the 3d manifold is narrow and the bonding in the cluster largely due to 4s-4p type electrons. Therefore the highly localised 3d-orbitals are not expected to contribute directly to the bonding in the clusters and other groups[22] suggested that they thus could be described by ECP's. However, it is known that 3d-orbitals are directly involved in a large number of chemisorption bonds and they at least provide an efficient way to rehybridise and to reduce the Pauli repulsion with the adsorbed molecule, which is important in the formation of a chemical bond. Our method of explicitly treating the valence d-orbitals on all nickel atoms seems in this light a more reliable method. More experimental or computational data based on different methodologies is therefore very interesting and necessary to draw more conclusions on CH$_3$ adsorption. Both Ni$_7$ and Ni$_{13}$ seem appropriate models. Especially the 3-fold adsorbate-substrate stretch frequency on the Ni$_{7,3}$- and Ni$_{7,3,3}$-clusters are too high. On the basis of both CH$_3$- and H adsorption on the various cluster models, the Ni$_7$- and Ni$_{13}$-clusters seem the most suitable substrate models.

3.3.2   CH$_2$, CH, and C adsorption on nickel clusters

To study the decomposition of CH$_{3a}$ to CH$_{2a}$, CH$_a$ and eventually C$_a$ on nickel and cobalt, we have used the 7-atom cluster and the 13-atom cluster. In this section we will discuss the results for nickel, which are displayed in table 3.2 and fig. 3.2. For completeness, we have also added the CH$_3$ and H chemisorption data on these clusters. CH$_2$ prefers the 3-fold site on both clusters with a chemisorption energy of 312 kJ/mol on Ni$_7$ and 378 kJ/mol on Ni$_{13}$. To allow for CH$_2$ relaxation in the gas phase, we have to shift the adsorption energies of CH$_2$ with 25 kJ/mol downward. This is the energy difference between CH$_2$ (^{1}A$_1$), which is the reference in our tables, and CH$_2$ ($^3\Sigma_g$), which is the experimental ground state. The barrier to move along the surface, again computed as the difference in chemisorption energy between most preferred site and next-most preferred site, is 49 kJ/mol on Ni$_7$ and 77 kJ/mol on Ni$_{13}$. CH prefers the 3-fold site on both clusters, but the chemisorption energy of 536 kJ/mol on Ni$_7$ and 537 kJ/mol on Ni$_{13}$ are almost the same. The barrier to move along the surface is now 48 kJ/mol on Ni$_7$ and 100 kJ/mol on Ni$_{13}$. C also prefers the 3-fold site on both clusters, with chemisorption energies of 559 kJ/mol on Ni$_7$ and 595 kJ/mol on Ni$_{13}$. The mobility barriers are now 54 kJ/mol on Ni$_7$ and 119 kJ/mol on Ni$_{13}$. We thus find the following order in mobility for both nickel clusters:

mobility(H) > mobility(CH$_3$) > mobility(CH$_2$) > mobility(CH) > mobility(C),

indicating that H is a very mobile adsorbate whereas C is very immobile. Siegbahn *et al.*[13] computed for CH$_2$ adsorption on Ni(111) modelled by a Ni$_3$ cluster, an adsorption energy of 324 kJ/mol and estimated it to be 368 kJ/mol. For CH they computed a value of 452 kJ/mol and estimated it to be 502 kJ/mol. They gave no results for C adsorption. Yang and Whitten[15] found for CH$_2$ a preference for the 3-fold site with an adsorption energy of 281 kJ/mol, and an adsorbate-substrate frequency of 430 cm^{-1}. For the 2-fold site, they computed an adsorption energy of 262 kJ/mol and an adsorbate-substrate frequency of 444 cm^{-1}. Finally, for the 1-fold site they found an adsorption energy of 152 kJ/mol and an adsorbate-substrate frequency of 501 cm^{-1}. Except for the 1-fold adsorption energy, which is significantly larger in our case, this is all in good agreement with our data on Ni$_7$. For CH adsorption they also found a preference for the 3-fold site with an adsorption energy of 302 kJ/mol and an adsorbate-substrate frequency of 556 cm^{-1}. For the 2-fold site they found an adsorption energy of 280 kJ/mol and an adsorbate-substrate frequency of 447 cm^{-1}. Finally for the 1-fold site they found an adsorption energy of 163 kJ/mol and an adsorbate-substrate frequency of 600 cm^{-1}. It is clear from table 3.2 that our adsorption energies on the 2-fold site and 3-fold site are very much higher as are our adsorbate-substrate stretch frequencies. For the 1-fold site the differences are smaller, but still fairly large.

Table 3.2. CH$_3$-, CH$_2$-, CH-, C-, and H chemisorption data on Ni$_7$, and Ni$_{13}$-clusters. z denotes the adsorbate-substrate distance, E_{ads} the adsorption energy, and ν denotes the adsorbate-substrate stretch frequency.

adsorbate	substrate	site	z(Å)	E_{ads} (kJ/mol)	ν (cm^{-1})
CH$_3$[a]	Ni$_7$	1-fold	2.06	97	387
CH$_3$	Ni$_7$	2-fold	1.92	61	245
CH$_3$	Ni$_7$	3-fold	1.96	64	307
CH$_3$	Ni$_{13}$	1-fold	1.99	179	465
CH$_3$	Ni$_{13}$	2-fold	1.87	152	292
CH$_3$	Ni$_{13}$	3-fold	1.90	143	271
CH$_2$[b]	Ni$_7$	1-fold	1.81	225	535
CH$_2$	Ni$_7$	2-fold	1.60	263	439
CH$_2$	Ni$_7$	3-fold	1.44	312	496
CH$_2$	Ni$_{13}$	1-fold	1.81	301	565
CH$_2$	Ni$_{13}$	2-fold	1.49	285	464
CH$_2$	Ni$_{13}$	3-fold	1.45	378	592
CH	Ni$_7$	1-fold	1.66	245	538
CH	Ni$_7$	2-fold	1.27	488	700
CH	Ni$_7$	3-fold	1.14	536	730
CH	Ni$_{13}$	1-fold	1.70	347	771
CH	Ni$_{13}$	2-fold	1.35	437	555
CH	Ni$_{13}$	3-fold	1.25	537	594
C	Ni$_7$	1-fold	1.66	359	705
C	Ni$_7$	2-fold	1.27	505	566
C	Ni$_7$	3-fold	1.14	559	742
C	Ni$_{13}$	1-fold	1.66	378	701
C	Ni$_{13}$	2-fold	1.26	476	551
C	Ni$_{13}$	3-fold	1.08	595	551
H	Ni$_7$	1-fold	1.48	203	1913
H	Ni$_7$	2-fold	1.04	229	1472
H	Ni$_7$	3-fold	0.90	241	1014
H	Ni$_{13}$	1-fold	1.51	235	1764
H	Ni$_{13}$	2-fold	1.13	253	1119
H	Ni$_{13}$	3-fold	1.12	272	1284

[a] All CH$_3$ adsorption energies drop 34 kJ/mol if we allow for CH$_3$ relaxation in the gas phase to adopt the preferred planar CH$_3$ (^{2}A$_2''$) configuration.

[b] All CH$_2$ adsorption energies drop 25 kJ/mol if we allow for CH$_2$ relaxation in the gas phase to adopt the preferred CH$_2$ ($^3\Sigma_g$) configuration.

Therefore, adsorption energies and adsorbate-substrate frequencies vary strongly on average between Siegbahn *et al.*, Yang and Whitten, and this work, but all groups find the following order in chemisorption energy:

$$E_{ads}(CH_3) < E_{ads}(H) < E_{ads}(CH_2) < E_{ads}(CH) < E_{ads}(C)$$

The largest difference is found in the case of CH adsorption at the 3-fold position on Ni(111), where Siegbahn gives a value of 502 kJ/mol and Yang and Whitten of 302 kJ/mol. A possible reason for these differences has already been discussed in section 3.3.1.

The decomposition of CH_4 to C_a and $4H_a$ is displayed in fig. 3.2. The first step, activation of one CH bond in gas phase CH_4 producing CH_{3a} and H_a (reaction (3.1)), is 142 kJ/mol endothermic on Ni_7. This is quite large and due to the weak bonding of CH_3 on this cluster. On the Ni_{13}-cluster this cluster defect is remedied and the endothermicity drops to 30 kJ/mol. This is quite close to the expected thermoneutrality of the reaction. The second step, abstraction of another hydrogen from CH_{3a} to form CH_{2a} and H_a (reaction (3.2)), is endothermic by 38 kJ/mol on the Ni_7-cluster and 24 kJ/mol on the Ni_{13}-cluster. The third step, decomposition of CH_{2a} to form CH_a and H_a (reaction (3.3)) is exothermic by 61 kJ/mol on Ni_7 and 27 kJ/mol on Ni_{13}, suggesting the thermodynamic instability of this species. This could explain why the group of Ceyer[1] could not find evidence for the existence of CH_2 on a Ni(111) surface, although Kaminsky *et al.*[2] claim experimental evidence of all CH_x-species. Finally, the reaction of CH_a to produce C_a and H_a (reaction (3.4)) is 92 kJ/mol endothermic on Ni_7 and 27 kJ/mol endothermic on Ni_{13}. We conclude that all reaction energies are lowered on the Ni_{13}-cluster compared to the Ni_7-cluster. Using the experimental CH bond scission energy in CH_4, which is 425 kJ/mol, and the maximum adsorption energies for H and CH_3, which are 259 kJ/mol and 162 kJ/mol, Yang and Whitten computed for reaction (3.1) an endothermicity of just 4 kJ/mol. In later work they give an endothermicity of 12 kJ/mol[23]. For reaction (3.2) they computed an endothermicity of 55 kJ/mol and for reaction (3.3) an endothermicity of 140 kJ/mol. Siegbahn *et al.* found the following reaction energies. For reaction (3.1), again using the experimental CH bond scission energy in CH_4, the experimental adsorption energy of hydrogen (264 kJ/mol), and their best estimates of the adsorption energy of CH_3 (209–230 kJ/mol[14]), they found an exothermicity of 48–69 kJ/mol. For reaction (3.2), they computed an endothermicity of 34–58 kJ/mol. For reaction (3.3) they found an endothermicity of 29 kJ/mol. Finally, for reaction (3.4) they found an exothermicity of 50 kJ/mol. It seems, that the value they give for reaction (3.1), i.e. 48–69 kJ/mol exothermic, do not coincide with the reported low sticking coefficients on these surfaces[24]. Only on reaction (3.2) do all authors agree that it is an endothermic reaction.
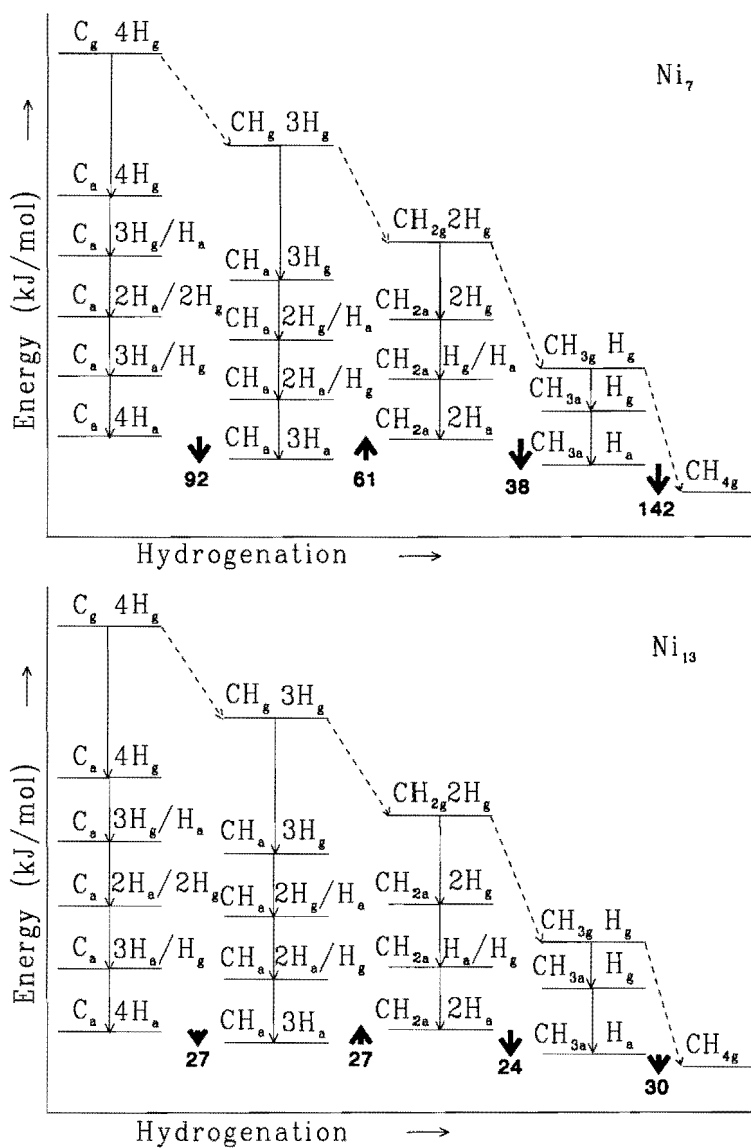
Fig. 3.2.
Energy scheme for CH$_4$ decomposition and subsequent dehydrogenation to C$_a$ and 4H$_a$ on Ni$_7$ (top) and Ni$_{13}$ (bottom). The adsorption energies of the H- and CH$_x$-species used for this scheme are given in table 3.2. Geometric and electronic data of these species is discussed in section 3.2.

3.3.3   CH$_3$, CH$_2$, CH, C and H adsorption on cobalt clusters

In this section we will discuss the chemisorption data for all CH$_x$-species and H on cobalt, which is displayed in table 3.3 and fig. 3.3. For CH$_3$, we find again a preference for the 1-fold site on both Co$_7$ and Co$_{13}$. The adsorption energies of 105 kJ/mol and 202 kJ/mol are somewhat higher than on the corresponding nickel clusters. The barrier to move along the surface is 35 kJ/mol on Co$_7$ and 42 kJ/mol on Co$_{13}$. CH$_2$ prefers the 3-fold site with adsorption energies of 361 kJ/mol on Co$_7$ and 397 kJ/mol on Co$_{13}$. The mobility barrier is 95 kJ/mol on Co$_7$ and 43 kJ/mol on Co$_{13}$. CH prefers the 3-fold site with adsorption energies of 586 kJ/mol on Co$_7$ and 564 kJ/mol on Co$_{13}$. This is the only case in which a fragment adsorbs stronger on a 7-atom cluster than a 13-atom cluster. The mobility barrier is 258 kJ/mol on Co$_7$ and 56 kJ/mol on Co$_{13}$. C prefers the 3-fold site with adsorption energies of 625 kJ/mol on Co$_7$ and 635 kJ/mol on Co$_{13}$. The mobility barrier is 190 kJ/mol on Co$_7$ and 86 kJ/mol on Co$_{13}$. Finally, H also prefers the 3-fold site with adsorption energies of 240 kJ/mol and 270 kJ/mol on Co$_7$ and Co$_{13}$ and mobility barriers of just 5 and 1 kJ/mol respectively. We thus find the same order in mobility for H and CH$_x$ as we found for the nickel clusters with the exception of CH on Co$_7$, which is very immobile. It is clear that the site preference for all adsorbates is the same for nickel and cobalt, i.e. 1-fold for CH$_3$ and 3-fold for all other species. The adsorption energies on cobalt are somewhat higher for all CH$_x$-species; for hydrogen they are the same. The same order in chemisorption energy is found on both metals, however the mobility barriers on the 13-atom cluster have now decreased compared to those on the 7-atom cluster, except for CH$_3$, which is just opposite to the results on the nickel clusters. Contrary to nickel, there is no much data available for adsorption on cobalt clusters. However, Zheng *et al.*[25], using extended Hückel calculations, gave bonding energies for CH$_3$ adsorption on slabs modelling Co(0001) of 360 kJ/mol for the 1-fold site, 255 kJ/mol for the 2-fold site, and 228 kJ/mol for the 3-fold site. We find the same order in site preference on both Co$_7$ and Co$_{13}$, but our energies are much lower. For CH$_2$ they found a preference for the 2-fold site with an adsorption energy of 613 kJ/mol, followed by an adsorption energy of 610 kJ/mol for the 1-fold site and 555 kJ/mol for the 3-fold site. Again our adsorption energies are much lower, and we find the opposite order for site preference. For CH they calculated a preference for the 3-fold site with an adsorption energy of 903 kJ/mol, followed by the 2-fold site with an adsorption energy of 873 kJ/mol and the 1-fold site with an adsorption energy of 853 kJ/mol. We have the same order for site preference, but again our energies are much lower. All the CH$_x$-species are very mobile on Co(0001) according to Zheng *et al.*.

Table 3.3. CH_3-, CH_2-, CH-, C-, and H chemisorption data on Co_7, and Co_{13}-clusters. z denotes the adsorbate-substrate distance, E_{ads} the adsorption energy, and ν denotes the adsorbate-substrate stretch frequency.

adsorbate	substrate	site	$z(\text{Å})$	E_{ads} (kJ/mol)	$\nu(\text{cm}^{-1})$
CH_3[a]	Co_7	1-fold	2.09	105	365
CH_3	Co_7	2-fold	1.94	70	251
CH_3	Co_7	3-fold	1.98	64	245
CH_3	Co_{13}	1-fold	2.08	202	556
CH_3	Co_{13}	2-fold	1.86	160	234
CH_3	Co_{13}	3-fold	1.93	151	284
CH_2[b]	Co_7	1-fold	1.80	266	719
CH_2	Co_7	2-fold	1.75	258	260
CH_2	Co_7	3-fold	1.37	361	418
CH_2	Co_{13}	1-fold	1.79	354	577
CH_2	Co_{13}	2-fold	1.53	329	391
CH_2	Co_{13}	3-fold	1.48	397	725
CH	Co_7	1-fold	1.65	328	729
CH	Co_7	2-fold	1.66	320	689
CH	Co_7	3-fold	1.20	586	599
CH	Co_{13}	1-fold	1.66	436	695
CH	Co_{13}	2-fold	1.40	508	758
CH	Co_{13}	3-fold	1.29	564	554
C	Co_7	1-fold	1.64	435	822
C	Co_7	2-fold	1.60	418	577
C	Co_7	3-fold	1.03	625	438
C	Co_{13}	1-fold	1.60	494	683
C	Co_{13}	2-fold	1.24	549	502
C	Co_{13}	3-fold	1.09	635	634
H	Co_7	1-fold	1.48	213	1425
H	Co_7	2-fold	1.06	235	2094
H	Co_7	3-fold	0.95	240	1056
H	Co_{13}	1-fold	1.50	242	1229
H	Co_{13}	2-fold	1.21	269	1746
H	Co_{13}	3-fold	1.03	270	1068

[a] All CH_3 adsorption energies drop 34 kJ/mol if we allow for CH_3 relaxation in the gas phase to adopt the preferred planar CH_3 ($^2A_2''$) configuration.

[b] All CH_2 adsorption energies drop 25 kJ/mol if we allow for CH_2 relaxation in the gas phase to adopt the preferred CH_2 ($^3\Sigma_g$) configuration.

The decomposition of CH_4 to C_a and $4H_a$ is displayed in fig. 3.3. Reaction (3.1) is endothermic by 135 kJ/mol on Co_7 and by 8 kJ/mol on Co_{13}. Again this difference is due to a cluster defect, which is remedied in the 13-atom cluster case. Reaction (3.2) is 3 kJ/mol exothermic on Co_7 and 29 kJ/mol endothermic on Co_{13}. Reaction (3.3) is exothermic by 60 kJ/mol on Co_7 and 32 kJ/mol on Co_{13}, indicating the thermodynamic instability of the CH_2-species also on cobalt. Finally, reaction (3.4) is endothermic by 77 kJ/mol on Co_7 and by 14 kJ/mol on Co_{13}. Again all reaction energies are thus lowered on the Co_{13}-cluster compared to the Co_7-cluster. For reaction (3.2) this effect results in inversion of the energetics from slightly exothermic on Co_7 to endothermic on Co_{13}.
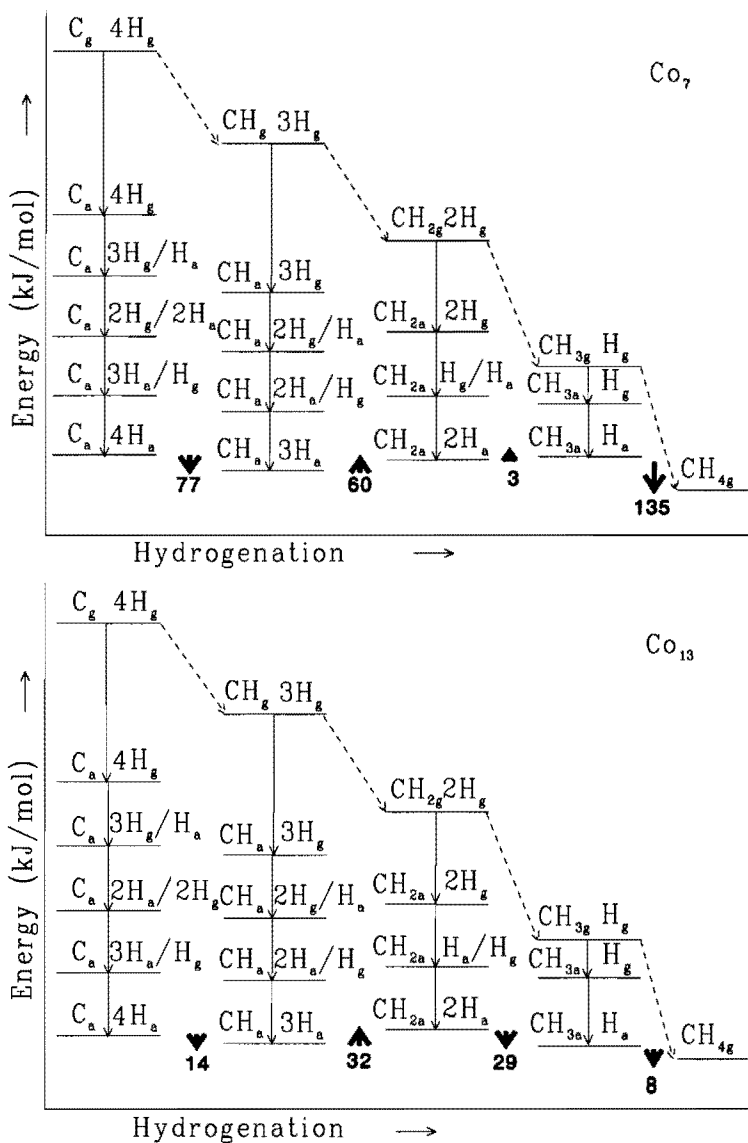
Fig. 3.3.
Energy scheme for CH_4 decomposition and subsequent dehydrogenation to C_a and $4H_a$ on Co_7 (top) and Co_{13} (bottom). The adsorption energies of the H- and CH_x-species used for this scheme are given in table 3.3. Geometric and electronic data of these species is discussed in section 3.2.

3.4   Conclusions

We have carried out DFT calculations to study the adsorption of CH_3 and H on nickel clusters of various size and -shape. We conclude that a one layer 7-atom model has at its main advantage that it models a Ni(111), Co(111) and Co(0001) surface. The most important disadvantage is that it suffers from boundary effects. These boundary effects are eliminated by adopting a spherical 13-atom cluster. The main disadvantage is now the transferability of our results on this cluster to those which are experimentally determined on surfaces. As a next step we have studied the adsorption of CH_3, CH_2, CH, C, and H on these clusters.

Starting from gas phase CH_4, the formation of CH_{3a} and H_a is endothermic on all clusters, but the endothermicity is strongly reduced on the 13-atom clusters (142 kJ/mol on Ni_7, 135 kJ/mol on Co_7, 30 kJ/mol on Ni_{13}, and 8 kJ/mol on Co_{13}). The formation of CH_{2a} and H_a from CH_{3a} is endothermic by 25–40 kJ/mol on all clusters, except on Co_7 (3 kJ/mol exothermic), mainly because of the much stronger adsorption of CH_2 on this cluster. The formation of CH_a and H_a from CH_{2a} is exothermic on all clusters, but the exothermicity differs a factor two between the 7- and 13-atom clusters (61 kJ/mol on Ni_7, 60 kJ/mol on Co_7, 27 kJ/mol on Ni_{13}, and 32 kJ/mol on Co_{13}). Finally, the formation of C_a and H_a from CH_a is strongly endothermic on the 7-atom clusters, but the endothermicity is again strongly reduced on the 13-atom clusters (92 kJ/mol on Ni_7, 77 kJ/mol on Co_7, 27 kJ/mol on Ni_{13}, and 14 kJ/mol on Co_{13}).

All authors agree on reaction (3.2) being endothermic. We found reaction (3.3) to be exothermic. This is in line with the observation of Ceyer's group[1] of CH_3 and CH but not of CH_2. Furthermore, we find all species to adsorb at 3-fold sites except for CH_3, which adsorbs at a 1-fold site. Zheng *et al.*, using extended Hückel calculations, agree with us on this last point, as they found that all species wanted to restore their missing bonds. They disagree with us and the groups of Siegbahn and Whitten on the point of adsorption site of the other species. Our computed CH_3 chemisorption energies seem too low on the 7-atom clusters, but this is remedied at the 13-atom clusters. It seems that Siegbahn *et al.* overestimate the CH_3 adsorption energy, because they report for reaction (3.1) an endothermicity of 48–69 kJ/mol, which does not coincide with the reported low sticking coefficients. No CH_x adsorption energies are known experimentally. The large differences between the calculated results remains controversial, but a possible origin is the different treatment of the nickel valence d-orbitals among the groups.

3.5 References

1. M.B. Lee, Q.Y. Yang, S.L. Tang, S.T. Ceyer, J. Chem. Phys. **85** (1986) 1693.
   M.B. Lee, Q.Y. Yang, S.T. Ceyer, J. Chem. Phys. **87** (1987) 2724.
   S.T. Ceyer, J.D. Beckerle, M.B. Lee, S.L. Tang, Q.Y. Yang, M.A. Hines,
   J. Vac. Sci. Tech. A **5** (1987) 501.

2. M. P. Kaminsky, N. Winograd, G. L. Geoffroy, M. A. Vannice,
   J. Am. Chem. Soc. **108** (1986) 1315.

3. Amsterdam density-functional (ADF) programme developed by Baerends *et al.*.
   E.J. Baerends, D.E. Ellis, P. Ros, Chem. Phys. **2** (1973) 41.
   P.M. Boerrigter, G. te Velde, E.J. Baerends, Int. J. Quantum Chem. **33** (1988) 87.
   G. te Velde, E.J. Baerends, J. Comput. Phys. **99** (1992) 84.
   D. Post, E.J. Baerends, J. Chem. Phys. **78** (1983) 5663.
   E.J. Baerends, A. Rozendaal, *Quantum chemistry: the challenge of transition metals and coordination chemistry*, edited by A. Veillard (Reidel, Dordrecht, 1986).
   P.J. van den Hoek, A.W. Kleyn, E.J. Baerends,
   Comm. Atom. Molec. Phys. **23** (1989) 93.

4. D.M. Ceperley, B.J. Alder, Phys. Rev. Lett. **45** (1980) 566.

5. S.H. Vosko, L. Wilk, M. Nusair, Can. J. Phys. **58** (1980) 1200.
   J.P. Perdew, A. Zunger, Phys. Rev. B **23** (1981) 5048.

6. A.D. Becke, Int. J. Quantum Chem. **27** (1985) 585.

7. A.D. Becke, Phys. Rev. A **38** (1988) 3098.

8. H. Stoll, C.M.E. Pavlidou, H. Preuss, Theor. Chim. Acta **49** (1978) 143.
   H. Stoll, E. Golka, H. Preuss, Theor. Chim. Acta **55** (1980) 29.

9. J.G. Snijders, E.J. Baerends, Mol. Phys. **36** (1978) 1789.
   J.G. Snijders, E.J. Baerends, P. Ros, Mol. Phys. **38** (1979) 1909.

10. N. Rösch, L. Ackermann, G. Pacchioni, Chem. Phys. Lett. **199** (1992) 275.

11. O. Kühnholz, M. Grodzicki, Lect. Notes Phys. **269** (1987) 198.

12. T. Ziegler, A. Rauk, Theor. Chim. Acta **46** (1977) 1.

13. P.E.M. Siegbahn, I. Panas, Surf. Sci. **240** (1990) 37.

14. J. Schüle, P.E.M. Siegbahn, U. Wahlgren,
    J. Chem. Phys. **89** (1988) 6982.

15. H. Yang, J.L. Whitten, Surf. Sci. **255** (1991) 193.

16. I. Panas, J. Schüle, P.E.M. Siegbahn, U. Wahlgren,
    Chem. Phys. Lett. **149** (1988) 265.
    I. Panas, P.E.M. Siegbahn, U. Wahlgren, *The challenge of d and f electrons. Theory and computation*, edited by D.R. Salahub and M.C. Zerner,
    (ACS, Washington DC, 1989).
17. K. Christmann, R.J. Behm, G. Ertl, M.A. Van Hove, W.H. Weinberg,
    J. Chem. Phys. **70** (1979) 4168.
18. K. Christmann, O. Schober, G. Ertl, M. Neumann,
    J. Chem. Phys. **60** (1974) 4528.
19. W. Ho, N.J. DiNardo, D.E. Plummer, J. Vac. Sci. Tech. **17** (1980) 314.
20. H. Yang, J.L. Whitten, J. Chem. Phys. **89** (1988) 5329.
21. L.G.M. Petterson, H. Akeby, P.E.M. Siegbahn, U. Wahlgren,
    J. Chem. Phys. **93** (1990) 4954.
22. C.F. Melius, T.H. Upton, W.A. Goddard III, Solid State Comm. **28** (1978) 501.
    O. Gropen, J. Almlöf, Chem. Phys. Lett. **191** (1992) 306.
    M.A. Nygren, P.E.M. Siegbahn, U. Wahlgren, H. Akeby,
    J. Phys. Chem. **96** (1992) 3633.
23. H. Yang, J.L. Whitten, J. Chem. Phys. **96** (1992) 5529.
24. T. P. Beebe, D. W. Goodman, B. D. Kay, J. T. Yates,
    J. Chem. Phys. **87** (1987) 2305.
25. C. Zheng, Y. Apeloig, R. Hoffmann, J. Am. Chem. Soc. **110** (1988) 749.

Chapter 4

Chemisorption of methane on nickel and cobalt. Electronic structure calculations and kinetics

abstract

The dissociative chemisorption of CH_4 on nickel and cobalt has been studied using different cluster models. Density functional theory is used to determine the structure and potential energy surface in the reactant-, transition state-, and product region. The transition state is explicitly determined on a one layer 7-atom cluster and a spherical 13-atom cluster. We find transition state barriers of 214 kJ/mol for the Ni_7-cluster, 216 kJ/mol for the Co_7-cluster, 121 kJ/mol for the Ni_{13}-cluster and 110 kJ/mol for the Co_{13}-cluster. The overall reaction energies are 142 kJ/mol, 135 kJ/mol, 30 kJ/mol, and 8 kJ/mol, respectively. The much higher and almost the same barrier for the 7-atom clusters compared to the single atom cases can be attributed to the intrinsic lower reactivity of the central atom embedded in the cluster and the similar electronic nature of the atoms in the clusters (open s- and d-shells). The lower barrier for the 13-atom clusters compared with the 7-atom clusters is a result of each surface atom now having five bonds, which gives a more balanced description of the substrate model. We have used transition state theory to compute rate constants in terms of rotational, vibrational and translational partition functions and we have also determined sticking coefficients. They are small, which is consistent with experiment. Kinetic isotope effects are much larger for dissociative adsorption compared to associative desorption.

4.1   Introduction

A very interesting and important reaction in heterogeneous catalysis is the Fischer-Tropsch synthesis, where CO and H_2 produce CH_4 among higher hydrocarbons[1]. It was concluded by Yates *et al.*[2] that the rate determining step to form CH_4 occurred in an earlier stage than the recombination of adsorbed methyl (CH_{3a}) and -hydrogen (H_a). Whether CH_4 or higher hydrocarbons are produced depends strongly on the metal catalyst and on reaction conditions. Over metals like Fe, Co and Ru a wide range of hydrocarbons is formed, whereas over Ni and Pd, CH_4 is the principle product, while Cu shows no reactions at all[3]. Thermal steam reforming to produce H_2 is another important industrial example of the activation of CH_4[4]. It is generally agreed that the rate determining step for this process is the dissociative chemisorption of CH_4. Feasible conversion levels, however, can only be achieved at high temperatures (1000 K), and in the presence of a transition metal catalyst[5]. The difficult decomposition of CH_4 is attributed to the barrier for breaking the CH bond. Many detailed surface science experiments and quantum chemical calculations have been carried out to probe the dissociation process in terms of the CH bond activation. The experiments showed up two main routes for this CH bond activation. One possibility is to raise the metal surface temperature T_s. The underlying model in this case is that the molecular species is in thermal equilibrium with the surface accounting for the strong activation with T_s (precursor model). The other possibility is to supply energy to CH_4 in the gas phase. This can be done by raising the gas temperature T_g, which affects the translation energy of the molecule or by raising the nozzle temperature, which results in vibrational exited CH_4 molecules. In all cases a significant isotope effect is reported. The experiments are described in detail elsewhere[6]. We focus here on a review of the computations performed by several groups.

In a series of papers Yang and Whitten have presented quantum chemical calculations on the dissociative chemisorption of CH_4 and the subsequent dehydrogenation of the adsorbed hydrocarbon species on a Ni(111) surface. In the first paper they described the chemisorption of atomic hydrogen on a Ni(111) surface[7]. The surface was modelled by a 26 atom three layer cluster, which was extracted from a larger cluster by an orbital localisation transformation to embed the cluster properly. *Ab initio* valence orbital CI calculations were then carried out on a local region of four nickel atoms to describe the binding process. The hydrogen atoms were found to bind strongly on both 3-fold and 2-fold (bridge) sites. Calculated adsorption energies ranged from 248 to 259 kJ/mol for optimised NiH bond lengths of 1.81–1.87 Å. Vibrational frequencies ranged from 1043 to 1183 cm^{-1}. The 1-fold (atop) position strongly deviated with an adsorption energy of only

187 kJ/mol, a NiH bond length of 1.61 Å and a vibrational frequency of 2332 cm^{-1}. In a subsequent paper[8] the reaction of chemisorbed CH and H on nickel was discussed. Here, however, a cluster consisting of 28 atoms was used. Again, a preference for both 3-fold and 2-fold sites was found for CH as well as CH$_2$. Adsorption energies ranged from 280 to 302 kJ/mol for CH adsorption and from 262 to 281 kJ/mol for CH$_2$ adsorption. Atop sites were again far less favourable with adsorption energies of 163 kJ/mol and 152 kJ/mol for CH and CH$_2$, respectively. The NiC bond lengths were almost equivalent for CH and CH$_2$ at 3-fold and 2-fold sites, ranging from 2.00 to 2.04 Å. The NiC bond length for adsorption of CH and CH$_2$ at the atop site was found to be 1.74 Å and 1.86 Å, respectively. NiC vibrational stretch frequencies ranged from 400 to 600 cm^{-1} for all species on all sites. The hydrogenation of CH to CH$_2$ was calculated to be exothermic by 140 kJ/mol, however, a significant barrier was calculated in moving H and CH to adjacent 3-fold sites. In a later paper they described the bonding of CH$_3$[9]. They computed adsorption energies of 162, 149 and 142 kJ/mol with corresponding NiC distances of 2.34, 2.34 and 2.03 Å at the 3-fold, 2-fold and 1-fold sites, respectively. Frequencies were 369–386 cm^{-1} for the 3-fold site, 296 cm^{-1} for the bridge site, and 416 cm^{-1} for the atop site. The hydrogenation of CH$_2$ into CH$_3$ was calculated to be exothermic by 55 kJ/mol, however once again a barrier was calculated to move CH$_2$ and H to adjacent 3-fold sites. Finally, the dissociative chemisorption of CH$_4$ was discussed by the same authors[10]. They now used a 41 atom, three layer embedded cluster as a model for the Ni(111) surface. Also the description of the local binding region was extended to 7 nickel atoms. The calculated activation energy of CH$_4$ adsorbed atop nickel was 70 kJ/mol. Dissociation to adsorbed CH$_3$ and H at infinite separation was computed to be exothermic by 12 kJ/mol.

The dissociation of CH$_4$ on a Ni(100) atop site has been studied by Swang *et al.*[11] using a 13 -atom 2 -layer cluster at the CASSCF-CI level. This is the only *ab initio* study thus far describing the central nickel atom at an all-electron level; the other atoms were described by one-electron effective core potentials. They calculated an activation barrier of 37 kJ/mol and by making an estimate for basis set superposition errors, finite basis set effects, finite cluster size and zero point vibrations, they arrived at a final estimate of 62–71 kJ/mol for the fully corrected barrier. They rigorously determined the transition state by optimising independently five degrees of freedom. In another study they modelled the Ni(111) surface, but now they investigated the chemisorption of CH$_3$[12] at atop sites and 3-fold hollow sites. Clusters of different size were used, but they were all prepared for bonding, which means that an orbital of the same symmetry as the binding adsorbate orbital is available at the substrate to bind. The authors found a preference for the 3-fold

hollow (fcc) site, mainly based on calculated frequency shifts with respect to $LiCH_3$, which they chose as a model system. Calculated NiC stretch frequencies for the 3-fold site ranged from 320 to 353 cm^{-1}, while the experimental value for this frequency is 370 cm^{-1}[13]. The computed CH_3 adsorption energy ranged from 188 to 209 kJ/mol. The estimated value, including corrections for basis set superposition errors, finite basis set effects, cluster size effects and zero-point vibration, ranged from 209 to 230 kJ/mol. Finally, CH stretch frequencies and adsorption energies were calculated for CH_3, CH_2 and CH on Ni(111) and Ni(100) again modelled by clusters of various size but all bond prepared[14]. Their best estimates for the adsorption energies on Ni(111) were 502 kJ/mol for CH, 368 kJ/mol for CH_2 and 205 kJ/mol for CH_3.

Luntz and Harris discussed various existing models[15] for CH_4 dissociation, but denounced them all, because none could explain all experimental observations. In subsequent papers they introduced a new model[16], arguing that the tunnel process could not be viewed in terms of a static one dimensional barrier, i.e., where the coupling between the tunnel barrier and the surface is ignored. Instead, a potential energy surface with a minimum of three degrees of freedom is needed including the distance of the molecule to the surface, a bond distance and a coordinate representing lattice vibrations. According to this model, both direct dissociation (CH_4) and precursor governed processes (higher order alkanes) are dominated by so-called thermally assisted tunneling effects, i.e., the thermal energy associated with a hot surface greatly enhances the tunneling probability. They thus suggested that a classical approach to CH_4 is not appropriate. However, we feel that under the condition of rapid energy exchange compared to the overall reaction time, which is valid in the case of a high activation barrier and at high temperatures and pressures, which are the industrial conditions of CH_4 steam reforming, transition state theory may be applicable. Also in the case of a wide activation barrier, the importance of tunneling will decrease.

The previous computational studies on CH_4 dissociation focussed mainly on electronic structure calculations or on treating the dynamics using a model for the potential energy surface. We have calculated both the potential energy surface using an *ab initio* density functional approach, and treated the kinetics of the system by employing transition state theory. Specifically, we have taken a Ni_7-, $Ni_{7,3}$-, $Ni_{7,3,3}$- and Ni_{19}-cluster to model the Ni(111) surface, and a Co_7-cluster to model the Co(0001) surface. We have also used a Ni_{13}- and a Co_{13}-cluster, which give a balanced description of the different adsorption sites.

The dissociative adsorption of CH_4 can thus be written as:

$$CH_4 + M_x \xrightarrow{k_{dis,ads}} CH_{3a} + H_a, \tag{4.1}$$
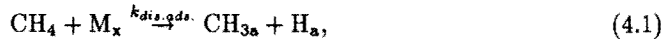
and the reverse reaction, a mobile recombination (association) of CH_{3a} and H_a on the surface followed by desorption, as:

$$CH_{3a} + H_a \xrightarrow{k_{ass,des}} CH_4 + M_x. \tag{4.2}$$
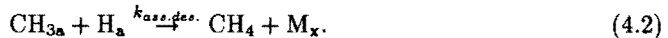
In eqns. (4.1)–(4.2) M = Ni or Co, and x = 7, 10, 13 or 19. Details of the calculations are discussed in section 4.2. In section 4.3 the electronic structure calculations are presented and discussed. In section 4.4 reaction kinetics is discussed and in section 4.5 we summerise results and draw conclusions.

4.2 Methods

We have performed quasi-relativistic calculations based on density functional theory (DFT) using the Amsterdam Density Functional programme package (ADF) developed by Baerends *et al.*[17]. The exchange-correlation potential used is based on quantum Monte Carlo simulations of Ceperley and Alder[18] of a homogeneous electron gas which are parametrised by Vosko, Wilk and Nusair[19]. To correct for the overbinding inherent to the local density approximation (LDA)[20], we haved used a gradient corrected exchange energy functional[21] in combination with the Stoll correction[22] for correlation. Molecular orbitals are expressed by the LCAO method using Slater orbitals, integrals are evaluated numerically and adsorption energies are calculated by Ziegler's transition state method[23]. For carbon a frozen core potential is used for the 1s electrons; for nickel and cobalt the electrons up to 3p are frozen. Relativistic effects were taken into account by first order perturbation theory[24]. Single ζ functions are used for core orthogonalisation. The basis sets are of double ζ quality with the exception of the nickel and cobalt d-orbitals which are triple ζ 's. On all atoms polarisation functions are included. As a first step, we have used the Ni_7-cluster to optimise geometrical parameters. As other models for the substrate, we have taken $Ni_{7,3}$-, $Ni_{7,3,3}$-, Ni_{13}-, and Ni_{19}-clusters, using the Ni_7 optimised geometrical parameters. Except for the Ni_{19}-cluster, which is displayed in fig. 4.1, all these clusters are displayed in fig. 3.1.
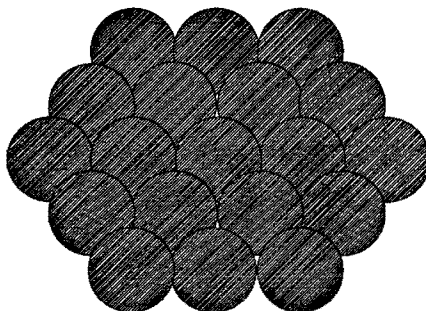
Fig. 4.1.
M_{19}-cluster modelling the substrate. The other substrate models are shown in fig. 3.1. For all clusters the bond distance of the bulk was used, i.e. 2.49 Å for Ni, 2.50 Å for Co.

As a second step we have also optimised the geometrical parameters rigorously on Ni_{13}-, Co_7- and Co_{13}-clusters. The 13-atom clusters do not model the Ni(111) or Co(0001) surface, but consist of a central metal atom surrounded by 12 atoms in a hexagonal-closed-packed fashion. In this cluster, all surface atoms form bonds with five other atoms and there are not low coordinated boundary atoms, eliminating possible boundary effects. For all nickel clusters the bond distance was fixed at the bulk value of 2.49 Å, for cobalt clusters at the bulk value of 2.50 Å. This results in a site area per atom of $5.38 \cdot 10^{-20}$ m^2 for nickel and $5.40 \cdot 10^{-20}$ m^2 for cobalt, which is used for the connection between the transition state theory rate constants $k^{TST}_{ass.des.}$ and $k^{TST}_{dis.ads.}$ and their equivalents in terms of surface- and volume concentrations $k_{ass.des.}$ and $k_{dis.ads.}$ (see appendix). The CH$_3$ fragment was kept fixed with CH distances of 1.09 Å and HCH angles of 109.48° as in CH$_4$. The basis for this assumption was the experimental result that the CH$_3$ fragment in the TS and the DS are very similar[13]. The transition state was explicitly calculated by a four dimensional grid in the MC and CH distances and the CH$_3$ tilt angle with respect to the activated CH bond (θ) and the MMC angle (α) for both the 7- and 13-atom clusters (fig. 4.2). The grid point energies were fitted to a second-order polynomial in the MC and CH distances, θ, and α. We included estimates of quantum chemical tunneling based on an unsymmetrical Eckart potential[25], if the reaction coordinate consisted of essentially one coordinate. Vibrational calculations were performed using the conventional GF-method[26], where G is the kinetic energy matrix and F the force constant matrix. Surface reaction kinetics was calculated according to transition state theory[27].
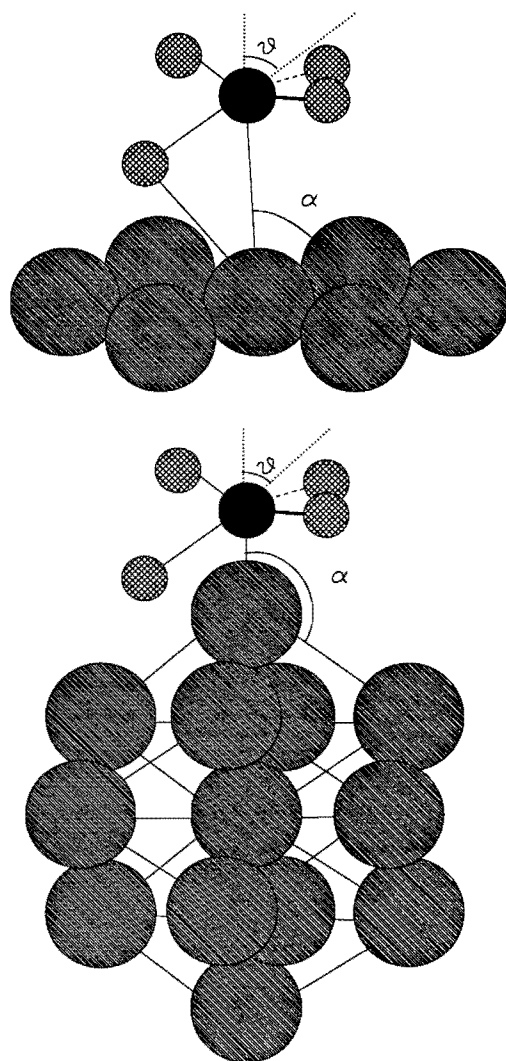
Fig. 4.2.
Definition of optimised parameters. Hydrogen atoms are denoted by diagonally cross-hatched circles, carbon by a filled black circle, and transition metal atoms by diagonally hatched circles. The dotted lines denote the C_{3v}-axes of the CH_3-group in the reactant- and the TS. The MC bond, the CH bond, together with the CH_3 tilt angle with respect to the activated bond (θ), and the MMC angle (α) were optimised.

4.3   Electronic structure calculations

Optimal parameters and adsorption energies of the Ni_7/CH_4 reactant, the transition state (TS) and the dissociated state (DS) are shown in table 4.1. The enormous increase (173 kJ/mol) in barrier height going from a single nickel atom to a Ni_7-cluster has two main origins. Firstly, the nearest neighbours of the central nickel atom in the first layer are now included resulting in a decrease in reactivity of the central nickel atom. Secondly, the activated CH bond is now 0.3 Å more stretched than in the single atom case.   For

Table 4.1. Geometries (Å) and energies (kJ/mol) of the reactant, the TS and the DS for the cluster models.

System	Method	R_{MC}	R_{MH}	R_{CH}	α	θ	E^a
Ni_7/CH_4 DS	DFT	2.06	1.70	∞	90.0°	0.0°	142
Ni_7/CH_4 TS	DFT	2.24	1.49	1.63	90.1°	26.4°	214
Ni_7/CH_4 reactant	DFT	∞	∞	1.08	-	0.0°	0
Ni_{13}/CH_4 DS	DFT	1.99	1.83	∞	135.0°	0.0°	30
Ni_{13}/CH_4 TS	DFT	2.07	1.49	1.80	116.8°	29.0°	121
Ni_{13}/CH_4 reactant	DFT	∞	∞	1.08	-	0.0°	0
Ni_{13}/CH_4 DS	MRCI + Q^b						
Ni_{13}/CH_4 TS	MRCI + Q	2.12	1.48	1.51	83.5°	27.0°	77
Ni_{13}/CH_4 reactant	MRCI + Q	∞	∞	1.09	-	0.0°	0
Co_7/CH_4 DS	DFT	2.09	1.66	∞	90.0°	0.0°	135
Co_7/CH_4 TS	DFT	2.21	1.48	1.52	88.2°	26.8°	216
Co_7/CH_4 reactant	DFT	∞	∞	1.08	-	0.0°	0
Co_{13}/CH_4 DS	DFT	2.08	1.77	∞	135.0°	0.0°	8
Co_{13}/CH_4 TS	DFT	2.10	1.48	1.79	119.9°	27.2°	110
Co_{13}/CH_4 reactant	DFT	∞	∞	1.08	-	0.0°	0

^{a} chemisorption energy H (3-fold) on Ni_7: 241 kJ/mol; chemisorption energy CH_3 (1-fold) on Ni_7: 97 kJ/mol.
   chemisorption energy H (3-fold) on Ni_{13}: 272 kJ/mol; chemisorption energy CH_3 (1-fold) on Ni_{13}: 179 kJ/mol.
   chemisorption energy H (3-fold) on Co_7: 240 kJ/mol; chemisorption energy CH_3 (1-fold) on Co_7: 105 kJ/mol.
   chemisorption energy H (3-fold) on Co_{13}: 270 kJ/mol; chemisorption energy CH_3 (1-fold) on Co_{13}: 202 kJ/mol.
^{b} modelling a Ni(100) surface, see ref[11].

the nickel clusters, the NiH bond distance was fixed at 1.49 Å. This distance is the optimal value for the TS of the Ni/CH_4 complex and it remained practically constant throughout nickel insertion in CH_4[6]. Swang *et al.*[11] optimised this parameter and found a value of 1.48 Å, which is almost the same as our value and exactly the same as their value for nickel insertion[28]. For the cobalt clusters, the CoH bond distance was fixed at 1.48 Å for the same reason. To investigate the energy effect of different orientations of the TS on our

cluster, we have computed energies at three other geometries: one in which the Ni_7-cluster is rotated by 30° around the surface normal (TS_2), one with the CH_3 fragment rotated by 180° (TS_3), and one with both the CH_3 fragment rotated by 180° and the cluster by 30° (TS_4). The initial transition state geometry (TS_1) is the only TS that has been optimised as mentioned in the previous section. The effect of cluster size and -shape on the energy of the TS is investigated by computing the height of the barrier for some larger clusters. The results are summarized in table 4.2.

Table 4.2. Barrier energies, E (kJ/mol), for CH_4 dissociative adsorption, Mulliken overlap populations (M.O.P.) for MC, MH, and CH bonds, together with the number of nearest neighbours (N_{nn}), next nearest neighbours (N_{nnn}), and next-next nearest neighbours (N_{nnnn}) for the nickel atom at which adsorption takes place.

cluster	geometry[a]	$M.O.P._{MC}$	$M.O.P._{MH}$	$M.O.P._{CH}$	E^b	N_{nn}^c	N_{nnn}^c	N_{nnnn}^c
Ni_7	TS_1	0.16	0.15	0.11	214	6	0	0
Ni_7	TS_2	0.16	0.14	0.12	214	6	0	0
Ni_7	TS_3	0.16	0.14	0.12	214	6	0	0
Ni_7	TS_4	0.16	0.14	0.14	212	6	0	0
Ni_{19}	TS_1	0.15	0.12	0.10	207	6	0	6
$Ni_{7,3}$	TS_4	0.16	0.16	0.12	201	9	0	0
$Ni_{7,3,3}$	TS_4	0.16	0.16	0.13	172	9	0	3
Ni_{13}	TS_1	0.16	0.18	0.11	100	5	2	4
Ni_{13}	TS	0.19	0.15	0.05	121	5	2	4
Co_7	TS	0.14	0.11	0.11	216	6	0	0
Co_{13}	TS	0.19	0.13	0.04	110	5	2	4

[a] TS_1: TS optimised on Ni_7, see fig. 4.2 (top); TS_2: Ni_7 cluster rotated 30°; TS_3: CH_3 fragment rotated 180°; TS_4: Ni_7 fragment rotated 30° and CH_3 fragment rotated 180°; TS: TS optimised on cluster it refers to.

[b] experimental CH_4 activation barrier Ni(111): 50/53 kJ/mol[13]/[29]; experimental CH_4 activation barrier Ni(100): 27/52 kJ/mol[29]/[32]; experimental CH_4 activation barrier Co(0001): 70 kJ/mol[33].

[c] N_{nn} for infinite Ni(111)/Co(0001): 9; N_{nnn} for infinite Ni(111)/Co(0001): 3; N_{nnnn} for infinite Ni(111)/Co(0001): 9.

We see that rotation of the CH_3 group and/or the cluster as discussed above does not effect the energy significantly. Extending the cluster by including more nickel atoms in the top layer only lowers the energy slightly (7 kJ/mol). Extending the surface by including a second layer of only three atoms has a more pronounced effect (13 kJ/mol), whereas the result of including an additional (third) layer of three atoms lowers the energy significantly (42 kJ/mol). The activation barrier (172 kJ/mol), however, is still too high. Beebe *et al.*[29] for example, estimate this barrier to be 53 kJ/mol, while Lee *et al.*[13] observe carbon deposition indicative of CH_3 formation on a Ni(111) surface at energies

above 50 kJ/mol. We can obtain a far lower activation barrier by choosing as a substrate a Ni_{13}-cluster, which gives a balanced description of the different adsorption sites. In this case the activation barrier reduces to 100 kJ/mol.

In table 4.2, we have also denoted the number of nearest neighbours (N_{nn}), next nearest neighbours (N_{nnn}) and next-next nearest neighbours (N_{nnnn}) for the nickel atom at which adsorption takes place for all substrate models. We observe that there is a correlation between these numbers and the cluster barrier height. The lowest barrier (172 kJ/mol) is calculated for the $Ni_{7,3,3}$ -cluster, when N_{nn} equals the value of an infinite Ni(111) surface $(N_{nn} = 9)$, and the discrepancy between N_{nnn}- and N_{nnnn}-values for the cluster and an infinite Ni(111) surface $(N_{nnn} = 3, N_{nnnn} = 9)$ is least. The next-lowest barrier (201 kJ/mol) is found for the $Ni_{7,3}$ cluster, where N_{nn} is still correct, but N_{nnn} and N_{nnnn} deviate more from the infinite Ni(111) surface values, etc. The only exception is the Ni_{13}-cluster, which yields the lowest barrier. In this case N_{nn} has its worst value (table 4.2.). All 12 surface atoms are equally unsaturated with bonds, i.e. 5 bonds instead of the bulk value of 12, and therefore form a relatively strong bond with activated CH_4. Also, the metal atom at which adsorption takes place has now five nearest neighbours, two next-nearest neighbours, and four next-next-nearest neighbours as holds for all surface atoms in this substrate model. In this respect it is a better model for any infinite surface plane than the 7-atom cluster.

Panas *et al.*[30] have studied H_2 dissociation on various transition metal clusters and found very significant oscillations in adsorption energy as a function of cluster size and -shape. For example, they calculated an adsorption energy for H of 165 kJ/mol on a $Ni_{3,7}$-cluster (experimental value: 264 kJ/mol). Including a third layer of 7 atoms ($Ni_{3,7,7}$-cluster) lowers the adsorption energy with almost 100 kJ/mol to 264 kJ/mol. Including a fourth layer of 3 atoms ($Ni_{3,7,7,3}$-cluster) resulted in an adsorption energy of 235 kJ/mol, which is almost 30 kJ/mol worse. They concluded on the basis of oscillations like these that the clusters should be bond prepared. Using bond prepared clusters, they compute adsorption energies of 291 kJ/mol, 264 kJ/mol, and 235 kJ/mol for respectively the $Ni_{3,7}$-, $Ni_{3,7,7}$-, and $Ni_{3,7,7,3}$-cluster. Although the adsorption energy is now a smoother function of cluster size, there is still a variation in adsorption energy of almost 60 kJ/mol. In addition, the worst energy is computed for the best cluster. In the light of these results our calculated variations in adsorption energy seem very reasonable.

We have also computed the Mulliken overlap populations of the MC bond, the MH bond and the CH bond, the most interesting ones at the TS for the different clusters. We see that for the Ni_7-cluster the differences are small or even negligible: 0.16 for the NiC bond, 0.14–0.15 for the NiH bond and 0.11–0.14 for the activated CH bond. This indicates

significant bond formation between Ni and C and between Ni and H, at the expense of the CH bond. This trend is also seen for the 10- and 13-atom clusters. The absolute value of the NiC and NiH bond overlap populations (0.15–0.19 for NiC and 0.12–0.18 NiH) are significantly smaller as for the single atom case (0.32 for NiC and 0.27 for NiH)[6]. Again this can be understood by the intrinsic decline in reactivity of the central nickel atom.

An electron density difference map constructed in the mirror plane of the TS with respect to the Ni$_7$-cluster and activated CH$_4$ is shown in fig. 4.3 (top). It is clear that the CH bond is activated. It is also clear that H and CH$_3$ are forming bonds with the central nickel atom. These conclusions are supported by the Mulliken overlap populations. The involvement of the nickel d-orbitals lowers the CH$_4$ dissociation barrier.
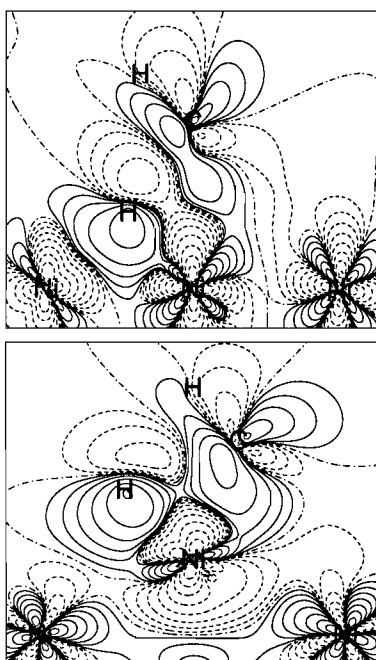
Fig. 4.3.
Contour plots of the electron density differences:
ρ (Ni$_7$CH$_4{}^{TS}$) - ρ (Ni$_7$) - ρ (CH$_4{}^{TS}$) (top), and ρ (Ni$_{13}$CH$_4{}^{TS}$) - ρ (Ni$_{13}$) - ρ (CH$_4{}^{TS}$) (bottom).
Solid contours denote increase, dashed lines denote decrease in electron density (in electrons Å^{-3}).
Contour values: $0.00, \pm 0.006, \pm 0.016, \pm 0.035, \pm 0.075, \pm 0.159, \pm 0.336, \pm 0.709, \pm 1.505,$ and ± 3.185.

As a next step we have optimised the TS rigorously on the Ni_{13}-, Co_7-, and Co_{13}-clusters. Optimal parameters and adsorption energies of the reactant, the TS and the DS of these systems are also shown in table 4.1. The results of Ni_7/CH_4 have already been discussed. Again, we see the enormous increase in barrier height in going from a single cobalt atom to a Co_7-atom cluster (137 kJ/mol), which has as its cause the inclusion of the nearest neighbours of the central cobalt atom at which adsorption takes place, which reduces strongly the reactivity of the central cobalt atom. Although the CH bond is more stretched in the TS of Ni_{13}/CH_4 and Co_{13}/CH_4 compared to the 7-atom clusters, the barrier height for CH_4 dissociation drops by 93 kJ/mol for nickel and by 106 kJ/mol for cobalt. This is due to two effects. Firstly the metal atom at which adsorption takes place has now five nearest neighbours, two next-nearest neighbours, and four next-next-nearest neighbours as holds for all surface atoms in this substrate model. In this respect it is a better model for any infinite surface plane than the 7-atom cluster, as discussed before. Also the average strength of the metal-metal bonds is now strongly moderated, as can be concluded by dividing the formation energy of the cluster through the number of bonds formed. In Ni_7 this average bond strength is 152 kJ/mol, in Ni_{13} 106 kJ/mol, whereas in bulk nickel the average bond strength is 71 kJ/mol according to Kittel[31]. For Co_7 we find a value of 102 kJ/mol, for Co_{13} a value of 80 kJ/mol and for bulk cobalt a value of 70 kJ/mol is given[31]. A surface atom of the 13-atom cluster can therefore form more easily a bond with an adsorbate than the 7-atom cluster. Secondly, the steric repulsion between the hydrogen atom of the activated CH bond and the surface is far less for the 13-atom cluster, because the surface plane is now more parallel with the dissociating bond (see fig. 4.2 (bottom)). The barrier for associative desorption raises for both nickel and cobalt with 20 kJ/mol relative to the 7-atom clusters. An electron density difference map constructed in the mirror plane of the TS with respect to the Ni_{13}-cluster and activated CH_4 is shown in fig. 4.3 (bottom). It is clear that density increases at the activated CH bond, but this is due to electron donation of nickel into an almost broken CH bond in activated CH_4. This is clear from the very elongated CH bond at the TS (1.80 Å, see table 4.1), and the very small overlap population (0.05, see table 4.2). It is also clear that H and CH_3 are forming bonds with the central nickel atom. This is again supported by the overlap populations (0.19 for NiC, 0.15 for NiH). The involvement of the nickel d-orbitals lowers the CH_4 dissociation barrier. The density difference maps of the TS on Co_7/Co_{13} are very similar and not given here. The Mulliken overlap populations for Co_7 are slightly smaller than those on Ni_7 for all bonds. The same observation holds for Co_{13}.

We can compare our Ni_7/CH_4 (TS) results to those of Swang *et al.*[11], who modelled the Ni(100) surface. They calculate a less extended CH bond, a shorter NiC bond distance,

and a smaller NiNiC angle. This suggests a more compact, tight transition state with a significant larger interaction energy between substrate and adsorbate as is indeed reflected in a much lower activation barrier. Compared to our Ni_{13}/CH_4 (TS) results their CH bond length is 0.3 Å shorter, resulting in a much lower barrier. The experimental energy barrier for CH activation on Ni(100) is unresolved. Chorkendorff *et al.*[32] measured an activation barrier of 53 kJ/mol, whereas Beebe *et al.*[29] gave a value of 27 kJ/mol. If the latter result is correct, Swang's result is a factor three too high. Beebe *et al.* give an activation energy of 53 kJ/mol for CH_4 on Ni(111). Geerlings *et al.*[33] report a CH_4 dissociation barrier on Co(0001) of 70 kJ/mol. According to our calculations, the barrier for CH_4 dissociation is the same on Ni_7 and Co_7, but somewhat lower on Co_{13} compared to Ni_{13}. Desorption is easier on nickel for both cluster models. Zaera[34] reports a desorption barrier of 71 kJ/mol on platinum which is in good agreement with our calculated barrier on Ni_7 (72 kJ/mol) and Ni_{13} (91 kJ/mol). As discussed in the introduction, many groups have computed adsorption energies and frequencies of H and CH_3 and their site preference on Ni(111). For H on Ni_7, we compute a preference for the 3-fold adsorption site with an adsorption energy of 241 kJ/mol, a H -surface distance of 0.90 Å, corresponding to a NiH bond length of 1.70 Å, and a NiH stretch frequency of 1014 cm^{-1}. CH_3 chemisorbs at a 1-fold site with an adsorption energy of 97 kJ/mol, a NiC bond length of 2.06 Å and a NiC stretch frequency of 387 cm^{-1}. The experimental site preference for H is 3-fold with a H -surface distance of 1.15 Å[35], an adsorption energy of 261 kJ/mol[36], and a NiH stretch frequency of 1120 cm^{-1}[37]. Therefore, our calculated H-surface distance is too short by 0.25 Å, our adsorption energy too low by 19 kJ/mol and our frequency too low by 106 cm^{-1}. For CH_3 only the experimental CH_3 surface stretch frequency is available: 370 cm^{-1}[13], which is in good agreement with our value of 387 cm^{-1}. Yang and Whitten[9] found much higher adsorption energies (142 kJ/mol), but comparable bond lengths (2.03 Å) for adsorption at the atop site. They found a preference for the 3-fold site. Schüle *et al.*[12] calculated similar adsorption energies for CH_3 adsorbed 1-fold and 3-fold, but a large difference in the NiC stretch frequency: approximately 600 cm^{-1} for the atop site, modelled by a single atom, and 320–353 cm^{-1} for the 3-fold site. On the basis of the calculated frequencies and frequency shifts, they assigned the 3-fold site to be the preferred site, whereas we would assign a 1-fold site preference. They estimate the CH_3 adsorption energy to be around 209–230 kJ/mol, which differs from our value by a factor of two.

4.4   Kinetic calculations

We have computed rate constants using transition state theory. An important advantage of this approach is that the complete potential energy surface is not required. Instead only the local parts at the reactant, the transition state, and the product state need to be determined to compute kinetics. In particular, rotational and vibrational frequencies together with masses of the intermediates and barrier heights determine the rate constant. The transition state theory formula for the rate coefficient for dissociative adsorption at the high pressure limit is given by[27]:

$$k_{dis.ads.}^{TST} = \frac{k_B T}{h} \frac{Q_v^\dagger}{Q_t Q_v Q_r} e^{\frac{-E_{crit}}{k_B T}} \tag{4.3}$$

and for associative desorption by

$$k_{ass.des.}^{TST} = \frac{k_B T}{h} \frac{Q_v^\dagger}{Q_t Q_v} e^{\frac{-E'_{crit}}{k_B T}} \tag{4.4}$$

In eqns. (4.3)–(4.4), k_B denotes Boltzmann's constant, T temperature, and h Planck's constant. Q_t, Q_v and Q_r are the translational, vibrational and rotational partition functions for the reactant, the TS and the DS. The translational partition function describes the relative translation of CH_4 with respect to the substrate or, on the substrate, the two absolute and relative translations of CH_{3a} and H_a thus implying a mobile DS. We have discussed in chapter 3 the mobility of various adsorbates, and we have concluded that both CH_3 and H are mobile species, which validates this assumption. A dagger ($\dagger$) denotes transition state partition functions. E_{crit} is the minimum energy at which reaction can occur classically (critical energy), and includes the zero-point vibrational energy differences. In the appendix we give the connection between $k_{ass.ads.}^{TST}$ and $k_{dis.ads.}$ and between $k_{ass.des.}^{TST}$ and $k_{ass.des.}$. To evaluate $k_{dis.ads.}^{TST}$ and $k_{ass.des.}^{TST}$, we need to calculate the translational, vibrational and rotational partition functions for the reactant, the DS and the TS. However, if partition functions are the same for the DS and the TS, or for the reactant and the TS, they will effectively cancel out and we need only to evaluate partition functions which differ. Also, if a vibrational frequency is high ($h\nu \gg k_B T$), the partition function yields a factor of 1.0 and does not effectively contribute to the rate constant.

To find out which degrees of freedom cancel, we characterised them at the different geometries bearing in mind that our cluster represents an (infinite) surface of infinite mass. Therefore overall translations and rotations of the cluster are irrelevant and internal lattice vibrations (phonons) are neglected. With these premises we have determined the degrees

of freedom at the TS. Three modes determine the absolute position of H: one MH stretch, one CH stretch and one vibration of H perpendicular to the mirror plane. Three modes determine the absolute position of the CH$_3$ group: one MC stretch, one MMC angle (α) and one vibration of CH$_3$ perpendicular to the mirror plane. Three modes determine the orientation of the CH$_3$ group: the CH$_3$ tilt angle in the mirror plane (θ), one CH$_3$ tilt perpendicular to the mirror plane, and one internal CH$_3$ rotation around the internal C$_{3v}$ axis. Finally, there are six internal CH$_3$ modes: three CH stretches and three internal bending modes adding up to a total of 15 degrees of freedom. For the reactant we have nine internal (vibrational) modes of CH$_4$, four of which are CH stretches, three are CH$_3$ internal bending modes, and two are wagging modes, one perpendicular to the mirror plane, and θ. Together with three rotations of CH$_4$ and three relative translations of CH$_4$ with respect to the surface, they make up 15 independent degrees of freedom. For the DS we have six internal CH$_3$ modes of which three are CH stretches, and three internal bending modes. Three modes determine the relative CH$_3$ position: two CH$_3$ wagging modes (θ, and one wagging mode perpendicular to the mirror plane), and one internal CH$_3$ rotation around the internal C$_{3v}$ axis. One mode determines the absolute position of CH$_3$ perpendicular to the surface: the MC stretch. Two (vibrational) modes determine the absolute position of CH$_3$ parallel to the surface, which are two translations in the mobile model. Analogously for H, one mode determines the absolute position of H perpendicular to the surface: the MH stretch. Two modes determine the absolute position of H parallel to the surface, which are again two translations in the mobile model. Together, these modes add up again to a total of 15 degrees of freedom. This choice of modes can result in the partition function cancellation as discussed before.

The six internal CH$_3$ modes cancel at all geometries. Also, one CH$_3$ rotation around the C$_{3v}$-axis at the TS and the DS cancels against one overall CH$_4$ rotation. Finally, the CH$_3$ wagging mode perpendicular to the mirror plane cancels at the reactant, the TS and the DS. For the reactant, this leaves us with three relative translations, two CH$_4$ overall rotations, one CH stretch and θ. At the TS we have left one CH stretch, the MC stretch, the MH stretch the CH$_3$ and H vibration perpendicular to the mirror plane, θ, and α At the DS we have left a MC stretch, a MH stretch, θ, two translations of CH$_3$ parallel to the surface and two translations of H parallel to the surface. The translations can be combined to two relative translations parallel to the surface and two translations of the centre of mass parallel to the surface. These modes need thus explicit computation. We have not explicitly calculated the MH stretch mode, because in the G-matrix only the mass of H is involved, which will result in a high frequency. As a consequence, the corresponding vibrational partition function will be 1.0.

As discussed in section 4.2, a harmonic vibrational analysis for the TS, the DS and for the reactant was carried out to compute vibrational partition functions. The frequencies are displayed in table 4.3 for both CH_4 and CD_4. For the reactant the frequencies can be

Table 4.3. Vibrational frequencies, ν_i (cm^{-1}), of the reactant, the TS, and the DS of the cluster models.

System	ν_1	ν_2	ν_3	ν_4	ν_5	ν_6
M_x/CH_4 reactant	2951	2438				
M_x/CD_4 reactant	2131	1929				
Ni_7/CH_4 TS	636	499	327	152	38 i	6
Ni_7/CD_4 TS	450	403	265	139	31 i	5
Ni_7/CH_4 DS	1663	1014	387			
Ni_7/CD_4 DS	1319	718	353			
Ni_{13}/CH_4 TS	875i	636^a	361	152^a	31	2
Ni_{13}/CD_4 TS	633i	450^a	332	139^a	24	2
Ni_{13}/CH_4 DS	1633	1284	465			
Ni_{13}/CD_4 DS	1298	908	424			
Co_7/CH_4 TS	629	505	167	150	133 i	5
Co_7/CD_4 TS	445	448	153	110	107 i	4
Co_7/CH_4 DS	1056	1001	365			
Co_7/CD_4 DS	747	794	333			
Co_{13}/CH_4 TS	954i	629^b	349	167^b	35	2
Co_{13}/CD_4 TS	690i	445^b	321	153^b	27	2
Co_{13}/CH_4 DS	1947	1068	556			
Co_{13}/CD_4 DS	1544	756	507			

^{a} parallel modes of the Ni_7-cluster.

^{b} parallel modes of the Co_7-cluster.

best compared with the normal frequencies of CH_4 and CD_4. We find for the CH stretch a frequency of 2951 cm^{-1} and for θ a frequency of 2438 cm^{-1}. For CD_4 these values are 2131 cm^{-1} and 1929 cm^{-1}, respectively. The experimental values are 2917/3019 cm^{-1} for the symmetrical/asymmetrical normal stretch mode, and 1534 cm^{-1} for the normal bending modes of CH_4. For CD_4 these values are 2109/2259 cm^{-1} and 1092 cm^{-1}, respectively[38]. Our values for the CH stretch seem thus correct, whereas for the CH_3 tilt they are 800–900 cm^{-1} too high. This is due to the fact that we calculated the pure stretch and θ and not the normal coordinates, which lower the frequencies. Our choice of modes, however, results in the partition function cancellation as discussed above. For the 7-atom clusters, the imaginary frequency at the TS is strongly dominated by a mixture of all modes. On the

13-atom clusters it consists almost purely of the CH stretch and in this case we estimated the quantum chemical tunneling effect on the reaction rate. The low vibrational frequencies indicate a loose transition state. Now, according to eqns. (4.3)–(4.4) rate constants can be calculated. The results are shown in table 4.4 for CH_4 and CD_4 at different temperatures. Sticking coefficients (S) are calculated as follows. First, we calculated the Hard Sphere pre-exponential (A^{HS}).

$$A^{HS} = \sqrt{\frac{k_B T}{2\pi\, m_{CH4}}}.$$

(4.5)

This is related to the number of collisions of CH_4 with the substrate per unit time, $dN^{col}_{CH_4}/dt$, via

$$\frac{d}{dt}N^{col}_{CH_4} = S\,\frac{N_{CH_4}}{V}A^{HS},$$

(4.6)

where N_{CH_4} is the number of CH_4 gas molecules, V is the volume, and S is the surface area (see also the appendix). The sticking coefficient is now simply the ratio of $k_{dis.ads.}$ and A^{HS} and is therefore effectively the reaction probability per hard sphere collision. Our computed sticking coefficients are clearly too low on the 7-atom clusters as a result of the very high dissociation barriers. This defect is remedied when we use the 13-atom models as substrate models. Beebe *et al.*[29] gave experimental values for the sticking coefficient at $T = 500$ K of 10^{-8}–10^{-7} for Ni(111), Ni(100) and Ni(110) surfaces. Our sticking coefficients on Ni_{13} at $T = 500$ K are of the order 10^{-10}, which is somewhat too small, and our dissociation barrier of 121 kJ/mol is somewhat too high. If we substitute for our calculated E_{crit} the experimental measured values by Lee *et al.*[13] (CH_4: 50 kJ/mol; CD_4: 59 kJ/mol), we obtain sticking coefficients of 10^{-8}–10^{-7} at $T = 500$ K. This illustrates that accurate sticking coefficients can be calculated with our model. The main remaining problem is a correct computation of the activation barrier. The isotope substitution ratio is almost constant for associative desorption (a factor two), but varies significantly for dissociative adsorption. Our (classical) computed ratio of 3.47/4.07 on Ni_7/Ni_{13} at $T = 750$ K is approximately half the value measured in this temperature region[13], but tunneling effects will decrease this discrepancy. An estimate of these tunneling effects is not as straightforward for the 7-atom clusters as for our single metal atom study, because now the reaction coordinate is not described by the CH stretch mode alone, instead it is a mixture of all modes. As a consequence, we did not make an estimate of tunneling effects for the 7-atom clusters. For the 13-atom clusters the imaginary frequency is almost the pure CH stretch mode and an estimate of tunneling effects can be made. Γ^* gives the ratio of quantum chemical rate to classical chemical rate, and the high imaginary frequency of the 13-atom clusters is reflected in the large values of Γ^*, especially at low temperatures.

Table 4.4. Rate constant for dissociative adsorption ($k_{dis.ads.}$) (m s^{-1}) and isotopic substitution ratio, rate constant for associative desorption ($k_{ass.des.}$) (m^2 s^{-1}) and isotopic substitution ratio, classical sticking coefficients (S^{TST}), quantum sticking coefficients (S^{QM}) and ratio of quantum chemical rate to classical chemical rate (Γ^*) for the cluster models.

System	T	$k_{dis.ads.}$	k^{CH_4}/k^{CD_4}	$k_{ass.des.}$	k^{CH_4}/k^{CD_4}	S^{TST}	S^{QM}	Γ^*
Ni$_7$/CH$_4$	250	$9.22 \cdot 10^{-39}$		$9.17 \cdot 10^{-22}$		$6.42 \cdot 10^{-41}$		
Ni$_7$/CD$_4$	250	$3.05 \cdot 10^{-40}$	30.27	$2.23 \cdot 10^{-22}$	4.11	$2.37 \cdot 10^{-42}$		
Ni$_7$/CH$_4$	500	$8.74 \cdot 10^{-19}$		$1.61 \cdot 10^{-14}$		$4.30 \cdot 10^{-21}$		
Ni$_7$/CD$_4$	500	$1.45 \cdot 10^{-19}$	6.03	$6.93 \cdot 10^{-15}$	2.32	$7.98 \cdot 10^{-22}$		
Ni$_7$/CH$_4$	750	$6.56 \cdot 10^{-12}$		$5.82 \cdot 10^{-12}$		$2.64 \cdot 10^{-14}$		
Ni$_7$/CD$_4$	750	$1.89 \cdot 10^{-12}$	3.47	$2.97 \cdot 10^{-12}$	1.96	$8.51 \cdot 10^{-15}$		
Ni$_7$/CH$_4$	1000	$2.31 \cdot 10^{-08}$		$1.27 \cdot 10^{-10}$		$8.03 \cdot 10^{-11}$		
Ni$_7$/CD$_4$	1000	$8.62 \cdot 10^{-09}$	2.68	$6.96 \cdot 10^{-11}$	1.82	$3.36 \cdot 10^{-11}$		
Ni$_{13}$/CH$_4$	250	$2.05 \cdot 10^{-18}$		$4.17 \cdot 10^{-23}$		$1.43 \cdot 10^{-20}$	$5.50 \cdot 10^{-20}$	3.862
Ni$_{13}$/CD$_4$	250	$5.14 \cdot 10^{-20}$	39.80	$6.27 \cdot 10^{-24}$	6.65	$4.00 \cdot 10^{-22}$	$7.48 \cdot 10^{-22}$	1.870
Ni$_{13}$/CH$_4$	500	$8.08 \cdot 10^{-08}$		$2.35 \cdot 10^{-14}$		$3.98 \cdot 10^{-10}$	$5.29 \cdot 10^{-10}$	1.330
Ni$_{13}$/CD$_4$	500	$1.12 \cdot 10^{-08}$	7.21	$7.86 \cdot 10^{-15}$	3.00	$6.17 \cdot 10^{-11}$	$7.14 \cdot 10^{-11}$	1.158
Ni$_{13}$/CH$_4$	750	$4.67 \cdot 10^{-04}$		$2.88 \cdot 10^{-11}$		$1.88 \cdot 10^{-06}$	$2.13 \cdot 10^{-06}$	1.134
Ni$_{13}$/CD$_4$	750	$1.15 \cdot 10^{-04}$	4.07	$1.21 \cdot 10^{-11}$	2.39	$5.16 \cdot 10^{-07}$	$5.51 \cdot 10^{-07}$	1.068
Ni$_{13}$/CH$_4$	1000	$4.58 \cdot 10^{-02}$		$1.18 \cdot 10^{-09}$		$1.59 \cdot 10^{-04}$	$1.24 \cdot 10^{-04}$	1.074
Ni$_{13}$/CD$_4$	1000	$1.47 \cdot 10^{-02}$	3.12	$5.42 \cdot 10^{-10}$	2.18	$5.72 \cdot 10^{-05}$	$5.94 \cdot 10^{-05}$	1.038
Co$_7$/CH$_4$	250	$1.94 \cdot 10^{-39}$		$1.76 \cdot 10^{-23}$		$1.35 \cdot 10^{-41}$		
Co$_7$/CD$_4$	250	$5.73 \cdot 10^{-41}$	33.86	$5.50 \cdot 10^{-24}$	3.20	$4.46 \cdot 10^{-43}$		
Co$_7$/CH$_4$	500	$6.37 \cdot 10^{-19}$		$3.31 \cdot 10^{-15}$		$3.13 \cdot 10^{-21}$		
Co$_7$/CD$_4$	500	$1.00 \cdot 10^{-19}$	6.37	$1.58 \cdot 10^{-15}$	2.09	$5.51 \cdot 10^{-22}$		
Co$_7$/CH$_4$	750	$7.31 \cdot 10^{-12}$		$5.82 \cdot 10^{-12}$		$2.94 \cdot 10^{-14}$		
Co$_7$/CD$_4$	750	$2.02 \cdot 10^{-12}$	3.62	$2.97 \cdot 10^{-12}$	1.96	$9.09 \cdot 10^{-15}$		
Co$_7$/CH$_4$	1000	$3.19 \cdot 10^{-08}$		$7.95 \cdot 10^{-11}$		$1.11 \cdot 10^{-10}$		
Co$_7$/CD$_4$	1000	$1.15 \cdot 10^{-08}$	2.78	$4.40 \cdot 10^{-11}$	1.81	$4.47 \cdot 10^{-11}$		
Co$_{13}$/CH$_4$	250	$4.27 \cdot 10^{-16}$		$3.90 \cdot 10^{-25}$		$2.97 \cdot 10^{-18}$	$1.63 \cdot 10^{-17}$	5.476
Co$_{13}$/CD$_4$	250	$1.05 \cdot 10^{-17}$	40.60	$5.56 \cdot 10^{-26}$	7.02	$8.19 \cdot 10^{-20}$	$1.75 \cdot 10^{-19}$	2.141
Co$_{13}$/CH$_4$	500	$1.07 \cdot 10^{-06}$		$2.20 \cdot 10^{-15}$		$5.29 \cdot 10^{-09}$	$7.44 \cdot 10^{-09}$	1.407
Co$_{13}$/CD$_4$	500	$1.47 \cdot 10^{-07}$	7.32	$7.04 \cdot 10^{-16}$	3.13	$8.08 \cdot 10^{-10}$	$9.62 \cdot 10^{-10}$	1.191
Co$_{13}$/CH$_4$	750	$2.48 \cdot 10^{-03}$		$5.83 \cdot 10^{-12}$		$9.97 \cdot 10^{-06}$	$1.16 \cdot 10^{-05}$	1.162
Co$_{13}$/CD$_4$	750	$6.01 \cdot 10^{-04}$	4.13	$2.36 \cdot 10^{-12}$	2.47	$2.70 \cdot 10^{-06}$	$2.92 \cdot 10^{-06}$	1.081
Co$_{13}$/CH$_4$	1000	$1.54 \cdot 10^{-01}$		$3.52 \cdot 10^{-10}$		$5.36 \cdot 10^{-04}$	$5.84 \cdot 10^{-04}$	1.089
Co$_{13}$/CD$_4$	1000	$4.87 \cdot 10^{-02}$	3.16	$1.57 \cdot 10^{-10}$	2.28	$1.90 \cdot 10^{-04}$	$1.98 \cdot 10^{-04}$	1.045

   Tunneling is easier through a sharply peaked barrier, which is characterised by a high imaginary frequency. The isotope effect is more clearly seen from fig. 4.4–4.5, which show Arrhenius plots for the adsorption/desorption of CH_4/CD_4 on Ni_7 (fig. 4.4 (top)), Co_7 (fig. 4.4 (middle)), Ni_{13} (fig. 4.5 (top)), and Co_{13} (fig. 4.5 (middle)). Fig. 4.4 (bottom) and fig. 4.5 (bottom) compare CH_4 adsorption/desorption on Ni_7/Co_7 and Ni_{13}/Co_{13} respectively. The plot data is summerised in table 4.5.   The electronic energy, E,

Table 4.5. Electronic energy (E) (kJ/mol), critical energy (E_{crit}) (kJ/mol), activation energy (E_{act}) (kJ/mol), and Arrhenius pre-exponential (A^{plot}) for dissociative adsorption (m s^{-1}) and associative desorption (m^2 s^{-1}) for the cluster models.

System	Reaction	E	E_{crit}	E_{act}	A^{plot}
Ni_7/CH_4	dissociative adsorption	214	188	194	$2.11 \cdot 10^{+02}$
Ni_7/CD_4	dissociative adsorption	214	194	200	$1.77 \cdot 10^{+02}$
Ni_7/CH_4	associative desorption	72	66	71	$5.15 \cdot 10^{-07}$
Ni_7/CD_4	associative desorption	72	68	73	$3.77 \cdot 10^{-07}$
Ni_{13}/CH_4	dissociative adsorption	121	96	104	$8.53 \cdot 10^{+03}$
Ni_{13}/CD_4	dissociative adsorption	121	103	111	$6.47 \cdot 10^{+03}$
Ni_{13}/CH_4	associative desorption	91	78	86	$2.70 \cdot 10^{-05}$
Ni_{13}/CD_4	associative desorption	91	81	89	$1.86 \cdot 10^{-05}$
Co_7/CH_4	dissociative adsorption	216	193	199	$5.41 \cdot 10^{+02}$
Co_7/CD_4	dissociative adsorption	216	199	206	$4.53 \cdot 10^{+02}$
Co_7/CH_4	associative desorption	81	75	81	$1.65 \cdot 10^{-06}$
Co_7/CD_4	associative desorption	81	77	83	$1.11 \cdot 10^{-06}$
Co_{13}/CH_4	dissociative adsorption	110	85	92	$7.24 \cdot 10^{+03}$
Co_{13}/CD_4	dissociative adsorption	110	91	99	$5.43 \cdot 10^{+03}$
Co_{13}/CH_4	associative desorption	102	88	95	$2.53 \cdot 10^{-05}$
Co_{13}/CD_4	associative desorption	102	91	98	$1.72 \cdot 10^{-05}$

gives the energy difference between the TS, the DS and the reactant on the electronic potential energy surface (not including zero point energies). In the critical energy, E_{crit}, the differences in zero point energy for the TS, the DS and the reactant have been taken into account. The slope of the Arrhenius plots is reflected in the activation energy, E_{act}, and the intercept in the pre-exponential, A^{plot}. We see that inclusion of zero-point energies lowers the dissociation barrier of Ni_7/CH_4 by 26 kJ/mol reflecting the relatively low frequencies at the TS and the high stretch frequency of CH_4. Isotopic substitution lowers vibrational frequencies for both the TS and Ni_7/CH_4. The barrier is therefore reduced by only 20 kJ/mol.
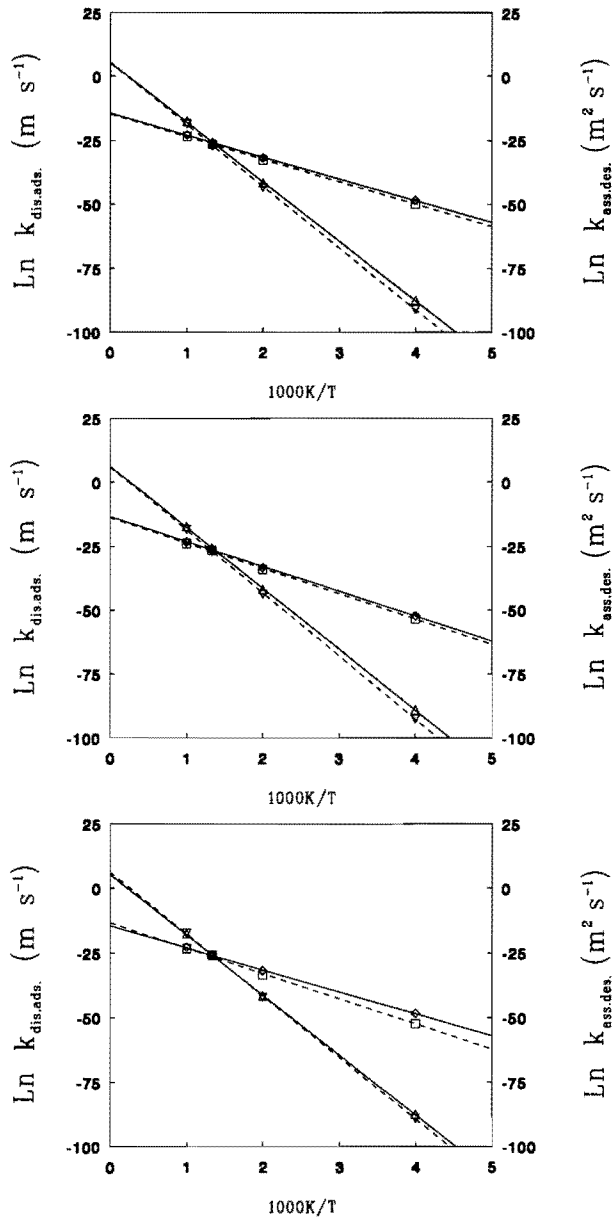
Fig. 4.4.
Arrhenius plots for dissociative adsorption ($k_{dis.ads.}$) and associative desorption ($k_{ass.des.}$) of $Ni_7/CH_4/CD_4$ (top), $Co_7/CH_4/CD_4$ (middle), and $Ni_7/Co_7/CH_4$ (bottom). Markers are: $\triangle$: $k_{dis.ads.}$ $Ni_7/Co_7/CH_4$, ∇: $k_{dis.ads.}$ $Ni_7/Co_7/CD_4$, $\diamond$: $k_{ass.des.}$ $Ni_7/Co_7/CH_4$, $\square$: $k_{ass.des.}$ $Ni_7/Co_7/CD_4$.
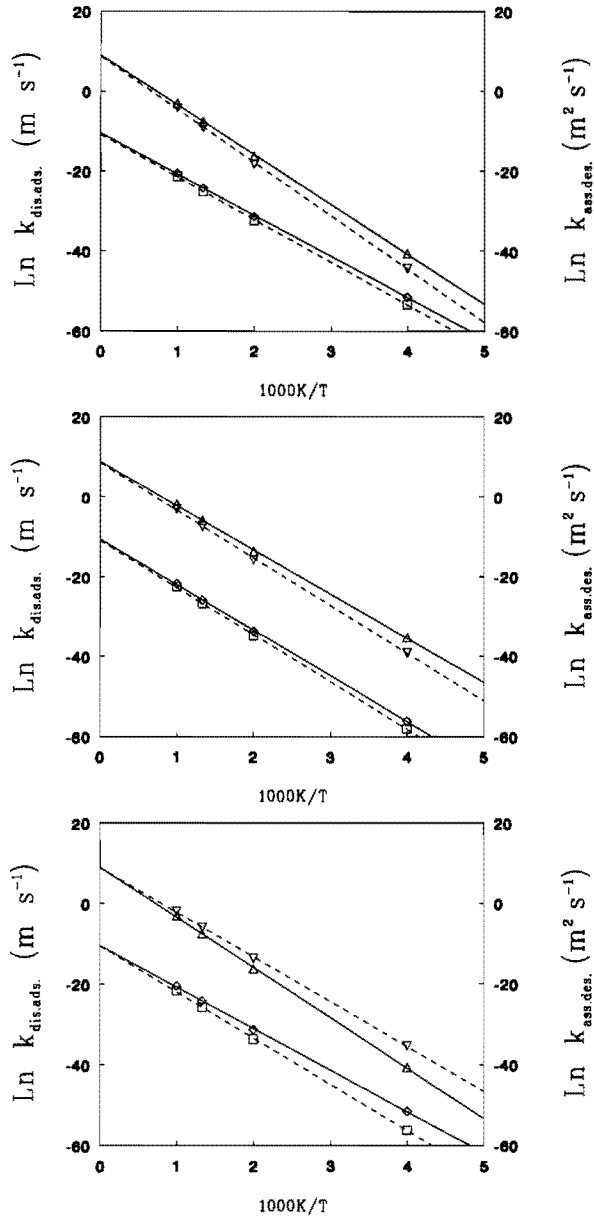
Fig. 4.5.
Arrhenius plots for dissociative adsorption ($k_{dis.ads.}$)/ associative desorption ($k_{ass.des.}$) of $Ni_{13}/CH_4/CD_4$ (top), $Co_{13}/CH_4/CD_4$ (middle), and $Ni_{13}/Co_{13}/CH_4$ (bottom). Markers are: $\triangle$: $k_{dis.ads.}$ $Ni_{13}/Co_{13}/CH_4$, $\triangledown$: $k_{dis.ads.}$ $Ni_{13}/Co_{13}/CD_4$, $\diamond$: $k_{ass.des.}$ $Ni_{13}/Co_{13}/CH_4$, $\square$: $k_{ass.des.}$ $Ni_{13}/Co_{13}/CD_4$.

We see a similar trend for the desorption barrier, but the effect is less pronounced (6 kJ/mol for Ni_7/CH_4 and 4 kJ/mol for Ni_7/CD_4). The activation energy, E_{act}, displays the effect on the barrier, when excited rotational and vibrational levels are populated: a temperature-averaged barrier. The population of high vibrational frequency excited levels, e.g. the CH stretch mode in the reactant or the MH stretch mode in the DS, will remain small at elevated temperatures due to their high frequency and thereby associated high energy. On the contrary, the population of relatively low vibrational frequency excited levels, as those found in the TS, will strongly increase. This is reflected in both the vibrational partition functions and the increase of the insertion barrier (6 kJ/mol for $Ni_7/CH_4/CD_4$ adsorption, 5 kJ/mol for $Ni_7/CH_4/CD_4$ desorption). The absolute value of the temperature-averaged barrier will depend on the values of the translational, vibrational and rotational partition functions at the TS, the DS and the reactant for different temperatures. Similar behaviour is seen for the adsorption/desorption of Ni_{13}/CH_4, Ni_{13}/CD_4, Co_7/CH_4, Co_7/CD_4, Co_{13}/CH_4, and Co_{13}/CD_4.

The pre-exponential factor is connected with the change in entropy in going from reactant to the TS, the entropy of activation ($\Delta S^{\ddagger}$), and is thus a measure of the gain or loss in entropy. If $\Delta S^{\ddagger}$ equals zero, the pre-exponential is approximately 10^2 m s^{-1} for an adsorption reaction and 10^{-6} m^2 s^{-1} for a bimolecular desorption reaction[27]. The pre-exponentials for adsorption denote therefore that there is essentially no entropy of activation. This can be understood by realising that although three relative translations are lost going from Ni_7/CH_4 to the TS, the vibrations at TS are very loose modes and the activated CH_4 can rotate freely on the surface. For the desorption reaction some entropy is lost. Four translation modes are lost in going from the DS to the DS, but this is once again counteracted by the very loose vibrations in the TS, thus limiting the overall effect.

4.5 Conclusions

We have carried out DFT calculations to determine the TS, the DS, height and origin of the barrier for reactions (4.1)–(4.2). In addition, we calculated rotational and vibrational frequencies and used transition state theory to calculate rate constants and sticking coefficients. On a Ni_7-cluster a barrier for dissociative chemisorption of 214 kJ/mol was found. The barrier for associative desorption is 72 kJ/mol. The higher dissociation barrier with respect to our single nickel atom study is attributed to the intrinsic decrease in reactivity of the central nickel atom at which the activated CH_4 chemisorbs, due to the surrounding neighbouring nickel atoms. In addition the CH bond is more stretched than in the one atom case. Our kinetic analysis showed that we can reproduce experimental sticking coefficients, provided we use the experimental barrier height. Therefore, the main remaining problem is an accurate computation of the height of the dissociation barrier. Although our Ni_7-cluster does not represent an infinite Ni(111) surface properly, the error made in adopting this cluster is the same for both the TS and the DS, thus providing an accurate account of the association barrier height. We have shown that extending the cluster by adding more atoms in a single layer or including second or third layers does indeed lower the energy, but only for the Ni_{13}-cluster does the dissociation barrier decrease dramatically. However, in making these comparisons we have not explicitly optimised the TS. On Co_7 the CH_4 dissociation barrier is 216 kJ/mol. The CH_3/H association barrier is 9 kJ/mol lower on Ni_7 and the value of 72 kJ/mol for nickel compares very well with the reported value of Zaera[34] of 71 kJ/mol on platinum. When explicitly optimising the TS on the 13-atom clusters, the CH_4 dissociation barrier drops sharply to 121 kJ/mol for nickel and 110 kJ/mol for cobalt. The association barriers are now 91 kJ/mol on nickel and 102 kJ/mol on cobalt. Also the endothermicity now drops to 30 kJ/mol for nickel and 8 kJ/mol on cobalt.

Calculated frequencies and rate coefficients could only partially be compared with experimental data. Frequencies for CH_4 are too high, because normal modes were not calculated. The frequency shift for CD_4 appears to be correct. Calculated pre-exponentials were connected with change in entropy for dissociation and association. They indicate a loose transition state.

Calculated sticking coefficients on the Ni_{13}-cluster at $T = 500$ K are two orders of magnitude away from the experimental ones. This is due to the computed barrier height (121 kJ/mol), which is still significantly higher than the experimental value (53 kJ/mol). We also made an estimate of hydrogen and deuterium tunneling effects for the 13-atom clusters, which turned out to be small, except at low temperatures.

4.6 References

1. F. Fischer, H. Tropsch, Brennst. Chem. **7** (1926) 97.
   F. Fischer, H. Tropsch, Chem. Ber. **59** (1926) 830.

2. J.T. Yates Jr., S.M. Gates, J.N. Russell Jr., Surf. Sci. **164** (1985) L839.

3. R.C. Brady III, R. Pettit, J. Am. Chem. Soc. **102** (1980) 6181.
   R.C. Brady III, R. Pettit, J. Am. Chem. Soc. **103** (1981) 1287.

4. J.P. Van Hook, Catal. Rev. Sci. Eng. **21** (1980) 1.

5. J.R. Rostrup-Nielsen, *Catalysis- science and technology, Vol. 5,*
   edited by J.R. Anderson and M. Boudart (Springer-Verlag, Berlin, 1984).

6. H. Burghgraef, A.P.J.Jansen, R.A. van Santen, J. Chem. Phys. **98** (1993) 8810.

7. H. Yang, J.L. Whitten, J. Chem. Phys. **89** (1988) 5329.

8. H. Yang, J.L. Whitten, J. Chem. Phys. **91** (1989) 126.

9. H. Yang, J.L. Whitten, J. Am. Chem. Soc. **113** (1991) 6442.

10. H. Yang, J.L. Whitten, J. Chem. Phys. **96** (1992) 5529.

11. O. Swang, K. Faegri Jr, O. Gropen, U. Wahlgren, P.E.M. Siegbahn,
    Chem. Phys. **156** (1991) 379.

12. J. Schüle, P.E.M. Siegbahn, U. Wahlgren, J. Chem. Phys. **89** (1988) 6982.

13. M.B. Lee, Q.Y. Yang, S.L. Tang, S.T. Ceyer, J. Chem. Phys. **85** (1986) 1693.
    M.B. Lee, Q.Y. Yang, S.T. Ceyer, J. Chem. Phys. **87** (1987) 2724.
    S.T. Ceyer, J.D. Beckerle, M.B. Lee, S.L. Tang, Q.Y. Yang, M.A. Hines,
    J. Vac. Sci. Tech. A **5** (1987) 501.

14. P.E.M. Siegbahn, I. Panas, Surf. Sci. **240** (1990) 37.

15. A.C. Luntz, D.S. Bethune, J. Chem. Phys. **90** (1989) 1274.

16. A.C. Luntz, J. Harris, Surf. Sci. **258** (1991) 397.
    A.C. Luntz, J. Harris, J. Vac. Sci. Tech. A **10** (1992) 2292.

17. Amsterdam density-functional (ADF) programme developed by Baerends *et al.*.
    E.J. Baerends, D.E. Ellis, P. Ros, Chem. Phys. **2** (1973) 41.
    P.M. Boerrigter, G. te Velde, E.J. Baerends, Int. J. Quantum Chem. **33** (1988) 87.
    G. te Velde, E.J. Baerends, J. Comput. Phys. **99** (1992) 84.
    D. Post, E.J. Baerends, J. Chem. Phys. **78** (1983) 5663.
    E.J. Baerends, A. Rozendaal, *Quantum chemistry: the challenge of transition metals and coordination chemistry,* edited by A. Veillard (Reidel, Dordrecht, 1986).
    P.J. van den Hoek, A.W. Kleyn, E.J. Baerends,
    Comm. Atom. Molec. Phys. **23** (1989) 93.

18. D.M. Ceperley, B.J. Alder, Phys. Rev. Lett. **45** (1980) 566.

19. S.H. Vosko, L. Wilk, M. Nusair, Can. J. Phys. **58** (1980) 1200.
    J.P. Perdew, A. Zunger, Phys. Rev. B **23** (1981) 5048.
20. A.D. Becke, Int. J. Quantum Chem. **27** (1985) 585.
21. A.D. Becke, Phys. Rev. A **38** (1988) 3098.
22. H. Stoll, C.M.E. Pavlidou, H. Preuss, Theor. Chim. Acta **49** (1978) 143.
    H. Stoll, E. Golka, H. Preuss, Theor. Chim. Acta **55** (1980) 29.
23. T. Ziegler, A. Rauk, Theor. Chim. Acta **46** (1977) 1.
24. J.G. Snijders, E.J. Baerends, Mol. Phys. **36** (1978) 1789.
    J.G. Snijders, E.J. Baerends, P. Ros, Mol. Phys. **38** (1979) 1909.
25. H.S. Johnston, J. Heicklen, J. Phys. Chem. **66** (1962) 532.
    H.S. Johnston, D. Rapp, J. Am. Chem. Soc. **83** (1961) 1.
26. E.B. Wilson, J.C. Decius, P.C. Cross, *Molecular vibrations. Theory of infrared and raman vibrational spectra* (McGraw-Hill, New York, 1955).
27. R.G. Gilbert, S.C. Smith, *Theory of unimolecular and recombination reactions* (Blackwell, Oxford, 1990).
    M. Boudart, G. Djéga-Mariadassou, *Kinetics of heterogeneous catalytic reactions* (Princeton University Press, Princeton, N.J 1984).
28. M.R. Blomberg, U. Brandemark, P.E.M. Siegbahn, J. Am. Chem. Soc. **105** (1983) 5557.
    M.R. Blomberg, P.E.M. Siegbahn, U. Nagashima, J. Wennerberg, J. Am. Chem. Soc. **113** (1991) 424.
29. T.P. Beebe, D.W. Goodman, B.D. Kay, J.T. Yates, J. Chem. Phys. **87** (1987) 2305.
30. I. Panas, P.E.M. Siegbahn, U. Wahlgren, *The challenge of d and f electrons. Theory and computation*, edited by D.R. Salahub and M.C. Zerner, (ACS, Washington DC, 1989).
31. C. Kittel, *Introduction to solid state physics* (Wiley, New York, 1953).
32. I. Chorkendorff, I. Alstrup, S. Ullmann, Surf. Sci. **227** (1990) 291.
33. J.C.C. Geerlings, M.C. Zonnevylle, C.P.M. de Groot, Surf. Sci. **241** (1991) 302.
34. F. Zaera, Surf. Sci. **262** (1992) 335.
35. K. Christmann, R.J. Behm, G. Ertl, M.A. Van Hove, W.H. Weinberg, J. Chem. Phys. **70** (1979) 4168.
36. K. Christmann, O. Schober, G. Ertl, M. Neumann, J. Chem. Phys. **60** (1974) 4528.
37. W. Ho, N.J. DiNardo, D.E. Plummer, J. Vac. Sci. Tech. **17** (1980) 314.
38. *CRC Handbook of chemistry and physics*, edited by D.R. Lide, (CRC Press, Boca Raton, 1990).

4.7   Appendix: derivation of rate constant equations

As a starting point, we can write down the following for the dissociative adsorption:

$$\frac{d}{dt}\,N_{CH_{4a}} = k^{TST}_{dis.ads.}\,N_{CH_4}. \tag{4.7}$$

Here, $N_{CH_{4a}}$ is the number of dissociatively adsorbed CH_4 molecules. N_{CH_4} is the number of CH_4 molecules in the gas phase, and $k^{TST}_{dis.ads.}$ is the transition state theory reaction rate constant given by:

$$k^{TST}_{dis.ads.} = \frac{k_B T}{h}\,\frac{Q^{\dagger}_{v_1}\,..\,Q^{\dagger}_{v_6}}{Q_{t_1}Q_{t_2}Q_{t_3}Q_{r_1}Q_{r_2}Q_{v_1}Q_{v_2}}e^{\frac{-E_{crit}}{k_B T}}. \tag{4.8}$$

The translational partition functions Q_{t_1}, Q_{t_2}, and Q_{t_3} can be combined to

$$(2\pi m_{CH_4} k_B T/h^2)^{3/2}\,V. \tag{4.9}$$

All vibrational partition functions Q_v are of the form

$$\frac{1}{1 - e^{-\frac{h\nu}{k_B T}}}. \tag{4.10}$$

The rotational partition functions Q_{r_1}, and Q_{r_2} are each of the form

$$\frac{C\,I_{CH4}k_B T}{2\pi^2 h^2}. \tag{4.11}$$

In eqns. (4.8)–(4.11), k_B denotes Boltzmann's constant, T temperature, h Planck's constant, E_{crit} the barrier energy including zero-point energy differences, ν the frequency of the particular vibrational mode, V the volume of the gas container, m_{CH_4} the CH_4 mass, I_{CH_4} the moment of inertia of CH_4, and C a constant depending on the symmetry factor of the species.

As a consequence of our loose TS, the activated CH_4 is not bound to one specific site, and the partition functions for the two vibrational modes parallel to the surface, i.e., the CH stretch and a combination of the CH_3 and H modes parallel to the surface and perpendicular to the mirror plane, yield an additional factor N_{sites}, the number of sites. Instead of changing the partition function, we can also multiply the right-hand-site of eq. (4.7) by N_{sites}, which results in

$$\frac{d}{dt} N_{CH_{4a}} = k_{dis.ads.}^{TST} N_{sites} N_{CH_4},$$ (4.12)

or equivalently,

$$\frac{d}{dt} N_{CH_{4a}} = k_{dis.ads.}^{TST} \frac{S}{\sigma_{site}} N_{CH_4},$$ (4.13)

where S is the total surface area and σ_{site} the site area, which is $5.38 \cdot 10^{-20}$ m^{-2} for a Ni(111) surface. eq. (4.13) can be rearranged in terms of surface concentrations (left-hand-side) and volume concentrations (right-hand-side) to

$$\frac{1}{S}\frac{d}{dt} N_{CH_{4a}} = \frac{k_{dis.ads.}^{TST}}{\sigma_{site}} V[CH_4],$$ (4.14)

or

$$\frac{d}{dt} [CH_4]_a = k_{dis.ads.}[CH_4].$$ (4.15)

We therefore have $k_{dis.ads.} = (k_{dis.ads.}^{TST} V)/\sigma_{site}$

Note that the volume V in eqns. (4.9) and (4.14) cancels.

As a starting point for the associative desorption per site, we can write down the following:

$$\frac{d}{dt} N_{CH_{4a}} = -k_{ass.des.}^{TST} N_{CH_{3a}} N_{H_a}. \tag{4.16}$$

Here, $N_{CH_{4a}}$ is the number of associatively desorbing CH_4 molecules. $N_{CH_{3a}}$ and N_{H_a} are the number of CH_{3a} and H_a particles adsorbed on the surface, and $k_{ass.des.}^{TST}$ is the transition state theory formula for the rate constant for mobile adsorption:

$$k_{ass.des.}^{TST} = \frac{k_B T}{h} \frac{Q_{v_1}^{\dagger} \cdot\cdot Q_{v_6}^{\dagger}}{Q_{t_1,CM} Q_{t_2,CM} Q_{t_1,\mu} Q_{t_2,\mu} Q_{v_1} \cdot\cdot Q_{v_3}} e^{\frac{-E'_{crit}}{k_B T}}. \tag{4.17}$$

We have discussed before the form of the vibrational partition functions. The absolute translational partition functions $Q_{t1,CM}$ and $Q_{t2,CM}$ can be combined to

$$\frac{2\pi M_{CH_3 H} k_B T}{h^2} S. \tag{4.18}$$

The relative translational partition functions $Q_{t1,\mu}$ and $Q_{t2,\mu}$ can be combined to

$$\frac{2\pi \mu_{CH_3 H} k_B T}{h^2} S. \tag{4.19}$$

In eqns. (4.18)–(4.19) $M_{CH_3 H}$ is the absolute mass of CH_3 and H, $\mu_{CH_3 H}$ is the reduced mass of CH_3 and H, and S the total surface area as discussed before.

Taking into account the mobility of our transition state, eq. (4.16) results in:

$$\frac{d}{dt} N_{CH_{4a}} = -k_{ass.des.}^{TST} \frac{S}{\sigma_{site}} N_{CH_{3a}} N_{H_a}, \tag{4.20}$$

or

$$\frac{1}{S} \frac{d}{dt} N_{CH_{4a}} = -\frac{k_{ass.des.}^{TST}}{\sigma_{site}} N_{CH_{3a}} N_{H_a}, \tag{4.21}$$

or equivalently

$$\frac{1}{S} \frac{d}{dt} N_{CH_{4a}} = -\frac{k_{ass.des.}^{TST}}{\sigma_{site}} S S \frac{N_{CH_{3a}}}{S} \frac{N_{H_a}}{S}, \tag{4.22}$$

which in terms of surface concentrations results eventually in

$$\frac{d}{dt} [CH_4]_a = -k_{ass.des.}[CH_3]_a [H]_a. \tag{4.23}$$

We therefore have $k_{ass.des.} = (k_{ass.des.}^{TST} S S)/\sigma_{site}$

Note that the surface S in eqns. (4.18)–(4.19) and (4.22) cancels.

Chapter 5

CC coupling on nickel and cobalt. Electronic structure calculations and kinetics

abstract

The CC coupling of C and CH (methylidyne), C and CH_2 (methylene), and C and CH_3 (methyl) on nickel has been studied with density functional theory using 7- and 13-atom cluster models. Formation of CCH_3 (ethylidyne) turned out to be the most exothermic reaction on both clusters. Experimentally, CCH_3 has been identified unambiguously with a structure perpendicular to the metal surface. Thus, for the C/CH_3 coupling forming CCH_3, we have determined the structure and potential energy surface in the coadsorbed state, transition state, and CC-formed state. The transition state is explicitly determined on the 7-atom cluster and the 13-atom cluster of both nickel and cobalt. We find transition state barriers of 57 kJ/mol for the Ni_7-cluster, 55 kJ/mol for the Co_7-cluster, 84 kJ/mol for the Ni_{13}-cluster and 47 kJ/mol for the Co_{13}-cluster. The overall reaction energies are -215 kJ/mol, -184 kJ/mol, -66 kJ/mol, and -89 kJ/mol, respectively. Analysis of the TS shows a dominant contribution of the CC bond to the reaction coordinate. Cluster size effects play a role in all studied CC coupling reactions.

5.1   Introduction

A very interesting and important topic in heterogeneous catalysis is the conversion of CH_4 to higher hydrocarbons. A well known method for CH_4 activation is its steam reforming producing CO and H_2 followed by the so-called Fischer-Tropsch synthesis to various hydrocarbons[1]. Whether CH_4 or higher hydrocarbons are produced depends strongly on the metal catalyst and on reaction conditions, but on Fe, Co and Ru a wide range of hydrocarbons is formed, whereas over Ni and Pd CH_4 is the principal product, while Cu shows no reaction at all[2]. Kaminsky *et al.*[3] have detected CH_3, CH_2, and CH as intermediates on Ni(111). An alternative, direct route is dissociation of CH_4 to CH_x-species over a transition metal catalyst at temperatures between 600–900 K, followed by CC coupling and hydrogenation at temperatures around 370 K[4]. Again, the role of the metal is important: Ru and Co give a wide range of products as does Ni but in much lower yields, Pt yields only C_1- and C_2 products, while Cu and Pd show no CC coupling at all. Goodman and coworkers have identified C, CH, CCH_2 (vinylidene), and CCH_3 on Ru for this reaction using HREELS and TPD[5]. Belgued *et al.*[6] reported conversion of CH_4 on Pt producing higher hydrocarbons up to C_6-species.

Another important reaction in catalysis is C_2H_4 (ethylene) adsorption and its subsequent decomposition, which is well studied on Pt(111). Various mechanisms for C_2H_4 decomposition have been suggested, but almost all agree on CCH_3 as the main product. Suggested intermediate structures are $CHCH_2$ (vinyl) and CCH_2[7], CH_2CH_3 (ethyl) and $CHCH_3$ (ethylidene)[8], or only $CHCH_3$[9] or $CHCH_2$[10]. Somorjai *et al.*[8] suggested a further decomposition of CCH_3 to CCH_2 and CCH (ethynyl). However, CCH_3 remains the only species from C_2H_4 decomposition on Pt(111), which has been identified unambiguously by various methods[11]. According to Fairbrother *et al.*[12], studying the reactions of adsorbed CH_3 on Pt(111), CH_3 reacts with H to form CH_4 or dehydrogenates to CH_2 and eventually C as shown by Zaera *et al.*[13]. These species can then form a CC bond. Again, CCH_3 has been identified. According to them, C_2H_4, CH_2CH_3 ,$CHCH_3$ and $CHCH_2$ can all be ruled out, leaving CCH_2 and CCH as the most likely other candidates. For the mechanism of CCH_3 formation Fairbrother *et al.*[12] suggest coupling of C and CH_3.

Zheng *et al.*[14] studied the CC coupling reactions of CH_3/CH_3, CH_3/CH_2 and CH_2/CH_2 on various transition metals using tight binding extended Hückel calculations and found a barrier for coupling CH_3/CH_3 and CH_3/CH_2 and an overall endothermicity. In contrast, the coupling between CH_2/CH_2 proceeded without a barrier and turned out to be exothermic. De Koster *et al.*[15] using atom superposition electron delocalisation molecular orbital (ASED-MO)-theory found on Rh(111) high barriers for coupling CH_3/CH_2, which they at-

tributed to strong steric repulsion between the hydrogen atoms. Koerts *et al.*[16], also using ASED-MO theory searched for a low coupling barrier between C/C, C/CH, C/CH$_2$, and C/CH$_3$. Except for C/CH$_2$, where a barrier of 95 kJ/mol was calculated, they found rather high barriers, but slightly exothermic overall reactions. The barrier height again correlated with the number of CH bonds, i.e. the highest barrier was found for C/CH$_3$ coupling followed by C/CH and C/C coupling. Kang and Anderson[7] studied theoretically ethylene and acetylene chemisorption on Pt(111) using again ASED-MO theory. They determined transition states and could thus compute activation barriers for their suggested intermediates. For CCH$_3$ they predicted a structure perpendicular to the surface, which is also found experimentally[17], for CCH$_2$ a bent structure, and the energetics of perpendicular and bent CCH turned out to be almost the same with a slight preference for the perpendicular structure. However, they computed a small barrier for CCH decomposition to form C and CH. Furthermore, for the rearrangement of CCH$_2$ to CCH$_3$ they computed a barrier of 203 kJ/mol and an endothermicity of 77 kJ/mol, which suggests no formation of CCH$_3$ at all, contrary to experiment. Instead, they suggested formation of CCH, which according to them is exothermic by 13 kJ/mol. Carter and Koel[18] estimated surface reaction energies and used these data to eliminate possible reaction pathways. According to them C$_2$H$_4$ adsorbs, isomerises to CH$_3$CH, dehydrogenates to CCH$_3$, which isomerises to CH$_2$CH, which dehydrogenates further to CHCH, CCH and finally CC. One of their conclusions is the absence of C and CCH$_2$. They predict that CH$_2$ is the most stable C$_1$-species and ethylidene (CHCH$_3$) the most stable C$_2$-species. Shustorovich *et al.*[19] used a bond order conservation (BOC)-model to study the decomposition of C$_2$H$_2$ (acetylene). According to them, this species is dehydrogenated to CHCH$_2$, followed by dehydrogenation to CCH$_2$, which is then predicted to isomerise to adsorbed CHCH, which then desorbs. In their model CCH$_3$ is not likely to form, contrary to experimental observations.

We can conclude that in both direct CH$_4$ dissociation and C$_2$H$_4$ decomposition CCH$_3$ plays an important role. In addition, almost every possible C$_2$H$_x$-species is proposed as an intermediate by theoreticians as well as experimentalists. We think that it is interesting to investigate the reaction between a fully dehydrogenated C-species and a CH$_3$-species, thereby avoiding the steric repulsion between hydrogen atoms, which results in a very high activation barrier as shown by others. Furthermore, the product CCH$_3$ has been detected by various methods and on various substrates, as discussed above. Therefore, we have calculated the potential energy surface at the coadsorbed state (CS), the transition state (TS) and the CC-formed state (CC^{f}S) of C/CH$_3$ using an *ab initio* density functional approach, and treated the kinetics of the system by employing transition state theory.

Specifically, we have taken a one layer 7-atom cluster, and a 13-atom spherical cluster of Ni and Co to model the substrate. Thus we have studied the following reactions:

$$CH_{3a} + C_a \overset{k^f_{cc}}{\rightleftharpoons} CCH_{3a}, \tag{5.1}$$

and

$$CCH_{3a} \overset{k^c_{cc}}{\rightleftharpoons} CH_{3a} + C_a. \tag{5.2}$$

In section 5.2 we give computational details, in section 5.3 we discuss the electronic structure results, in section 5.4 the kinetic results, and in section 5.5 we draw some conclusions.

5.2   Methods

We have performed quasi-relativistic calculations based on density functional theory (DFT) using the Amsterdam Density Functional programme package (ADF) developed by Baerends *et al.*[20]. The exchange-correlation potential used is based on quantum Monte Carlo simulations of Ceperley and Alder[21] of a homogeneous electron gas which has been parametrised by Vosko, Wilk and Nusair[22]. To correct for the overbinding inherent to the local density approximation (LDA)[23], we haved used a gradient corrected exchange energy functional[24] in combination with the Stoll correction[25] for correlation. For carbon a frozen core potential is used for the 1s electrons; for nickel and cobalt the electrons up to 3p are frozen. Relativistic effects were taken into account by first order perturbation theory[26]. The basis sets are of double ζ quality, with the exception of the nickel- and cobalt d-orbitals, which are triple ζ's. On all atoms polarisation functions are included. As models for the substrate, we have used a one layer 7-atom cluster and a spherical 13-atom cluster (fig. 3.1), which have been discussed extensively before. For nickel clusters the bond distance was fixed at the bulk value of 2.49 Å, for cobalt clusters at the bulk value of 2.50 Å. Adsorption energies are calculated using Ziegler's transition state method[27] and are given relative to the gas phase fragments with the same geometry. The CS was calculated by coadsorbing the two fragments at separated 3-fold sites at optimal adsorbate-substrate distances determined in previous studies[28]. The additional degrees of freedom of the CH_x fragments were not allowed to relax, i.e. for all CH_x species we kept the CH distances at 1.08 Å, the HCH angles at 109.48°, the substrate-CH angles of CH_3 at 109.48°, the substrate-CH angles of CH_2 at 125.26° and the substrate-CH angles of CH at 180°.

The TS of CCH$_3$ was explicitly calculated by a four dimensional grid in the MC$_1$, MC$_2$, and CC distances and the CH$_3$ tilt angle with respect to the activated CC bond (θ) (fig. 5.1). The grid point energies were fitted to a second-order polynomial in the MC$_1$, MC$_2$, and CC distances and θ. The CC^{f}S was determined by optimising the MC$_1$ and
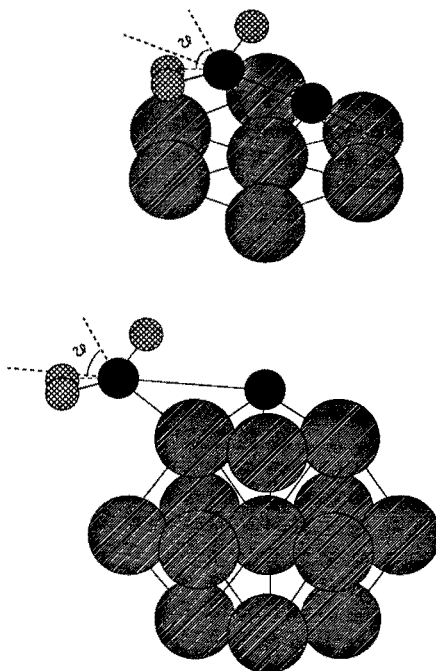
Fig. 5.1.
Definition of optimised parameters. Hydrogen atoms are denoted by diagonally cross-hatched circles, carbon atoms by filled black circles, and transition metal atoms by diagonally hatched circles. One dotted line is the extension of the CC bond. The other dotted lined gives the C$_{3v}$-axis of the CH$_3$-group with respect to this bond. The MC$_1$ bond (C), the MC$_2$ bond (CH$_3$), the CC bond, together with the CH$_3$ tilt angle with respect to the CC bond (θ) were optimised.

CC distances, keeping the product CCH$_x$ at a 3-fold site, and keeping substrate-CC angles all at 180° (perpendicular positions). Vibrational calculations were performed using the conventional GF-method[29], where G is the kinetic energy matrix and F the force constant matrix. Kinetic properties were calculated according to transition state theory[30].

5.3   Electronic structure calculations

Optimal parameters and energies of the CS and the CC^{f}S of C/CH and C/CH$_2$ on Ni$_7$ and Ni$_{13}$, together with the CS, the TS and the CC^{f}S of C/CH$_3$ on Ni$_7$, Ni$_{13}$, Co$_7$, and Co$_{13}$ are shown in table 5.1.   We conclude that formation of CCH (CC^{f}S) is endothermic

Table 5.1. Geometries (Å) and energies (kJ/mol) of the coadsorbed state (CS), the transition state (TS) and the CC-formed state (CC^{f}S) for the 7- and 13-atom cluster models.

System	R_{MC1}	R_{MC2}	R_{CC}	θ	E
Ni$_7$/C/CH (CS)	1.84	1.84	2.88	0.0°	0
Ni$_7$/CCH (CC^{f}S)	1.98	3.03	1.31	0.0°	62
Ni$_7$/C/CH$_2$ (CS)	1.84	2.04	2.89	0.0°	0
Ni$_7$/CCH$_2$ (CC^{f}S)	1.90	3.02	1.41	0.0°	-152
Ni$_7$/C/CH$_3$ (CS)	1.84	2.43	2.99	0.0°	0
Ni$_7$/CCH$_3$ (TS)	1.81	2.32	2.39	43.3°	57
Ni$_7$/CCH$_3$ (CC^{f}S)	1.85	3.09	1.57	0.0°	-215
Ni$_{13}$/C/CH (CS)	1.80	1.91	6.40	0.0°	0
Ni$_{13}$/CCH (CC^{f}S)	2.03	3.09	1.31	0.0°	61
Ni$_{13}$/C/CH$_2$ (CS)	1.80	2.04	6.60	0.0°	0
Ni$_{13}$/CCH$_2$ (CC^{f}S)	1.95	3.07	1.41	0.0°	-14
Ni$_{13}$/C/CH$_3$ (CS)	1.80	2.39	7.05	0.0°	0
Ni$_{13}$/CCH$_3$ (TS)	1.82	2.16	2.15	25.9°	84
Ni$_{13}$/CCH$_3$ (CC^{f}S)	1.91	3.17	1.56	0.0°	-66
Co$_7$/C/CH$_3$ (CS)	1.77	2.45	3.04	0.0°	0
Co$_7$/CCH$_3$ (TS)	1.79	2.30	2.33	43.3°	55
Co$_7$/CCH$_3$ (CC^{f}S)	1.88	3.14	1.58	0.0°	-184
Co$_{13}$/C/CH$_3$ (CS)	1.81	2.41	7.10	0.0°	0
Co$_{13}$/CCH$_3$ (TS)	1.83	2.15	2.09	23.8°	47
Co$_{13}$/CCH$_3$ (CC^{f}S)	1.96	3.21	1.55	0.0°	-89

on both clusters by 61–62 kJ/mol.   Formation of CCH$_2$ (CC^{f}S) and CCH$_3$ (CC^{f}S) is strongly exothermic on Ni$_7$, but the exothermicity is reduced on Ni$_{13}$. For the Ni$_{13}$-clusters we also optimised the adsorption energy of CCH$_x$ (CC^{f}S) as a function of the MC$_1$ and CC distances for optimal CH distances of CCH$_x$ in the gas phase. Although the effect on the CH distance was pronounced (optimal CH distances of 1.09 Å, 1.11 Å, and 1.13 Å for CCH, CCH$_2$, and CCH$_3$, respectively), the effect on the adsorption energies was maximal 3 kJ/mol. For the most exothermic reaction, the formation of CCH$_3$, we determined the TS on Ni$_7$, Ni$_{13}$, Co$_7$, and Co$_{13}$. We find transition state barriers of 57 kJ/mol on Ni$_7$, 84

kJ/mol on Ni_{13}, 55 kJ/mol on Co_7, and 47 kJ/mol on Co_{13}. The geometry of the TS differs significantly between the 7- and 13-atom clusters of the same metal, but are quite similar for the 7-atom clusters as well as for the 13-atom clusters. Analysis of the TS shows a dominant contribution of the CC distance to the imaginary frequency, which characterises the reaction coordinate. Therefore, we expect a correlation between CC bond distance and barrier height. Indeed, the TS of Ni_7/CCH_3 with a CC bond of 2.39 Å gives a slightly higher barrier (57 kJ/mol) than the TS of Co_7/CCH_3 with a CC bond of 2.33 Å and a barrier height of 55 kJ/mol. The effect is more pronounced on the 13-atom clusters: The TS of Ni_{13}/CCH_3 has a CC bond distance of 2.15 Å and a barrier height of 84 kJ/mol, whereas the TS of Co_{13}/CCH_3 has a CC bond distance of 2.09 Å and a barrier height of only 47 kJ/mol. Although in both cases the difference in CC bond length is 0.06 Å, the effect on barrier height is very different. We attribute this to the more compact TS at the 13-atom clusters. Except for the MC_1 distance, the MC_2- and CC distances and the tilt angle are significantly smaller on the 13-atom clusters, which results in a larger effect on the transition state barrier height, when the CC bond length changes. The same conclusion can be drawn starting from the CC^fS state. For Ni_7/CCH_3 the CC bond changes from 1.57 Å to 2.39 Å, an increase of 0.82 Å in going from the CC^fS to the TS. The barrier height for this CC cleavage reaction is 272 kJ/mol. For Co_7/CCH_3 the CC bond changes from 1.58 Å to 2.33 Å, an increase of 0.75 Å with a corresponding barrier height of 239 kJ/mol. For Ni_{13}/CCH_3 and Co_{13}/CCH_3 the changes in CC bond length are respectively 0.59 Å and 0.54 Å with corresponding barrier heights of 150 kJ/mol and 136 kJ/mol.

Comparison of our CS results with the infinitely separated state (ISS) of adsorbed C/CH_x showed up the existence of cluster size effects. This can be seen from table 5.2, which shows the charge on C, C of CH_x, H of CH_x, the CH_x fragment, and on the cluster for all studied systems, together with the difference in energy between the adsorbed C/CH_x in the ISS and the CS. The large positive energy difference indicates that adsorption in the CS is far more favourable than in the ISS. The magnitude and sign of this energy difference clearly prohibits interpretation in terms of a barrier to move along the surface. We discuss first the results for C/CH. The CC^fS shows a positive charge on C (0.33e on Ni_7, 0.55e on Ni_{13}). Also, the total charge on the cluster is by more than two electrons positive on the CS at Ni_7 (2.06e), and by almost two electrons on Ni_{13} (1.99e). The CH fragment is strongly polarised at the CS and the CC^fS as a result of excessive (negative) charge on C and positive charge on H of CH. The total charge on the CH fragment is as a result also strongly negative at the CS and to a lesser extend at the CC^fS. All these observations hold for C/CH_2 too, but they are less pronounced.

Table 5.2. Charge (in electrons) on C (q_{C1}), on C of CH_3 (q_{C2}), on H of CH_x(Σq_H), on CH_x (q_{CHx}), and on M_x (Σq_{Mx}) based on a Mulliken population analysis for the infinitely separated state (ISS) of adsorbed C/CH_x, the coadsorbed state (CS), the transition state (TS) and the CC-formed state (CC^fS), together with the energy difference (kJ/mol) between the ISS and the CS for the 7- and 13-atom cluster models.

System	q_{C1}	q_{C2}	Σq_H	q_{CHx}	Σq_{Mx}	E_{ISS}-E_{CS}
Ni_7/C/CH (ISS)	-0.39	-0.39	0.13	-0.26	0.65	
Ni_7/C/CH (CS)	-0.57	-1.75	0.26	-1.49	2.06	474
Ni_7/CCH (CC^fS)	0.33	-1.13	0.19	-0.94	0.61	
Ni_7/C/CH_2 (ISS)	-0.39	-0.42	0.30	-0.12	0.51	
Ni_7/C/CH_2 (CS)	-0.56	-1.59	0.82	-0.77	1.33	399
Ni_7/CCH_2 (CC^fS)	0.04	-1.19	0.60	-0.59	0.55	
Ni_7/C/CH_3 (ISS)	-0.39	-0.30	0.33	0.03	0.36	
Ni_7/C/CH_3 (CS)	-0.59	-1.53	1.36	-0.17	0.76	303
Ni_7/CCH_3 (TS)	-0.60	-1.37	1.30	-0.07	0.67	
Ni_7/CCH_3 (CC^fS)	-0.35	-1.17	1.02	-0.15	0.50	
Ni_{13}/C/CH (ISS)	-0.52	-0.46	0.10	-0.36	0.88	
Ni_{13}/C/CH (CS)	-0.65	-1.65	0.31	-1.34	1.99	518
Ni_{13}/CCH (CC^fS)	0.55	-1.20	0.13	-1.07	0.52	
Ni_{13}/C/CH_2 (ISS)	-0.52	-0.53	0.28	-0.25	0.77	
Ni_{13}/C/CH_2 (CS)	-0.65	-1.72	0.92	-0.80	1.45	453
Ni_{13}/CCH_2 (CC^fS)	0.01	-1.20	0.64	-0.56	0.55	
Ni_{13}/C/CH_3 (ISS)	-0.52	-0.41	0.27	-0.14	0.66	
Ni_{13}/C/CH_3 (CS)	-0.66	-1.70	1.47	-0.23	0.89	335
Ni_{13}/CCH_3 (TS)	-0.58	-1.49	1.42	-0.07	0.65	
Ni_{13}/CCH_3 (CC^fS)	-0.34	-1.23	1.08	-0.15	0.49	
Co_7/C/CH_3 (ISS)	-0.46	-0.38	0.36	-0.02	0.48	
Co_7/C/CH_3 (CS)	-0.59	-1.55	1.37	-0.18	0.77	280
Co_7/CCH_3 (TS)	-0.55	-1.39	1.32	-0.07	0.62	
Co_7/CCH_3 (CC^fS)	-0.22	-1.21	1.00	-0.21	0.43	
Co_{13}/C/CH_3 (ISS)	-0.60	-0.54	0.45	-0.09	0.69	
Co_{13}/C/CH_3 (CS)	-0.58	-1.72	1.53	-0.19	0.77	300
Co_{13}/CCH_3 (TS)	-0.53	-1.60	1.57	-0.03	0.56	
Co_{13}/CCH_3 (CC^fS)	-0.25	-1.27	1.08	-0.19	0.44	

It is expected that C/CH attracts more charge than C/CH_2, resulting in a negatively charged CH_x fragment and a positively charged substrate, but the charge effects seem a bit large. The charge effects at the $CC'S$ of C/CH and C/CH_2 could have their cause in the restriction of the $CC'S$ to be perpendicular to the surface, whereas they have probably bent structures. However, the charge effects at the CS and the absence of them at the ISS, together with the large energy difference between ISS and CS suggests the occurrence of finite cluster size effects. For C/CH_3 the charge is always slightly positive on the metal substrate, slightly negative on the CH_3 fragment, and slightly more negative on C in all cases. This is in line with our expectation. The polarisation within the CH_3 fragment is however again very strong. This effect is present at the CS, the TS, and the $CC'S$ and we feel therefore that the relative energetics at these parts of the potential energy surface can be compared. Again the large charge effects are absent at the ISS. Table 5.2 shows that the energy difference between ISS and CS is largest for C/CH, followed by C/CH_2, and C/CH_3 on Ni_7 as well as Ni_{13}. The difference is always largest on the 13-atom clusters. Studies on adsorption of H/CH_3 showed an energy difference between the ISS and the CS of -29 kJ/mol. Also, no large charge effects were observed. Therefore, in this case the energy difference can be interpreted as a barrier, which has to be overcome to move infinitely separated adsorbed H and CH_3 to adjacent 3-fold sites. Studies on different coadsorbed positions of C/CH_3 showed an energy difference of -22 kJ/mol between separated 3-fold sites and adjacent 3-fold sites. In this case the large charge effects were again observed for both positions, suggesting the comparability of the relative energetics. The energy difference of 22 kJ/mol thus indicates a barrier of this size to overcome to move coadsorbed C/CH_3 to adjacent positions. We conclude that when both C and CH_x are adsorbed (CS, TS or $CC'S$), this gives rise to large charge effects, due to the finite size of our cluster models. This effect is absent at the ISS and in the coadsorption of H/CH_3.

Carter and Koel[18] estimated surface reaction energies for many C_xH_x-species. For the CC coupling of C/CH, C/CH_2, and C/CH_3 on Pt(111) forming CCH, CCH_2, and CCH_3, they estimated reaction energies of respectively -84 kJ/mol, -92 kJ/mol, and -218 kJ/mol. Thus, according to them al these reactions are thermodynamically favourable on Pt(111). However, for the CCH, and CCH_2 products they assumed bi-coordinated structures and for CCH_3 a perpendicular structure, while we restricted the CCH, CCH_2 and CCH_3 products to perpendicular positions to the surface for reasons of symmetry. Demuth and Ibach[31] did not find CC stretch frequencies on Ni(111) indicative of perpendicular CCH or CCH_2-species. Thus should these species be formed, they agree with Carter and Koel that the CC-axis is not perpendicular to the surface.

The work of Shustorovich *et al.*[19] is interesting, because they computed chemisorption data of C_xH_x on both Ni(111) and Pt(111). Mono-coordinated C_2H_x-species with a CC-axis perpendicular to the surface and bi-coordinated C_2H_x-species with a skewed CC-axis have comparable adsorption energies according to the BOC-model. For the CC coupling of C/CH, C/CH$_2$, and C/CH$_3$ on Pt(111) forming CCH, CCH$_2$, and CCH$_3$, they estimated reaction energies of respectively 0 kJ/mol, -75 kJ/mol, and +33 kJ/mol. On Ni(111) these enthalpies are +105 kJ/mol, +8 kJ/mol, and +88 kJ/mol, respectively. For the CC bond formation of C/CH$_3$, Shustorovich gives activation barriers of 79 kJ/mol on Pt(111) and 121 kJ/mol on Ni(111), and for the bond cleavage 46 kJ/mol on Pt(111) and 33 kJ/mol on Ni(111). Thus, according to Shustorovich, Pt(111) is the more reactive metal for CC bond formation, although all chemisorption energies are larger on Ni(111). In fact, CC coupling does not take place at all on Ni(111), according to Shustorovich. Also, his reaction enthalpies on Pt(111) are less exotherm or even endotherm compared to those of Carter and Koel. For the C/CH$_3$ reaction on Pt(111), Carter *et al.* and Shustorovich give very different results: according to the first it is exothermic by 218 kJ/mol, while Shustorovich gives an endothermicity of 33 kJ/mol. We can compare our results with those of Carter and Koel and those of Shustorovich. On first sight, our exothermicity of 215 kJ/mol for the C/CH$_3$ coupling on Ni$_7$ compares very well with the exothermicity of 218 kJ/mol for the same reaction on Pt(111) given by Carter and Koel. If we keep in mind the alleged lesser reactivity of Ni(111), it seems better to compare with our 13-atom cluster results. In that case our reaction energies of +61 kJ/mol, -14 kJ/mol, and -66 kJ/mol for C/CH, C/CH$_2$, and C/CH$_3$ coupling show the same trend as those of Carter and Koel of respectively -84 kJ/mol, -92 kJ/mol, and -218 kJ/mol on Pt(111). This is also in agreement with Shustorovich' notion that Pt(111) is the more reactive metal. Shustorovich' model probably underestimates the exothermicity of the studied surface reactions, as can be concluded from the comparison of his results on Pt(111) with those of Carter and Koel. We disagree with Shustorovich that the transition state barriers for CC bond formation are higher than those of CC bond cleavage.

Kang *et al.*[7] have computed the structure of CCH$_3$ on Pt(111). They found a structure perpendicular to the surface with an adsorbate-substrate distance of 1.20 Å, a CC bond distance of 1.70 Å, CH bond distances of 1.20 Å, and CCH bond angles of 108°. For CCH they also found a preference for a structure perpendicular to the surface, but at a 1-fold site, with an adsorbate-substrate distance of 1.55 Å, a CC bond distance of 1.36 Å, and a CH bond distance of 1.15 Å. Koestner *et al.*[32] using a LEED analysis, found on Rh(111) a perpendicular CCH$_3$ species at a 3-fold site with a CC bond distance of 1.45 Å, and a MC bond distance of 2.03 Å, which corresponds with an adsorbate-substrate

distance of 1.31 Å. For Pt(111) they give values of 1.50 Å for the CC bond distance and 2.00 Å for the MC distance, which corresponds with an adsorbate-substrate distance of 1.19 Å. It is clear that the computed and experimentally determined CC bond distance on Pt(111) differ significantly. Our computed MC_1 distances of CCH_3 (CC^fS) of 1.85 Å on Ni_7 and 1.88 Å on Co_7, corresponding with adsorbate-substrate distances of 1.16 Å and 1.21 Å respectively, and our CC bond lengths of 1.57 Å on Ni_7 and 1.58 Å on Co_7 seem to be reasonable values.

5.4 Kinetic calculations

We have computed rate constants using transition state theory. An important advantage of this approach is that the complete potential energy surface is not required. Instead, only the local parts at the coadsorbed state, the transition state, and the CC-formed state need to be determined to compute kinetics. In particular, rotational and vibrational frequencies together with masses of the intermediates and barrier heights determine the rate constant. The formula for CC bond formation is given by:

$$k_{CC}^f{}^{TST} = \frac{k_B T}{h} \frac{Q_v^\dagger}{Q_t Q_v} e^{\frac{-E_{crit}}{k_B T}} \tag{5.3}$$

and for CC bond cleavage by

$$k_{CC}^c{}^{TST} = \frac{k_B T}{h} \frac{Q_v^\dagger}{Q_v} e^{\frac{-E'_{crit}}{k_B T}} \tag{5.4}$$

The translational partition function describes the two translations of CH_3, which is a mobile species[28], on the substrate. The connection between $k_{CC}^f{}^{TST}$ and k_{CC}^f and between $k_{CC}^c{}^{TST}$ and k_{CC}^c is discussed in the appendix. To evaluate $k_{CC}^f{}^{TST}$ and $k_{CC}^c{}^{TST}$, we need to calculate the translational, and vibrational partition functions for the CS, the TS and the CC^fS.

To find out which degrees of freedom cancel, we characterised them at the different geometries bearing in mind that our cluster represents an (infinite) surface of infinite mass. Therefore, overall translations and rotations of the cluster are irrelevant and internal lattice vibrations (phonons) are neglected. With these premises we have determined the degrees of freedom at the TS. Three modes determine the absolute position of C: one MC stretch (MC_1), and two vibrations of C parallel to the surface (one in the mirror plane and one perpendicular to it). Three modes determine the absolute position of CH_3: one MC stretch

(MC_2), one CC stretch, and one vibration of CH_3 parallel to the surface and perpendicular to the mirror plane. Three modes determine the orientation of CH_3: the CH_3 tilt in the mirror plane (θ), the CH_3 tilt perpendicular to the mirror plane, and one internal CH_3 rotation around the internal C_{3v}-axis. Finally, there are six internal CH_3 modes: three CH stretches and three internal bending modes adding up to a total of 15 degrees of freedom. For the CS we have again the six internal modes of CH_3 and the three modes determining its orientation. Furthermore, we have the MC_2 stretch and the two vibrational modes parallel to the surface, which are translations, because CH_3 is a very mobile species. Together with the MC_1 stretch and the two vibrations of C parallel to the surface (one in the mirror plane and one perpendicular to it), they add up to 15 degrees of freedom. For the CC^fS we have again the six internal CH_3 modes and the three modes determining its orientation. Furthermore, we have one MC_1 stretch, the two vibrational modes of C parallel to the surface (one in the mirror plane and one perpendicular to it), one CC stretch, and the two vibrational modes of CH_3 parallel to the surface (one in the mirror plane and one perpendicular to it). Together, these modes add up again to a total of 15 degrees of freedom. The six internal CH_3 modes, the internal CH_3 rotation and the CH_3 tilt perpendicular to the mirror plane cancel at all geometries. Therefore, only the following modes need explicit computation. For the CS two translations of CH_3 on the surface, the MC_1 stretch, the MC_2 stretch, the two vibrations of C parallel to the surface (one in the mirror plane and one perpendicular to it), and θ. For the TS the CC stretch, the MC_1 stretch, MC_2 stretch, the two vibrations of C parallel to the surface (one in the mirror plane and one perpendicular to it), one vibration of CH_3 parallel to the surface and perpendicular to the mirror plane, and θ. For the CC^fS the MC_1 stretch, the CC stretch, the two vibrations of C parallel to the surface (one in the mirror plane and one perpendicular to it), the two vibrations of CH_3 parallel to the surface (one in the mirror plane and one perpendicular to it) , and θ. C was kept at a 3-fold site at all geometries, because it was shown to be very immobile[28]. Therefore, the MC_1 stretch and one vibration of C parallel to the surface and in the mirror plane are always varied such that their combination keeps C at the 3-fold site. Effectively, this reduces our degrees of freedom to be optimised from seven to six. The frequencies are displayed in table 5.3 for the 7- and 13-atom clusters of nickel and cobalt. The imaginary frequency at the TS is dominated by the CC stretch in all cases.

Table 5.3. Vibrational frequencies, ν_i (cm^{-1}), of the CS, the TS, and the CC^{J}S, of the 7- and 13-atom cluster models.

System	ν_1	ν_2	ν_3	ν_4	ν_5	ν_6
Ni$_7$/C/CH$_3$ (CS)	1663	742	683	387		
Ni$_7$/CCH$_3$ (TS)	573	421	246	167 i	75	32
Ni$_7$/CCH$_3$ (CC^{J}S)	2166	1082	380	187	177	142
Ni$_{13}$/C/CH$_3$ (CS)	1633	551	530	465		
Ni$_{13}$/CCH$_3$ (TS)	531	421^a	336	233i	75^a	28
Ni$_{13}$/CCH$_3$ (CC^{J}S)	2040	950	354	187^a	177^a	121
Co$_7$/C/CH$_3$ (CS)	1001	895	438	365		
Co$_7$/CCH$_3$ (TS)	537	427	286	118	100 i	46
Co$_7$/CCH$_3$ (CC^{J}S)	2274	1058	395	161	153	110
Co$_{13}$/C/CH$_3$ (CS)	1068	634	556	529		
Co$_{13}$/CCH$_3$ (TS)	553	427^b	348	240i	118^b	28
Co$_{13}$/CCH$_3$ (CC^{J}S)	2114	910	340	161^b	153^b	121

^{a} modes of the Ni$_7$-cluster.

^{b} modes of the Co$_7$-cluster.

As discussed in section 5.1, CCH$_3$ has been identified experimentally by various methods. Wu *et al.*[5], Steiniger *et al.*[11], Parmeter *et al.*[33], Kesmodel *et al.*[34], Koel *et al.*[35], and Skinner *et al.*[36] give vibrational frequencies of CCH$_3$ (CC^{J}S) on Ru(1120), Ru(0001), Pt(111), Pd(111), Rh(111), and the organometallic cluster Co$_3$(CCH$_3$)(CO)$_9$. These groups measured the symmetrical and asymmetrical CH stretch, the symmetrical and asymmetrical scissors mode, and the rocking vibration of the CH$_3$-group, in addition to the CC stretch and the MC stretch. Our choice of modes results in the cancellation of various partition functions, which allows computation of rate constants. However, it makes comparison with this data less straightforward. Therefore, we will restrict the comparison to the CC stretch and the MC stretch. For the CC stretch frequency we found values of 1082 cm^{-1}, 1058 cm^{-1}, 950 cm^{-1}, and 910 cm^{-1} on Ni$_7$, Co$_7$, Ni$_{13}$ and Co$_{13}$, respectively. Experimentally they range between 1080–1163 cm^{-1}[5,11,33,34,35,36]. For the MC stretch frequency we found values of 380 cm^{-1}, 395 cm^{-1}, 354 cm^{-1}, and 340 cm^{-1} on Ni$_7$, Co$_7$, Ni$_{13}$ and Co$_{13}$, respectively. Experimentally they range between 220–600 cm^{-1}[5,11,33,34,35,36]. Although no data on Ni or Co surfaces could be found, it is clear from these data that our computed frequencies seem correct and are well-suited for the computation of rate constants via vibrational partition functions.

These rate constants for CC bond formation and -cleavage are calculated according to eqns. (5.3)–(5.4), and are shown in table 5.4 at different temperatures.   It is clear from

Table 5.4. Rate constants for CC bond formation (k^f_{CC}) (m^2 s^{-1}) and CC bond cleavage (k^c_{CC}) (s^{-1}) for the 7- and 13-atom cluster models for different temperatures.

System	T	k^f_{CC}	k^c_{CC}
Ni$_7$/CCH$_3$	250	$5.99 \cdot 10^{-17}$	$1.64 \cdot 10^{-40}$
Ni$_7$/CCH$_3$	500	$1.10 \cdot 10^{-11}$	$1.81 \cdot 10^{-13}$
Ni$_7$/CCH$_3$	750	$9.10 \cdot 10^{-10}$	$2.33 \cdot 10^{-04}$
Ni$_7$/CCH$_3$	1000	$9.62 \cdot 10^{-09}$	$9.07 \cdot 10^{+00}$
Ni$_{13}$/CCH$_3$	250	$4.91 \cdot 10^{-23}$	$1.36 \cdot 10^{-15}$
Ni$_{13}$/CCH$_3$	500	$8.62 \cdot 10^{-15}$	$4.37 \cdot 10^{-01}$
Ni$_{13}$/CCH$_3$	750	$6.80 \cdot 10^{-12}$	$3.64 \cdot 10^{+04}$
Ni$_{13}$/CCH$_3$	1000	$2.19 \cdot 10^{-10}$	$1.13 \cdot 10^{+07}$
Co$_7$/CCH$_3$	250	$4.51 \cdot 10^{-18}$	$2.21 \cdot 10^{-34}$
Co$_7$/CCH$_3$	500	$1.60 \cdot 10^{-12}$	$1.04 \cdot 10^{-10}$
Co$_7$/CCH$_3$	750	$1.56 \cdot 10^{-10}$	$1.01 \cdot 10^{-02}$
Co$_7$/CCH$_3$	1000	$1.73 \cdot 10^{-09}$	$1.08 \cdot 10^{+02}$
Co$_{13}$/CCH$_3$	250	$3.62 \cdot 10^{-16}$	$4.55 \cdot 10^{-13}$
Co$_{13}$/CCH$_3$	500	$1.93 \cdot 10^{-11}$	$5.23 \cdot 10^{+00}$
Co$_{13}$/CCH$_3$	750	$9.94 \cdot 10^{-10}$	$1.42 \cdot 10^{+05}$
Co$_{13}$/CCH$_3$	1000	$8.05 \cdot 10^{-09}$	$2.51 \cdot 10^{+07}$

table 5.4 that for all temperatures and for all clusters CC bond formation prevails over CC bond cleavage. We see that the rate constant for CC bond formation is a factor 6–13 larger on Ni$_7$ compared to Co$_7$ in the temperature range studied, although the barrier height on Ni$_7$ is slightly higher at the electronic potential energy surface. This is due to the effect of vibrational zero-point energies and temperature on the barrier height. This is more clearly seen from table 5.5, which gives the barrier heights at the electronic potential energy surface (E), including zero-point energy differences (E$_{crit}$), and including temperature effects (E$_{act}$). E$_{act}$ is given by the slope of Arrhenius plots, which are shown in fig. 5.2 for both Ni$_7$/Co$_7$ and Ni$_{13}$/Co$_{13}$. The intercepts of the Arrhenius plots give the pre-exponentials (A$_{plot}$), which are also given in table 5.5. We see that inclusion of zero-point energies lowers barrier heights for both CC bond formation as well as CC bond cleavage, reflecting the relatively low vibrational frequencies at the TS and the relatively high frequencies at the CS and the CC^{f}S.
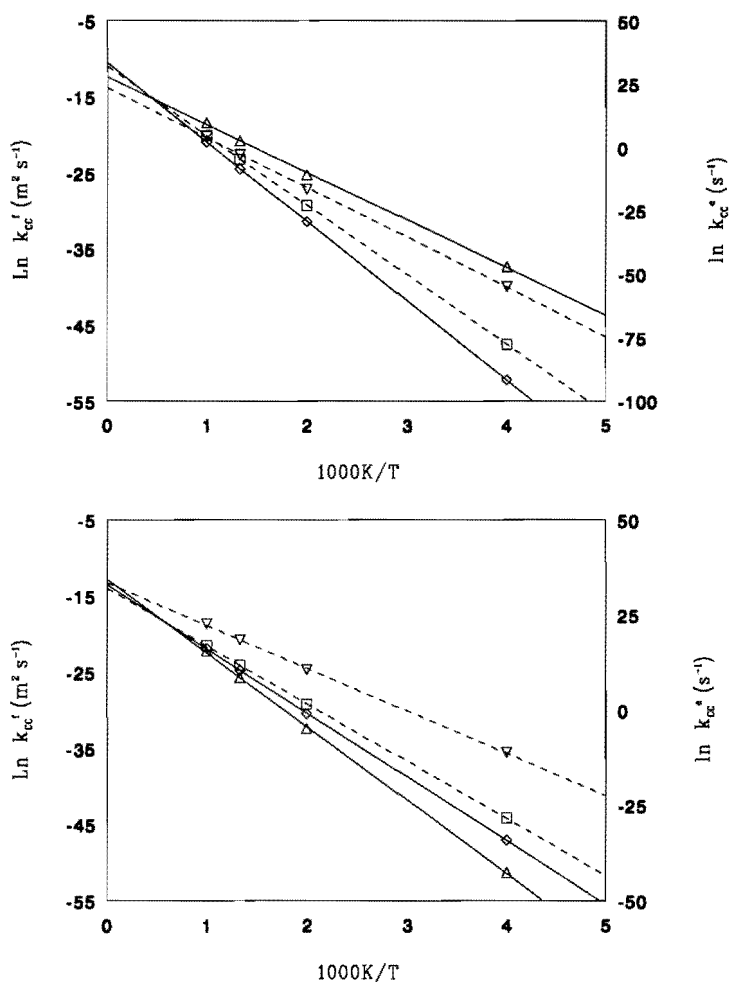
Fig. 5.2.
Arrhenius plots for bimolecular CC formation (k^f_{CC}) and unimolecular CC bond cleavage (k^c_{CC}) on $Ni_7/Co_7/C/CH_3$ (top), and on $Ni_{13}/Co_{13}/C/CH_3$ (bottom).
Markers are: $\triangle$: k^f_{CC} nickel; $\triangledown$: k^f_{CC} cobalt; $\diamondsuit$: k^c_{CC} nickel; $\square$: k^c_{CC} cobalt.

The effect of temperature is the population of excited levels, which affects the TS more strongly than the CS and the CC^fS, because of its lower frequencies. The temperature averaged barrier (E_{act}) will therefore be higher than the critical barrier E_{crit}, where only the zero-point energy differences are taken into account. For CC bond formation on Ni_{13} and Co_{13} the barrier height at the electronic potential energy surface (E), including zero-point energy differences (E_{crit}), and temperature averaged (E_{act}), is substantially lower on Co_{13}. Therefore, the rate constants on these clusters are far more larger on Co_{13} than on Ni_{13} at all temperatures.   If there is no entropy of activation, the pre-exponential

Table 5.5. Electronic energy (E) (kJ/mol), critical energy (E_{crit}) (kJ/mol), activation energy (E_{act}) (kJ/mol), and Arrhenius pre-exponential (A^{plot}) for CC bond formation ($m^2 s^{-1}$) and CC bond cleavage (s^{-1}) for the 7- and 13-atom cluster models.

System	Reaction	E	E_{crit}	E_{act}	A^{plot}
Ni_7/CCH_3	CC bond formation	57	44	52	$3.98 \cdot 10^{-06}$
Ni_7/CCH_3	CC bond cleavage	271	255	260	$2.96 \cdot 10^{+14}$
Ni_{13}/CCH_3	CC bond formation	84	73	80	$2.81 \cdot 10^{-06}$
Ni_{13}/CCH_3	CC bond cleavage	150	135	140	$1.99 \cdot 10^{+14}$
Co_7/CCH_3	CC bond formation	55	48	55	$1.00 \cdot 10^{-06}$
Co_7/CCH_3	CC bond cleavage	240	223	228	$7.25 \cdot 10^{+13}$
Co_{13}/CCH_3	CC bond formation	47	40	47	$1.81 \cdot 10^{-06}$
Co_{13}/CCH_3	CC bond cleavage	136	122	126	$8.37 \cdot 10^{+13}$

factor is approximately 10^{-6} m^2 s^{-1} for CC bond formation, which is a bimolecular surface reaction, and approximately 10^{+13} s^{-1} for CC bond cleavage, which is a unimolecular surface reaction[30]. The pre-exponentials for CC bond formation denote therefore that there is essentially no entropy of activation and that thus the entropy in the CS and the TS is essentially the same. In combination with the computed frequencies, we conclude that our TS is rather tight. The pre-exponentials for CC bond cleavage denote that there is a slight gain in entropy in going from the CC^fS to the TS, which seems natural. Inspection of table 5.3 shows that the frequencies of the CC^fS are indeed higher than those of the TS.

5.5 Conclusions

We have studied the CC coupling of C/CH, C/CH$_2$, and C/CH$_3$ on Ni$_7$- and Ni$_{13}$ cluster models using density functional theory. Formation of CCH$_3$ turned out to be the most exothermic reaction on both clusters. Experimentally, CCH$_3$ has been identified unambiguously with the CC-axis perpendicular to the metal surface. Therefore, we have determined the structure and potential energy surface at the CS, the TS, and the CC^{f}S of C/CH$_3$ on Ni$_7$, Co$_7$, Ni$_{13}$ and Co$_{13}$. We find CC coupling barriers of 57 kJ/mol for the Ni$_7$-cluster, 55 kJ/mol for the Co$_7$-cluster, 84 kJ/mol for the Ni$_{13}$-cluster and 47 kJ/mol for the Co$_{13}$-cluster. The overall reaction energies are -215 kJ/mol, -184 kJ/mol, -66 kJ/mol, and -89 kJ/mol, respectively. Analysis of the TS shows a dominant contribution of the CC bond to the reaction coordinate, and the barrier height correlates with the change of the CC bond in going from the CS to the TS and from the CC^{f}S to the TS. The magnitude of this effect is different for the 7-clusters and the 13-clusters.

Finite cluster size effects were observed for all CC coupling reactions by comparing the charge distributions on C, CH$_x$, and on the substrate at all studied parts of the potential energy surface, in combination with the energy difference between the adsorbed C/CH$_x$ in the ISS and the CS. For the CC^{f}S of C/CH and C/CH$_2$ a possible cause of the positive charge on C is the restriction of geometries perpendicular to the surface. For C/CH$_3$ the charge is always slightly positive on the substrate, slightly negative on CH$_3$, and slightly more negative on C, which is in line with our expectation. However, the polarisation within the CH$_3$ fragment is again very strong. This effect is present at the CS, the TS, and the CC^{f}S and we feel therefore that the relative energies at these parts of the potential energy surface are comparable. Coadsorption of H/CH$_3$ showed no finite cluster effects.

We have seen that the rate constant for CC bond formation is a factor 6–13 larger on Ni$_7$ compared to Co$_7$, although the barrier height on Ni$_7$ is slightly higher at the electronic potential energy surface. This is due to the effect of vibrational zero-point energies and temperature on the barrier height. For CC bond formation on Ni$_{13}$ and Co$_{13}$ the barrier height is always substantially lower on Co$_{13}$, whether zero-point energies and temperature effects are included or not. Therefore, the rate constants on these clusters are always far more larger on Co$_{13}$ than on Ni$_{13}$. The TS was shown to be rather tight.

5.6   References

1. F. Fischer, H. Tropsch, Brennst. Chem. **7** (1926) 97.
   F. Fischer, H. Tropsch, Chem. Ber. **59** (1926) 830.

2. R.C. Brady III, R. Pettit, J. Am. Chem. Soc. **102** (1980) 6181.
   R.C. Brady III, R. Pettit, J. Am. Chem. Soc. **103** (1981) 1287.

3. M.P. Kaminsky, N. Winograd, G.L. Geoffroy, M.A. Vannice,
   J. Am. Chem. Soc. **108** (1986) 1315.

4. T. Koerts, R.A. van Santen, J. Chem. Soc. Chem. Comm. (1991) 1281.
   T. Koerts, M.J.A.G. Deelen, R.A. van Santen, J. Catal. **138** (1992) 101.

5. M.C. Wu, D.W. Goodman, J. Am. Chem. Soc. **116** (1994) 1364.
   M.C. Wu, D.W. Goodman, G.W. Zajac, Catal. Lett. **24** (1994) 23.
   M.C. Wu, P. Lenz-Solomun, D.W. Goodman, J. Vac. Sci. Tech. A **12** (1994) 2205.

6. M. Belgued, P. Pareja, A. Amariglio, H. Amariglio, Nature **352** (1991) 789.

7. D.B. Kang, A.B. Anderson, Surf. Sci. **155** (1985) 639.

8. G.A. Somorjai, M.A. Van Hove, B.E. Bent, J. Phys. Chem. **92** (1988) 973.

9. R.G. Windham, B.E. Koel, J. Phys. Chem. **94** (1990) 1489.

10. F. Zaera, J. Am. Chem. Soc. **111** (1989) 4240.

11. H. Steiniger, H. Ibach, S. Lehwald, Surf. Sci. **117** (1982) 341.
    M. Salmeron, G.A. Somorjai, J. Phys. Chem. **86** (1982) 341.
    J.R. Creighton, J.M. White, Surf. Sci. **129** (1983) 327.
    M.R. Albert, L.G. Sneddon, W. Eberhardt, F. Greuter, T. Gustafson,
    E.W. Plummer, Surf. Sci. **120** (1982) 19.

12. D.H. Fairbrother, X.D. Peng, R. Viswanathan, P.C. Stair, M. Trenary, J. Fan,
    Surf. Sci. Lett. **285** (1993) L455.

13. F. Zaera, H. Hoffmann, J. Phys. Chem. **95** (1991) 6297.

14. C. Zheng, Y. Apeloig, R. Hoffmann, J. Am. Chem. Soc. **110** (1988) 749.

15. A. de Koster, R.A. van Santen, J. Catal. **127** (1991) 141.

16. T. Koerts, R.A. van Santen, J. Mol. Catal. **70** (1991) 119.

17. L.L. Kesmodel, L.H. Dubois, G.A. Somorjai, Chem. Phys. Lett. **56** (1978) 267.
    L.L. Kesmodel, L.H. Dubois, G.A. Somorjai, J. Chem. Phys. **70** (1979) 2180.

18. E.A. Carter, B.E. Koel, Surf. Sci. **226** (1990) 339.

19. E. Shustorovich, Surf. Sci. **205** (1988) 336.
    E. Shustorovich, A.T. Bell, Surf. Sci. **205** (1988) 492.
    E. Shustorovich, Advances in Cat. **37** (1990) 101.

20. Amsterdam density-functional (ADF) programme developed by Baerends *et al.*.
    E.J. Baerends, D.E. Ellis, P. Ros, Chem. Phys. **2** (1973) 41.
    P.M. Boerrigter, G. te Velde, E.J. Baerends, Int. J. Quantum Chem. **33** (1988) 87.
    G. te Velde, E.J. Baerends, J. Comput. Phys. **99** (1992) 84.
    D. Post, E.J. Baerends, J. Chem. Phys. **78** (1983) 5663.
    E.J. Baerends, A. Rozendaal, *Quantum chemistry: the challenge of transition metals and coordination chemistry*, edited by A. Veillard (Reidel, Dordrecht, 1986).
    P.J. van den Hoek, A.W. Kleyn, E.J. Baerends,
    Comm. Atom. Molec. Phys. **23** (1989) 93.
21. D.M. Ceperley, B.J. Alder, Phys. Rev. Lett. **45** (1980) 566.
22. S.H. Vosko, L. Wilk, M. Nusair, Can. J. Phys. **58** (1980) 1200.
    J.P. Perdew, A. Zunger, Phys. Rev. B **23** (1981) 5048.
23. A.D. Becke, Int. J. Quantum Chem. **27** (1985) 585.
24. A.D. Becke, Phys. Rev. A **38** (1988) 3098.
25. H. Stoll, C.M.E. Pavlidou, H. Preuss, Theor. Chim. Acta **49** (1978) 143.
    H. Stoll, E. Golka, H. Preuss, Theor. Chim. Acta **55** (1980) 29.
26. J.G. Snijders, E.J. Baerends, Mol. Phys. **36** (1978) 1789.
    J.G. Snijders, E.J. Baerends, P. Ros, Mol. Phys. **38** (1979) 1909.
27. T. Ziegler, A. Rauk, Theor. Chim. Acta **46** (1977) 1.
28. H. Burghgraef, A.P.J. Jansen, R.A. van Santen, Surf. Sci. **324** (1995) 345.
29. E.B. Wilson, J.C. Decius, P.C. Cross, *Molecular vibrations. Theory of infrared and raman vibrational spectra* (McGraw-Hill, New York, 1955).
30. R.G. Gilbert, S.C. Smith, *Theory of unimolecular and recombination reactions* (Blackwell, Oxford, 1990).
    M. Boudart, G. Djéga-Mariadassou, *Kinetics of heterogeneous catalytic reactions* (Princeton University Press, Princeton, N.J. 1984).
31. J.E. Demuth, H. Ibach, Surf. Sci. **78** (1978) L238.
32. R.J. Koestner, M.A. van Hove, G.A. Somorjai, Surf. Sci. **121** (1982) 321.
33. J.E. Parmeter, M.M. Hills, W.H. Weinberg, J. Am. Chem. Soc. **108** (1986) 3563.
34. L.L. Kesmodel, J. A. Gates, Surf. Sci. **111** (1981) L747.
35. B.E. Koel, B.E. Bent, G.A. Somorjai, Surf. Sci. **146** (1984) 211.
36. P. Skinner, M.W. Howard, I. A. Oxton, S.F.A. Kettle, D.B. Powell, N. Sheppard,
    J. Chem. Soc. Far. Trans. **77** (1981) 1203.

5.7   Appendix: derivation of rate constant equations

We can write down the following for CC bond formation:

$$\frac{d}{dt} N_{CCH_{3a}} = k_{CC}^{f}{}^{TST} N_{C_a} N_{CH_{3a}}, \tag{5.5}$$

where, $N_{CCH_{3a}}$ is the number of adsorbed CCH_3 molecules, N_{C_a} is the number of adsorbed C molecules, and $N_{CH_{3a}}$ is the number of adsorbed CH_3 molecules. $k_{CC}^{f}{}^{TST}$ is the transition state theory reaction rate constant given by:

$$k_{CC}^{f}{}^{TST} = \frac{k_B T}{h} \frac{Q_{v_1}^{\ddagger} .. Q_{v_5}^{\ddagger}}{Q_{t_1} Q_{t_2} Q_{v_1} .. Q_{v_4}} e^{\frac{-E_{crit}}{k_B T}}. \tag{5.6}$$

The translational partition functions Q_{t_1}, and Q_{t_2} can be combined and are of the form

$$(2\pi m_{CH_3} k_B T/h^2)\ S. \tag{5.7}$$

All vibrational partition functions Q_v are of the form

$$\frac{1}{1 - e^{-\frac{h\nu}{k_B T}}}. \tag{5.8}$$

In eqns. (5.6)–(5.8), k_B denotes Boltzmann's constant, T temperature, h Planck's constant, E_{crit} the barrier energy including zero-point energy differences, ν the frequency of the particular vibrational mode, S the surface area, and m_{CH_3} the mass of CH_3. The translational modes of CH_3 enter because CH_3 is a mobile species. As a consequence of our tight TS, the activated CCH_3 is immobile and bound to one specific site.

Changing to surface concentrations eq. (5.5) can be written as

$$\frac{1}{S}\frac{d}{dt} N_{CCH_{3a}} = k_{CC}^{f}{}^{TST} S \frac{N_{C_a}}{S} \frac{N_{CH_{3a}}}{S}, \tag{5.9}$$

or equivalently,

$$\frac{d}{dt} [CCH_3]_a = k_{CC}^{f}{}^{TST} S [C]_a [CH_3]_a, \tag{5.10}$$

or

$$\frac{d}{dt} [CCH_3]_a = k_{CC}^{f} [C]_a [CH_3]_a. \tag{5.11}$$

We therefore have $k_{CC}^f = k_{CC}^f{}^{TST} S$.

Note that the surface area S in eqns. 5.7 and 5.10 cancel.

For the CC bond cleavage we can write down the following:

$$\frac{d}{dt} N_{CCH_{3a}} = -k_{CC}^c{}^{TST} N_{CCH_{3a}}. \tag{5.12}$$

Here, $N_{CCH_{3a}}$ is again the number of adsorbed CCH_3 molecules, and $k_{CC}^c{}^{TST}$ is the transition state theory rate constant for CC bond cleavage given by:

$$k_{CC}^c{}^{TST} = \frac{k_B T}{h} \frac{Q_{v_1}^\dagger \,..\, Q_{v_5}^\dagger}{Q_{v_1} \,..\, Q_{v_6}} e^{\frac{-E'_{crit}}{k_B T}}. \tag{5.13}$$

Changing to surface concentrations eq. (5.12) can be written as

$$\frac{1}{S} \frac{d}{dt} N_{CCH_{3a}} = -k_{CC}^c{}^{TST} \frac{1}{S} N_{CCH_{3a}}, \tag{5.14}$$

or equivalently,

$$\frac{d}{dt}[CCH_3]_a = -k_{CC}^c{}^{TST}[CCH_3]_a, \tag{5.15}$$

or

$$\frac{d}{dt}[CCH_3]_a = -k_{CC}^c[CCH_3]_a. \tag{5.16}$$

Therefore, k_{CC}^c and $k_{CC}^c{}^{TST}$ are equivalent.

Summary

In this thesis we investigated two classes of reactions, which are very important in catalysis: CH bond activation and CC bond activation on transition metal surfaces. We have chosen to study the transition metals nickel and cobalt, because much experimental data on CH bond activation is available for nickel, while cobalt has been shown in this laboratory to be much more active in CC bond formation reactions. To model the metal surface, the cluster approach is used throughout this thesis. Much effort has been made to investigate various cluster models to find the best possible cluster. 'Best' meaning being able to reproduce experimental findings as good as possible within the computational limits.

In chapter 1 we started, after a general introduction, by discussing density functional theory, in particular the local density approximation (LDA-method). This method describes the electron density of a molecule locally by a uniform electron gas. The main advantages of this approach over conventional Hartree-Fock theory are the local exchange potential, the inclusion of correlation, and the applicability to large systems. We continued by discussing the concept of partition function, and we derived partition function formulae for translational, rotational, and vibrational degrees of freedom. Together with the barrier height and the rate of crossing the barrier, they determine the transition state theory formula for the rate constant.

In chapter 2 we discussed a first model for the activation of methane by starting from the simplest possible case: the single metal atom. We have compared the electronic structure results with those of Blomberg et al. We found a significantly less stretched CH bond resulting in a much lower transition state barrier. We have compared our computed rate constants with the experimental ones of the nickel cation. It turned out that the experimental rate constants for the cation are significantly higher, which is in line with our expectation.

We continued in chapter 3 by investigating clusters of various size and -shape to find a suitable model for the metal surface. We have judged the various cluster models by comparing the adsorption behaviour of the expected and experimentally detected products of methane dissociation: adsorbed methyl and hydrogen. A one layer 7-atom cluster and a 13-atom spherical cluster turned out to be the best cluster models. In addition to adsorbed methyl and hydrogen, we have also studied all subsequent dehydrogenation steps on both clusters leading to methylene, methylidyne, and eventually carbon. It turned out that all species prefer the 3-fold site, except methyl, which prefers a 1-fold site.

On average, adsorption energies on cobalt are larger than those on nickel, but for both metals we have found the following order in chemisorption energy:

$$E_{ads}(CH_3) < E_{ads}(H) < E_{ads}(CH_2) < E_{ads}(CH) < E_{ads}(C)$$

Hydrogen and methyl are contrary to methylene, methylidyne, and carbon, very mobile species for both nickel and cobalt. Reaction energies are strongly moderated on 13-atom clusters compared to 7-atom clusters. On all clusters methane dissociation is (more or less) endothermic, as is the final dehydrogenation step: the formation of carbon and hydrogen out of methylidyne. Formation of methylidyne and hydrogen out of methylene is exothermic on all clusters.

In chapter 4 we have studied in more detail methane dissociation producing adsorbed methyl and hydrogen. We determined barrier heights on both clusters and both metals and made a kinetic analysis by computing rate constants and sticking coefficients. When the reaction coordinate consisted mainly of one mode, we made an estimate of tunneling effects. The effect of isotopic substitution was also considered. Our computed sticking coefficients are somewhat too small, but we have shown that we can reproduce experimental values, if the barrier heights are computed correctly. On both 7-atom clusters the reaction is strongly endothermic. This endothermicity is strongly reduced on the 13-atom clusters.

In chapter 5 we have studied the alternative class of reactions which can occur, once adsorbed methyl and hydrogen are formed: CC bond formation reactions. We studied the formation of ethynyl (CCH) from carbon and methylidyne, vinylidene (CCH_2) from carbon and methylene, and ethylidyne (CCH_3) from carbon and methyl. This last reaction was studied in more detail by determining the transition state, because ethylidyne is unambiguously detected experimentally. The transition state barrier for CC bond formation of ethylidyne is significantly lower than the barrier for CC bond cleavage. As a result, formation of ethylidyne is strongly exothermic on both nickel and cobalt. The CC bond formation of C/CH_3 is comparable on the 7-atom clusters. On the 13-atom clusters cobalt is significantly more active. However, we observed finite cluster size effects for all studied CC bond formation reactions by comparing coadsorption and adsorption at infinitely separated sites. This was shown more clearly by comparing the charges on the adsorbate and the substrate at the various parts of the potential energy surface.

Samenvatting

In dit proefschrift hebben we twee typen reacties bestudeerd, die erg belangrijk zijn in de katalyse: CH bindingsactivering en CC bindingsactivering aan overgangsmetaaloppervlakken. We hebben de overgangsmetalen nikkel en kobalt bestudeerd, omdat er voor nikkel veel experimentele gegevens beschikbaar zijn aangaande CH bindingsactivering, terwijl in dit laboratorium is aangetoond dat kobalt veel actiever is dan nikkel met betrekking tot de vorming van CC bindingen. Om het metaal te modelleren is het clustermodel gebruikt, waarbij we veel moeite hebben gedaan om het 'beste' clustermodel te vinden. In dit verband moet 'beste' worden opgevat als het cluster dat de experimenteel bekende gegevens het best reproduceert binnen de rekentechnische mogelijkheden.

In hoofdstuk 1 zijn we begonnen, na een algemene schets van het probleem, met een discussie over dichtheidsfunctionaaltheorie en dan met name de benadering om lokaal de electronendichtheid van een molekuul te beschrijven als die van een uniform electronengas. De belangrijkste voordelen van deze aanpak boven de conventionele Hartree-Fock theorie zijn de lokale beschrijving van de 'exchange' potentiaal, een quantummechanische term zonder klassiek analogon, het meenemen van correlatiebijdragen en de toepasbaarheid op redelijk grote systemen. Vervolgens is het concept verdelingsfunctie besproken en hebben we uitdrukkingen voor translatie-, rotatie- en vibratie-vrijheidsgraden afgeleid. Samen met de barrièrehoogte en de snelheid waarmee de barrière gepasseerd wordt, bepalen zij binnen de theorie van het geactiveerde complex de reactiesnelheidsconstante.

In hoofdstuk 2 hebben we methaanactivering door één metaalatoom bestudeerd en de verkregen electronenstructuur vergeleken met de berekeningen van Blomberg c.s. De geactiveerde CH binding was in ons geval significant korter, wat resulteert in een lagere barrière. Onze kinetische berekeningen hebben we vergeleken met experimentele reactiesnelheidsconstanten van het nikkel kation. Het blijkt, dat onze berekende reactiesnelheidsconstanten een paar orden van grootte kleiner zijn dan de experimentele waarden, die op het kation betrekking hebben. Dit is ook wat we verwachten.

In hoofdstuk 3 hebben we verschillende clustermodellen bestudeerd om een model te vinden, dat het metaaloppervlak goed representeert. Aangezien de gevormde producten van methaandissociatie geadsorbeerd waterstof en methyl zijn, hebben we het adsorptiegedrag van deze producten bestudeerd. Een éénlaags 7-atomig model en een sferisch 13-atomig model blijken het beste te voldoen. Op deze clusters hebben we dan ook alle mogelijke dehydrogeneringsreacties onderzocht, die leiden tot geadsorbeerd methyleen, methylidyne en tenslotte koolstof. Het blijkt dat alle onderzochte verbindingen de drievoudig gecoördineerde adsorptieplaats prefereren, met uitzondering van geadsorbeerd methyl,

dat de enkelvoudig gecoördineerde positie prefereert. Over het geheel genomen zijn de adsorptie-energieën op kobalt wat groter dan op nikkel, maar voor beide metalen vinden we de volgende volgorde in adsorptie-energie:

$$E_{ads}(CH_3) < E_{ads}(H) < E_{ads}(CH_2) < E_{ads}(CH) < E_{ads}(C).$$

Verder zijn geadsorbeerd waterstof en methyl erg mobiel op zowel nikkel als kobalt, dit in tegenstelling tot methyleen, methylidyne en koolstof. De reactiewarmte van alle onderzochte oppervlaktereacties is altijd minder groot op de 13-atomige clusters vergeleken met de 7-atomige clusters. Op alle bestudeerde clustermodellen is methaandissociatie altijd (min of meer) endotherm, evenals de dehydrogeneringsstap van methylidyne tot koolstof en waterstof. De vorming van methylidyne en waterstof uit methyleen is op alle clusters exotherm.

In hoofdtuk 4 hebben we in meer detail de dissociatie van methaan bestudeerd. We hebben voor beide metalen en voor beide clustermodellen de overgangstoestand expliciet bepaald. Verder hebben we reactiesnelheidsconstanten en stickingcoefficienten uitgerekend. In het geval de reactiecoördinaat voornamelijk uit één vibratie-vrijheidsgraad bestond, hebben we een afschatting van de quantummechanische tunnelingseffecten gemaakt. We hebben ook het effect van deuterium substitutie onderzocht. De berekende stickingcoefficienten waren aan de kleine kant, maar we hebben aangetoond dat de experimentele stickingcoefficienten goed reproduceerbaar zijn, als we in ons model de experimentele barrièrehoogtes gebruiken. De endothermiciteit van methaandissociatie is groot op de 7-atomige clusters, maar beduidend kleiner op de 13-atomige modellen.

Tot slot hebben we in hoofdstuk 5 de vorming van CC bindingen aan nikkel- en kobaltoppervlakken bestudeerd. Het gaat dan met name om de koppeling van koolstof met methylidyne tot ethynyl, (CCH), de koppeling van koolstof en methyleen tot vinylideen (CCH_2), en de koppeling van koolstof en methyl tot ethylidyne (CCH_3). Aangezien deze laatste verbinding als enige experimenteel is vastgesteld, hebben we voor deze CC koppelingsreactie de overgangstoestand weer expliciet bepaald. De barrière om de overgangstoestand te bereiken met geadsorbeerd koolstof en methyl als reactant en ethylidyne als product, is een stuk lager dan voor de omgekeerde reactie geldt. De vorming van deze CC binding is dus sterk exotherm op zowel nikkel als kobalt. Voor de 7-atomige clusters geldt, dat er weinig onderscheid is tussen nikkel en kobalt, dit in tegenstelling tot de 13-atomige clusters, waar kobalt een stuk actiever is. Voor alle CC koppelingsreacties hebben we echter eindige clustereffecten kunnen waarnemen door co-adsorptie van de reactanten te vergelijken met adsorptie op oneindige, onderlinge afstand. Een ladingsanalyse bevestigt dit beeld.

List of Publications

1. H. Burghgraef, A.P.J. Jansen, R.A. van Santen,
   Theoretical investigation of the insertion of nickel in the CH bond of methane.
   Electronic structure calculations and dynamics,
   J. Chem. Phys. **98** (1993) 8810.

2. H. Burghgraef, A.P.J. Jansen, R.A. van Santen,
   Electronic structure calculations and dynamics of the chemisorption of methane
   on a Ni(111) surface,
   Chem. Phys. **177** (1993) 407.

3. H. Burghgraef, A.P.J. Jansen, R.A. van Santen,
   Theoretical investigation of methane decomposition on nickel:
   Electronic structure calculations and dynamics,
   Faraday Discuss. **96** (1993) 337.

4. H. Burghgraef, A.P.J. Jansen, R.A. van Santen,
   Electronic structure calculations and dynamics of methane activation
   on nickel and cobalt,
   J. Chem. Phys. **101** (1994) 11012.

5. H. Burghgraef, A.P.J. Jansen, R.A. van Santen,
   Methane activation and dehydrogenation on nickel and cobalt. A computational study,
   Surf. Sci. **324** (1995) 345.

6. H. Burghgraef, A.P.J. Jansen, R.A. van Santen,
   Electronic structure calculations and dynamics of CC coupling on nickel and cobalt,
   J. Chem. Phys. *submitted.*

Dankwoord

In dit dankwoord wil ik mij graag richten tot diegenen, die in positieve zin een bijdrage hebben verricht aan het tot stand komen van dit proefschrift. In de eerste plaats betreft het hier mijn promotor Rutger van Santen, die mij in de gelegenheid heeft gesteld dit onderzoek te beginnen. Je hebt nooit gebrek aan creatieve ideeen gehad, waarvan sommige ook in dit proefschrift terug te vinden zijn. In de tweede plaats is het passend om op deze plaats de persoon te bedanken die bij cruciale fases in het onderzoek onontbeerlijk is geweest: Tonek Jansen. Ik mag wel stellen dat jouw betrokkenheid bij dit onderzoek in sterke mate heeft bijgedragen aan het niveau. Vooral in de beginfase van het onderzoek heb ik veel aan je begeleiding gehad. Je was ook altijd bereid om met mij van gedachten te wisselen, als ik daar behoefte aan had.

Op het persoonlijke vlak wil ik graag nog enkele personen bij deze mijn waardering laten blijken. In de eerste plaats mijn ouders, die tijdens mijn studie altijd bereid waren mij te ondersteunen. Henk Eding, tijdens mijn periode bij de vakgroep organische chemie en daarna herinner ik me o.a. heel wat gezellige voetbaluurtjes, waarbij de alcohol rijkelijk vloeide. Verder wil ik Caroline Gerrard bedanken. Je hebt in belangrijke mate bijgedragen aan mijn welzijn in mijn eerste Eindhovense jaren. Tot slot wil ik mijn lieve vriendin Arian Kanters bedanken. Wie had gedacht dat onze ontmoeting in Egypte nog zo'n lang staartje zou krijgen? Bedankt voor je steun!

Curriculum Vitae

Hielke Burghgraef werd op 21 september 1966 geboren te Stedum. Na het doorlopen van het basisonderwijs begon hij in 1978 aan de VWO opleiding aan het Tromp college te Steenwijk. In 1984 werd dit diploma behaald aan het Ommelander college te Appingedam. Datzelfde jaar schreef hij zich in voor de studie chemie aan de Rijksuniversiteit Groningen. In 1989 werd het diploma (met genoegen) behaald binnen de vakgroep chemische fysica, met als hoofdvak theoretische chemie onder leiding van Prof. Dr. W.C. Nieuwpoort met als bijvak theoretische natuurkunde en vaste stof chemie. In november 1989 begon hij zijn promotieonderzoek aan de Technische Universiteit Eindhoven bij de vakgroep organische chemie met als doel de opheldering van reactiemechanismes van fotochemische reacties. Na een turbulent eerste jaar onder Prof. Dr. H.M. Buck besloot hij zijn promotieonderzoek voort te zetten onder leiding van Prof. Dr. R.A. van Santen. Dit onderzoek is beschreven in diverse publicaties en in dit proefschrift.

Stellingen

behorende bij het proefschrift

A Quantum Chemical Study of

CH and CC Bond Activation

on Transition Metals

H. Burghgraef

1. Hoewel Blomberg c.s. aangeeft dat het van het grootste belang is de $d^n s^2$, $d^{n+1} s^1$, en d^{n+2}-toestanden van overgangsmetaalatomen goed te beschrijven als men een reactie met een één-atoom wil bestuderen, geven zij slechts één energieverschil voor de methode, waarvan zij beweren dat het de beste is. Bovendien betreft het dan ook nog een energieverschil tussen twee $d^{n+1} s^1$ sub-toestanden.

M.R.A. Blomberg, P.E.M. Siegbahn, M. Svensson, J. Phys. Chem. **95** (1991) 4313.

2. Bij de vergelijking van semi-empirische- en *ab initio* methoden om het experimentele energieverschil tussen cycloheptatrieen en norcaradieen zo goed mogelijk te reproduceren, is het opmerkelijk dat Warner concludeert, dat de *ab initio* methoden RHF/MP2 en BLYP-DFT onbevredigende resultaten geven, terwijl de door hem in het vervolg gebruikte semi-empirische methoden het genoemde energieverschil een stuk slechter reproduceren.

P.M. Warner, J. Am. Chem. Soc. **116** (1994) 11059.

3. Hoewel Schüle c.s. verschillende clustermodellen gebruikt om enkelvoudig- en drievoudig gecoördineerde adsorptie te modelleren, is het eigenaardig dat ze voor de enkelvoudige positie alleen voor het één-atoom model de $Ni-CH_3$-strekfrequentie uitrekenen en dit resultaat representatief achten voor een oppervlak. Vervolgens wordt op grond van bovengenoemde frequentie geconcludeerd, dat CH_3 drievoudig gecoördineerd aan het oppervlak adsorbeert.

J. Schüle, P.E.M. Siegbahn, U. Wahlgren, J. Chem. Phys. **89** (1988) 6982.

4. In tegenstelling tot de bewering van Sasanuma vertoont de conformatie van 1,2-dimethoxypropaan helemaal geen opmerkelijke afhankelijkheid van het oplosmiddel, aangezien zowel in de gasfase als voor alle onderzochte oplosmiddelen de gauche+ conformatie energetisch het gunstigst is, en het verschil tussen deze conformatie en de overige conformaties zich in alle gevallen in het interval 1.3–2.5 kJ/mol bevindt.

Y. Sasanuma, J. Phys. Chem. **98** (1994) 13486.

5. Hoewel Yang c.s. nergens expliciet spreekt over oscillaties in de adsorptie-energie als functie van de clusterkeuze, blijkt dit verschijnsel wel degelijk bij hen op te treden, zoals kan worden geconcludeerd uit het vergelijken van eerdere en latere publicaties.

H. Yang, J.L. Whitten, J. Chem. Phys. **89** (1988) 5329.
H. Yang, J.L. Whitten, Surf. Sci. **255** (1991) 193.

6. Auteurs, maar zeker referees, zouden er op moeten toezien, dat als gesproken wordt over 'de' adsorptie-energie van een verbinding, duidelijk wordt aangegeven of de geadsorbeerde verbinding aan het oppervlak gerelaxeerd is, en wat de geometrie en electronische toestand van het fragment in de gasfase is.

7. Disputen in de vakliteratuur kunnen leiden tot vele (ongewenste) publicaties.

B.D. Kay, M.E. Coltrin, Surf. Sci. **205** (1988) L805.
T.C. Lo, G. Ehrlich, Surf. Sci. **205** (1988) L813.

8. De conclusie van Corma c.s., dat in de bereiding van zeoliet MCM-22 een toename in de verhouding OH/SiO_2 bij gelijkblijvende overige verhoudingen een negatieve invloed heeft op de kristalliniteit van het sample, kan pas getrokken worden als de reactietijd van de samples even lang is.

A. Corma, C. Corell, J. Perez-Pariente, Zeolites **15** (1995) 2.

9. Men kan zich ernstig afvragen of de experimenten van Beebe c.s., waarin o.a. de activeringsbarriere van CH_4 dissociatie op Ni(100) wordt bepaald, wel reproduceerbaar zijn, aangezien zij in hetzelfde artikel opmerken dat de op grond van deze gemeten activeringsbarrière berekende stickingcoefficienten een factor 100–200 groter zijn dan de experimenteel gemeten sticking coefficienten. In dit licht bezien is het niet zo vreemd dat Chorkendorff c.s. een tweemaal zo hoge activeringsbarriere vindt voor dezelfde reactie.

T.P. Beebe, D.W. Goodman, B.D. Kay, J.T. Yates, J. Chem. Phys. **87** (1987) 2305.
I. Chorkendorff, I. Alstrup, S.Ullmann, Surf. Sci. **227** (1990) 291.

10. Indien men op grond van een literatuuronderzoek het aantal theoretisch mogelijke CH_xCH_x-intermediairen dat kan optreden aan metaaloppervlakken enigszins wil beperken, dan zal dit niet lukken. Alle mogelijke CH_xCH_x-species worden zo niet door de ene, dan wel door de andere groep voorgesteld als belangrijke intermediairen.

Hoofstuk 5 van dit proefschrift.

11. In plaats van belastinggeld te besteden aan verkiezingscampagnes (b.v. zangduetten met Gordon), zouden politici een stuk serieuzer genomen worden en opkomstpercentages bij verkiezingen een stuk hoger uitvallen, indien dit geld in de vorm van een stempremie bij de actieve kiezers zou terugkomen.

12. Sportwedstrijden zouden eerlijker verlopen, indien zuivere speeltijd zou worden ingevoerd en reguliere scheidsrechters advies zouden krijgen van een hulp-scheidsrechter, die beschikt over uitgebreid beeldmateriaal en herhalingen.

13. Elke stelling is verdedigbaar.